GROUNDWATER OF PAHVANT VALLEY, MILLARD COUNTY, UTAH

by Greg Gavin, Paul Inkenbrandt, Trevor Schlossnagle, and Rebecca Molinari

SPECIAL STUDY 173
UTAH GEOLOGICAL SURVEY
UTAH DEPARTMENT OF NATURAL RESOURCES
2024

Blank pages are intentional for printing purposes.

GROUNDWATER OF PAHVANT VALLEY, MILLARD COUNTY, UTAH

by
Greg Gavin, Paul Inkenbrandt, Trevor Schlossnagle, and Rebecca Molinari

Cover photo: *A late winter storm covers the southern Pahvant Range above Meadow, Utah. View looking southeast toward Meadow, Hatton, and Kanosh from Tabernacle Hill. Corn Creek Canyon is visible on the far right, and Meadow Creek Canyon is visible left of center. The highly fractured and exposed Basalt of Tabernacle Hill is visible in the foreground. Photograph by Paul C. Inkenbrandt.*

Suggested citation:

Gavin, G., Inkenbrandt, P., Schlossnagle, T., and Molinari R., 2024, Groundwater of Pahvant Valley, Millard County, Utah: Utah Geological Survey Special Study 173, 57 p., 4 appendices, https://doi.org/10.34191/SS-173.

SPECIAL STUDY 173
UTAH GEOLOGICAL SURVEY
UTAH DEPARTMENT OF NATURAL RESOURCES
2024

STATE OF UTAH
Spencer J. Cox, Governor

DEPARTMENT OF NATURAL RESOURCES
Joel Ferry, Executive Director

UTAH GEOLOGICAL SURVEY
R. William Keach II, Director

PUBLICATIONS
contact
Natural Resources Map & Bookstore
1594 W. North Temple
Salt Lake City, UT 84116
telephone: 801-537-3320
toll-free: 1-888-UTAH MAP
website: utahmapstore.com
email: geostore@utah.gov

UTAH GEOLOGICAL SURVEY
contact
1594 W. North Temple, Suite 3110
Salt Lake City, UT 84116
telephone: 801-537-3300
website: geology.utah.gov

CONTENTS

ABSTRACT 1
INTRODUCTION 1
Purpose and Scope 1
Study Area 2
Geography 2
Population 2
Land Use 2
Groundwater and Irrigation Districts 2
History 5
Previous Work 5
Geologic Setting 5
Hydrostratigraphy 6
Groundwater 7
Surface Water 8
METHODS 8
Change in Storage 8
Water Rights and Well Data 9
Field Measurements 9
Aquifer Properties and Storage Change Estimation 9
Subsidence Analysis 11
Evapotranspiration and Spring Discharge 11
OpenET 11
Clear Lake 11
NDVI Change Over Time 12
Phreatophyte Evapotranspiration 12
Well Depletions 14
Agricultural Pumping 14
Water Use Calculations 14
Monte Carlo Model 14
Consumptive Use 15
Changes in Water Use 15
Chemistry 15
Sampling 15
Age Dating 17
Clustering Analysis 17
Flow Measurements of Surface Water in Pahvant Valley 18
RESULTS AND DISCUSSION 18
Change in Storage 18
Introduction 18
Water Level Change and Potentiometric Map 18
Comparison Between Field Campaigns 18
Year-to-Year Comparison 22
Hydrostratigraphy and Lithologic Profiles 22
Aquifer Areas 23
Interpretation 23
Aquifer Property Estimates 27
Subsidence 27
Discharge 30
Wells 30
Consumptive Use 30
Clear Lake 36
Other Springs and Shallow Groundwater 40
Groundwater Budget 40
Groundwater Chemistry and Environmental Tracer Data 40
Introduction 40

Groundwater Temperature 40
Total Dissolved Solids 40
Groundwater Types 43
Stable Isotopes 45
Radioactive Isotopes 48
CONCLUSION 50
Conceptual Groundwater Model 50
Conceptual Groundwater Zones 51
Groundwater Budget and Water Use Effects 53
ACKNOWLEDGMENTS 54
REFERENCES 54
APPENDICES 58
APPENDIX A—Depth to groundwater and groundwater elevation data 59
APPENDIX B—Clear Lake Spring flow by calendar year (Division of Water Rights, 2023) 63
APPENDIX C—Map of ET fraction for Pahvant Valley 64
APPENDIX D—Tabulated geochemical data for Pahvant Valley 65

FIGURES

Figure 1. Pahvant Valley location map 3
Figure 2. Groundwater districts of Pahvant Valley 4
Figure 3. Conceptual block diagram of Pahvant Valley 6
Figure 4. Zones of phreatophytes and shallow groundwater delineated for OpenET calculations 13
Figure 5. Location of water chemistry samples collected during this study 16
Figure 6. Significant watersheds of the Canyon Mountains and Pahvant Range 19
Figure 7. Potentiometric surface map of Pahvant Valley 20
Figure 8. Interpolated groundwater level changes recorded in the Pahvant region from 1986 to 2022 21
Figure 9. Hydrographs showing consistent groundwater elevation declines 22
Figure 10. Average groundwater level changes over time for Pahvant Valley unconsolidated valley fill 23
Figure 11. Location of cross sections and lithologic boreholes 24
Figure 12. Schematic geologic cross sections 25
Figure 13. Aquifer areas and coverage of confinement during 1986 and 2022 26
Figure 14. Estimated distributions of aquifer storage properties 27
Figure 15. Vertical ground displacement based on InSAR analysis 28
Figure 16. Time series of ground deformation based on InSAR analysis and groundwater levels at USGS well 385650112243601 29
Figure 17. Pahvant Valley groundwater pumping records over time 32
Figure 18. Result of pixel-wise Mann-Kendall trend analysis of summer NDVI values from 1989 to 2021 33
Figure 19. NDVI changes over time in three example fields 34
Figure 20. Increase in agricultural production in Millard County over time 34
Figure 21. Change in evapotranspiration in the arable parts of Pahvant Valley from 2000 to 2021 35
Figure 22. Annual discharge at Spring Lake based on measurements at the Spring Lake discharge channel 37
Figure 23. Comparison between Spring Lake discharge and pumping discharge 38
Figure 24. Groundwater temperatures throughout the Pahvant study area 44
Figure 25. Total dissolved solid concentrations grouped by water source 45
Figure 26. Total dissolved solid concentrations of water quality samples plotted by location 46
Figure 27. Piper diagram of general chemistry of water quality samples collected in Pahvant Valley 47
Figure 28. K-means multivariate cluster analysis of water quality samples plotted by location 48
Figure 29. Stable isotope ratios for water samples in the Pahvant region 49
Figure 30. Comparison of δ^2H ranges for water samples in the Pahvant region 49
Figure 31. Carbon isotopes in groundwater samples and simple mixing lines 50
Figure 32. Conceptual groundwater zones within Pahvant Valley 52

TABLES

Table 1. Models used by the OpenET group that are used in calculating the ensemble values 12
Table 2. Flow statistics from existing USGS streamflow measurements 19
Table 3. Zonal statistics of vertical ground deformation in the Pahvant Valley unconsolidated aquifer 29
Table 4. Point in time count of wells by type in Pahvant Valley and their estimated withdrawals for 2022 30
Table 5. Pumping duration and rate measurements of agricultural irrigation wells in Pahvant Valley 31
Table 6. Change in evapotranspiration from 2000 to 2021 and estimated net evapotranspiration during the irrigation season 36
Table 7. Evapotranspiration and net evapotranspiration during the irrigation season by water source 36
Table 8. Pearson's correlation coefficient between Clear Lake Spring flow, groundwater pumping, and Flowell precipitation 37
Table 9. Estimated net evapotranspiration of phreatophytes, springs, and wetlands from 2016 to 2023 39
Table 10. Summary of discharge values in 2022 calculated for Pahvant Valley. 41
Table 11. Estimated groundwater discharge values from 2016 to 2022 for Pahvant Valley 41
Table 12. Estimated groundwater recharge from 1960 to 2022 42
Table 13. Total dissolved solids concentration statistics of groundwater districts in Pahvant Valley 46
Table 14. Tritium and radiocarbon concentrations, carbon isotope ratios, and radiocarbon model age results 50

GROUNDWATER OF PAHVANT VALLEY, MILLARD COUNTY, UTAH

by Greg Gavin, Paul Inkenbrandt, Trevor Schlossnagle, and Rebecca Molinari

ABSTRACT

Pahvant Valley, located in Millard County, Utah, encompasses 1610 square miles and includes several small towns, agricultural districts, hot springs, and biologically important wetlands, all heavily reliant on groundwater. This study, conducted by the Utah Geological Survey during 2022 and 2023, aims to define Pahvant Valley's water recharge and discharge estimates, characterize its primary hydrogeologic units, and describe groundwater recharge and discharge areas. The research includes the collection of groundwater and surface water samples to estimate flow paths, sources of recharge and discharge, and residence times. Additionally, a water-level campaign was conducted in early March 2022 to create an updated potentiometric surface map for the region. Pahvant Valley's groundwater system comprises three main aquifers: the valley-fill aquifer, the volcanic aquifer of the Tabernacle Hill and Ice Springs lava flows, and the Black Rock Desert volcanics. For this study, we delineated these aquifers into three conceptual groundwater zones based on hydrogeologic, geochemical, and potentiometric characteristics.

Results of this study indicate significant groundwater level declines, particularly in agricultural areas, driven by overextraction and reduced recharge. Groundwater levels have declined by an average of 26 feet since 1986 and some areas have experienced declines of up to 160 feet. The study emphasizes the crucial role of streamflow from the Pahvant Range in recharging the valley-fill aquifer, with stable isotope and chemical analyses confirming that stream discharge significantly contributes to groundwater recharge. Additionally, groundwater quality varies across the valley and increased total dissolved solids could affect water usability in some areas.

The analysis of irrigation practices reveals a significant shift in the early 1990s from flood irrigation to pivot irrigation, which led to increased and more consistent crop density and health, as indicated by Normalized Difference Vegetation Index (NDVI) data. From 1992 to 2021, NDVI values rose substantially in both magnitude and duration, reflecting higher crop yields over time. This increase in crop density and vitality resulted in higher evapotranspiration per acre, while the extended duration of greenness demonstrated stable yields regardless of surface water availability. As irrigation shifted from surface water to groundwater sources, numerous high-capacity wells were established to meet demand. Consequently, groundwater pumping in areas no longer reliant on surface water led to declines in groundwater elevations. These decreases in groundwater levels have been linked to land subsidence, with Interferometric Synthetic Aperture Radar (InSAR) analysis detecting up to 5 inches of ground deformation in the Meadow area between 2014 and 2022, closely associated with changes in groundwater levels.

This study underscores the critical balance between groundwater extraction and recharge, the effects of irrigation practices on water use, and the importance of continuous monitoring and management to ensure sustainable groundwater resources. The findings highlight the need for sustainable groundwater management practices to maintain agricultural productivity and ecological health in Pahvant Valley.

INTRODUCTION

Purpose and Scope

The Pahvant Valley, located in Millard County, Utah, has been experiencing decline in spring flow and groundwater levels over the past 35 years (Holmes and Thiros, 1990; U.S. Geological Survey, 2024). In 2022, the Utah Division of Water Rights (DWRi) tasked the Utah Geological Survey (UGS) to conduct a hydrogeologic investigation into the causes and possible effects of these trends. Our study was conducted between 2022 and 2023.

Pahvant Valley is home to several small towns, extensive agricultural districts, hot springs, and biologically important wetlands, all of which are reliant on groundwater. Water in Pahvant Valley was initially sourced from surface water diverted from local streams until artesian groundwater conditions were discovered by drilling in the Flowell area, which prompted a shift to groundwater (well) diversions. Groundwater from springs and wells now provides the majority of Pahvant Valley's drinking water and agricultural water supply.

The primary goals of this study are to (1) estimate total groundwater pumping as it relates to Pahvant Valley's major agricultural centers; (2) characterize the hydrogeology of Pahvant Valley as it pertains to the occurrence and flow direction of groundwater; (3) determine storativity parameters for the valley-fill aquifer; (4) record groundwater quality in the valley-fill aquifer; and (5) develop a water budget for Pahvant Valley.

To achieve these goals, we defined water recharge and depletion estimates, primary hydrogeologic units, characterized principal valley-fill and volcanic aquifers, and categorized groundwater recharge and discharge areas for Pahvant Valley. We collected groundwater and surface water samples to estimate groundwater flow paths, sources of recharge/discharge, and residence time. A water-level campaign was conducted by UGS staff in spring 2022 to construct an updated potentiometric surface map for the region.

Study Area

Geography

The Pahvant Valley is located in west-central Utah on the eastern margin of the Basin and Range Province and encompasses an area of 1610 square miles. The valley is a broad north-south-trending hydrologic basin located in eastern Millard County, Utah. Pahvant Valley is bounded by the Canyon Mountains to the north, Pahvant Range to the east and southeast, the Black Rock Desert to the south, and the Cricket Mountains to the west (Figure 1). The lower elevations of Pahvant Valley span between 4600 feet above sea level by Clear Lake to 6000 feet along the foothills of the Pahvant Range. Topographic high-points in the mountain ranges surrounding the study area include Williams Peak (9200 feet) in the Canyon Mountains, Mine Camp Peak (10,222 feet) in the Pahvant Range, and an unnamed highpoint (7235 feet) in the Cricket Mountains.

Pahvant Valley's hydrology is shaped by its geographic features and limited natural drainage. The valley is topographically open to the north-northwest where no topographic features separate it from the Sevier Desert in the southern Bonneville Basin. Pahvant Valley is drained by Clear Lake Spring which is fed by groundwater that issues from the Ice Springs basalt, currently the primary source of natural discharge for the valley. The Beaver River channel is normally dry due to upstream diversions but does flow episodically into Pahvant Valley during years of higher precipitation when excess water is released from Minersville Reservoir, located 50 miles to the south of the study area. The Beaver River channel enters Pahvant Valley between the Black Rock Desert volcanic field and the southern extent of the Cricket Mountains and flows northward along its eastern extent before joining the Sevier River northwest of the Clear Lake Wildlife Management Area (WMA). The Cricket Mountains have no major streams that feed the Beaver River.

Population

Pahvant Valley has numerous towns and unincorporated communities. Recent census data (U.S. Census Bureau, 2021) show that Millard County had a population of 13,164 in 2021. Fillmore, population 2592, is the county seat and economic hub of Pahvant Valley (Dean, 2023). The town of Holden accommodates 438 inhabitants, Meadow has a population of 320, and Kanosh, known for its historical significance, has a population of 508. Various other towns collectively contribute with a combined population of 3566. Groundwater from wells provides the majority of the irrigation water with lesser amounts of surface water diverted from streams draining the Pahvant Range and Canyon Mountains. Springs and groundwater represent the primary sources of drinking-water supply for Pahvant Valley.

Land Use

Land use in Pahvant Valley is multifaceted and diverse. The predominant industry is irrigated agriculture, with lesser amounts of livestock ranching, serving as primary economic drivers for Millard County. The agricultural landscape mainly includes the cultivation of alfalfa, corn, and wheat, with alfalfa ranking as the leading crop in Millard County's farming endeavors (Feuz et al., 2020). Notably, in 2019, Millard County ranked second in agricultural production among all Utah counties, having a total of $201 million dollars in sales (Dean, 2023).

Groundwater and Irrigation Districts

Dennis et al. (1946) were the first to delineate and describe individual groundwater districts for Pahvant Valley. They divided the area into six groundwater districts based on geographic, geologic, and hydrologic conditions. From north to south, these are McCornick, Greenwood, Pahvant, Flowell, Meadow, and Kanosh (Figure 2). The arable land shown on Figure 2 includes agricultural land regardless of the crop rotational status, fallow, or type of farming activity.

Irrigation practices vary from district to district but the primary source of water is from groundwater. Groundwater is supplemented with surface water from major streams flowing from the Pahvant Range that is diverted into canal networks. Surface water diversions vary seasonally based on regional precipitation and temperature trends.

Historically, crop irrigation in the valley relied solely on surface water for farms adjacent to the Pahvant Range piedmont. Canals also conveyed water farther into the valley but increases in irrigated acreage and changes in irrigation practices and management strategies have shifted the region to rely more on groundwater. The Kanosh district is supplied by groundwater only. The Meadow district is supplied by groundwater and supplemented by surface water diverted from Meadow Creek and Corn Creek. The Flowell district relies chiefly on groundwater with lesser quantities of supplementary surface water supplied by Chalk Creek. The Greenwood and Pahvant districts are supplied by groundwater and supplemented by surface water diverted from Pioneer Creek. The McCornick district is supplied solely by groundwater, but did have historical surface water diversions from the Central Utah Canal and from Whiskey Creek, which drains the southern slope of the Canyon Mountains.

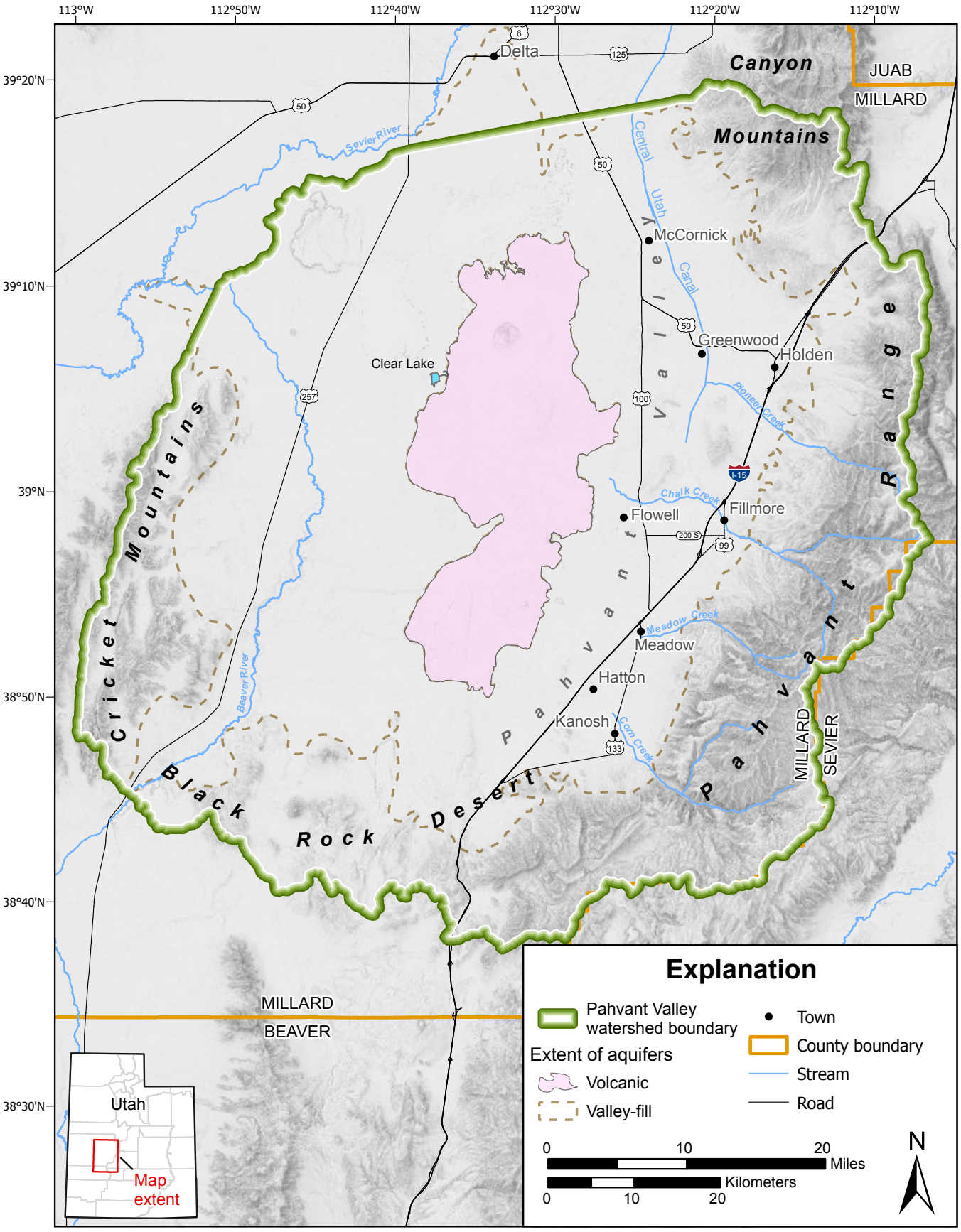

Figure 1. *Pahvant Valley location showing watershed boundary, the extent of the valley fill and volcanic aquifers, and streams draining into and out of Pahvant Valley.*

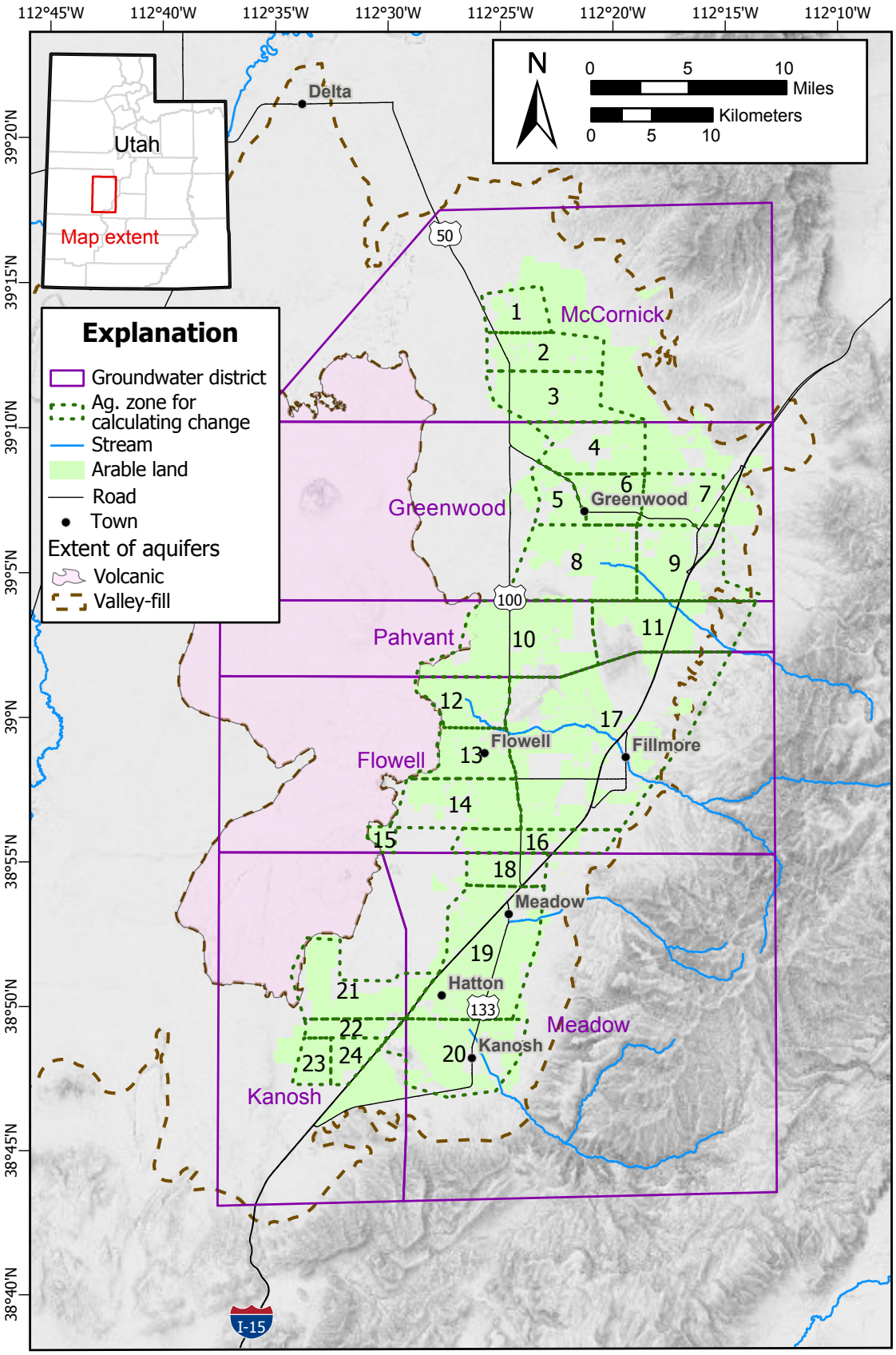

Figure 2. *Groundwater districts of Pahvant Valley with arable land shown in green and agricultural zones segmented by dashed lines. The numbered segments were used to analyze local changes over time.*

History

Pahvant Valley is named for the original inhabitants, the Pahvant band of the Ute Indian Tribe. Pahvant means "close to water" (Cuch, 2000). The town of Kanosh is named after Chief Kanosh (1821–1884) of the Pahvant band. The Ute tribe inhabited the valley and regions of the Great Basin for millennia prior to written records. Mormon settlers entered Pahvant Valley in 1851, building a small habitation adjacent to Chalk Creek in current day Fillmore. During that time, the first documented irrigation canals were dug to divert portions of Chalk Creek to supply water to the newly constructed Fort Pahvant in Fillmore (Lyman and Newell, 1999). From that original pioneer community established in Fillmore, multiple individuals and families spread out across the valley to ranch and farm.

Clear Lake is a spring-fed ecological hotspot in northwestern Pahvant Valley. Indigenous peoples visited the lake for many years as a source of refuge, water, and food. Later, the area approximately five miles west of Clear Lake was settled in 1880 as a railroad town for travelers (Kelsey, 1992) and named after the lake. The town of Clear Lake was located roughly halfway between Clear Lake, the spring-fed water source, and the Sevier River. In 1892 townsfolk began the construction of ditches, ponds, and dikes diverting water from Clear Lake to the town. Population in the town of Clear Lake expanded to 100 as of the 1900 census but declined to around 70 soon after. Populations in the town of Clear Lake fluctuated yearly between 1900 to 1930, but finally dwindled to almost zero during The Great Depression. The post office was the final business in town to close, which shuttered its doors December 31, 1936 (Kelsey, 1992). Once the town of Clear Lake was abandoned by its early 20th century settlers, the State of Utah purchased the land and water rights and soon after created the Clear Lake WMA.

The Clear Lake WMA is an important part of the intermountain flyway. Many avian species have been documented at the WMA with the area acting as a primary source of food and rest for migrating birds. The Clear Lake WMA is also home to the Least Chub (*Iotichthys phlegethontis*), a listed sensitive species of ray-finned fish (Dittmer et al., 2019). Least Chub habitat within Utah has been declining in recent years, and Clear Lake is one of its remaining critical habitats (Dittmer et al., 2019). Recreation is also an important facet of the Clear Lake WMA with waterfowl permits being a major draw for sportsmen. Waterfowl numbers harvested at Clear Lake WMA by sportsmen has declined rapidly in recent years, from 20,000 in the early to late 2000s to 0 harvested as of spring 2023 (Lynn Zubeck, Utah Division of Wildlife Resources [DWR], verbal communication, 2023).

Previous Work

Meinzer (1911) was the first to characterize the groundwater of the region. Meinzer (1911) plotted the location of 40 wells and more than 20 springs in the valley, including a chain of freshwater springs in the Flowell area. His study noted that the area was predominantly irrigated agriculture, fed at the time by springs and streams, with Chalk and Corn Creeks as the primary stream sources. At the time of Meinzer's observations in 1908, there were no flowing wells present in the area, and no wells used for irrigation.

In the 1940s, Livingston and Maxey (1944) measured aquifer leakage and artesian head of several wells in the Flowell area. The well with highest estimated natural artesian flow was from well (C-21-5) at 430 gallons per minute (gpm) with a static water level of +17.3 feet above ground surface. Their report also estimated vertical leakage between aquifer units and provided estimated flow rates. Livingston and Maxey (1944) also provided an estimate on the volume of groundwater not put to beneficial use resulting from uncapped artesian wells. Lastly, they provided guidance to area well owners to minimize leakage and loss from these wells.

Dennis et al. (1946) were the first to estimate a groundwater budget for the area and characterize the area hydrogeology in detail. Dennis et al. (1946) were also first to divide Pahvant Valley into groundwater districts as a means to distinguish the area's unique hydrogeology, topography, and geology. In addition, their report also summarized regional hydrogeochemistry grouped by groundwater district.

Mower (1965) worked in Pahvant Valley in the 1960s, refining the regional water budget and better characterizing the confined and unconfined valley-fill aquifer systems. Holmes and Thiros (1990) studied water quality changes in the valley-fill aquifer system, provided insights into mechanisms for water quality changes, and provided an updated water budget for the region. Many of the components of the Holmes and Thiros (1990) budget were derived from the Mower (1965) work.

Geologic Setting

Pahvant Valley is a syntectonic sedimentary basin composed of interbedded alluvial and lacustrine gravel, sand, and clay with volcanic rocks forming the center of the valley. The valley is located on the eastern margin of the Basin and Range physiographic province and is underlain by a west-dipping, low-angle normal fault known as the Sevier Desert detachment. The Sevier Desert detachment dips west between 3° and 4° at a depth between 1.2 and 2.5 miles below the surface (Allmendinger et al., 1983; Oviatt, 1991). Pahvant Valley formed during Basin and Range extensional normal faulting throughout late Tertiary to Quaternary time, which uplifted mountain blocks and subsided valley floors. The Quaternary valley fill and volcanic rocks form the principal aquifers of Pahvant Valley (Mower, 1965).

Geologic units in the valley floor of the study area are Quaternary unconsolidated deposits and Tertiary volcanic and sedimentary rocks (Hintze and Davis, 2005; Hintze et al., 2008).

Quaternary basaltic volcanic rocks dominate the valley fill in the central part of Pahvant Valley and are interbedded along their margins with the unconsolidated sedimentary deposits (Figure 3). The valley fill includes alluvial-fan and lacustrine deposits composed of gravel, sand, and silt near the mountains, with additional layers of clay found in the central part of the study area where the deposits become finer. The Tertiary Oak City Formation is predominantly a poorly to well-cemented conglomerate consisting of sandy, bouldery gravel deposited in alluvial fans. It underlies the base of the principal valley-fill aquifer in Pahvant Valley and forms the eastern and northeastern boundaries of that aquifer. The contact between the Oak City Formation and overlying Quaternary valley fill is an erosional unconformity that includes some paleotopography. This formation constitutes the central core of several valley hills, with Bald Mountain, Cedar Mountain, and West Mountain being the most prominent.

The Pahvant Range is structurally complex, containing thrust faults of the Sevier Orogeny and normal faults of later Basin and Range extension. Strata in the range includes Cambrian- to Tertiary-age sedimentary and metasedimentary rocks. The Pahvant thrust fault, which trends north-south along the west side of the range, thrust Cambrian strata over Triassic through Cretaceous rocks, mainly the Jurassic Navajo Sandstone (Steven, 1990; Hintze, 2005; Hintze, 2008). The Tertiary North Horn and Flagstaff Formations lie unconformably over these older rock units and are exposed in the central and eastern parts of the range. Similarly, in the southern part of the Pahvant Range, the Red Ridge thrust trends southwest from South Mountain to Dog Valley and placed Mississippian through Triassic units over the Jurassic Navajo Sandstone.

Hydrostratigraphy

The primary aquifers in the study area consist of the valley-fill aquifer, which is composed of unconsolidated interbedded sediments, and the volcanic aquifer, which is composed chiefly of basalt flows and minor rhyolite and ash deposits. The volcanic aquifer and the valley fill aquifer overlap in age and depth and are interbedded along their contact (Figure 3). Past research has categorized the groundwater system into an unconfined system and an artesian system (Meinzer, 1911; Livingston and Maxey, 1944; Dennis et al, 1946; Mower, 1965). The unconfined system comprises around 50 feet of saturated unconsolidated fill across most of the area and up to 100 feet of basalt interbedded with fill in the central region. The confined system, located in the Flowell area, occurs between 140 and

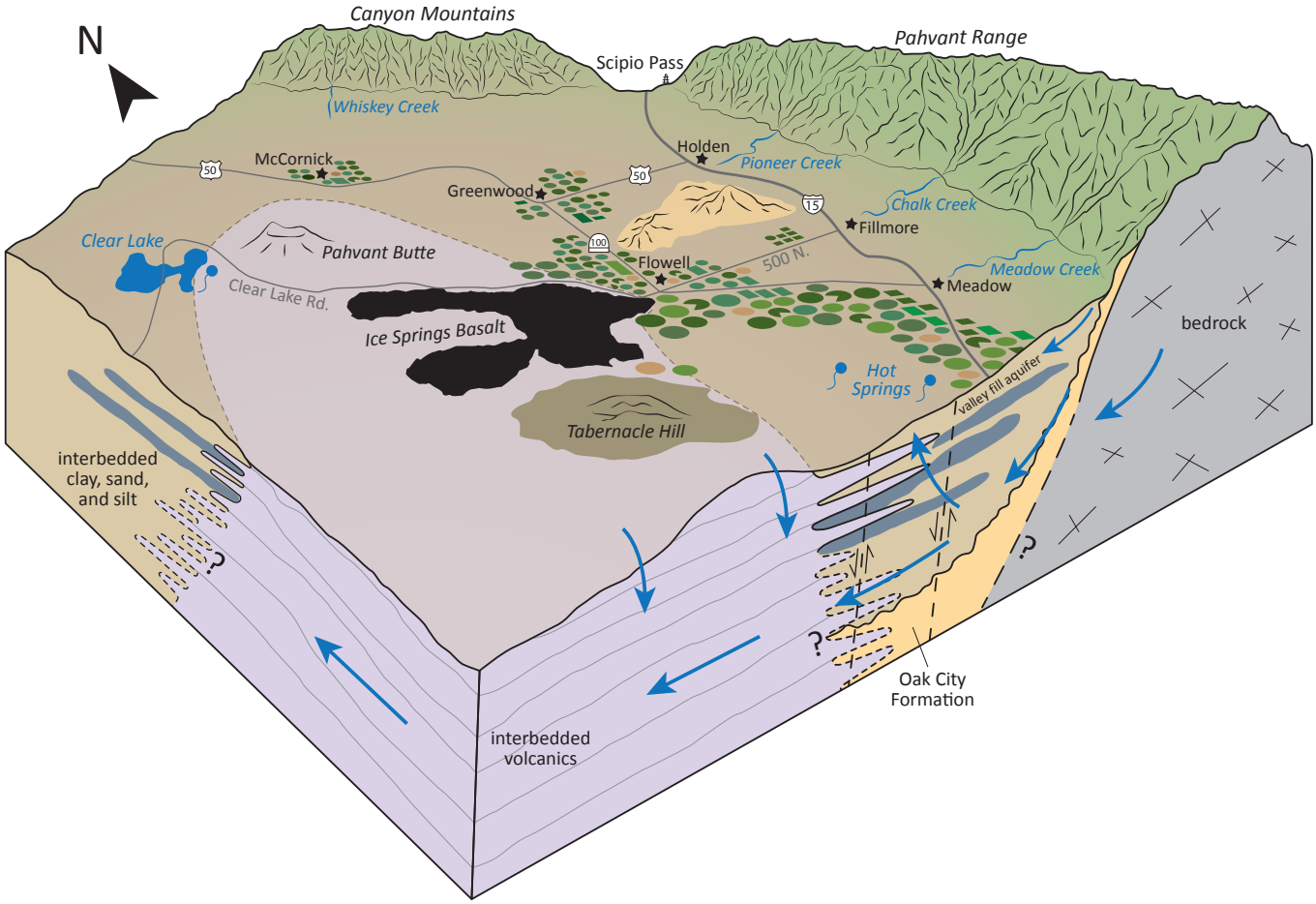

Figure 3. *Conceptual block diagram of Pahvant Valley illustrating likely groundwater flow paths.*

200 feet deep and is separated from the unconfined system by a 15- to 75-foot-thick layer of clay, creating artesian conditions.

In the mountains, some of the bedrock is fractured near the surface and contributes water to springs, but most of these rocks are relatively impermeable and hold little water. Generally, very little groundwater travels from the mountains to the valley through the bedrock. A minor amount of water does move through the top few feet of these rocks via fractures, joints, and layers, although this amount likely does not surpass the base flow of the mountain streams (Mower, 1965; Holmes and Thiros, 1990). The majority of water in these bedrock formations discharges at springs in the canyons, supporting the base flow of various small creeks. The debris at the mountain faces and bases, particularly the alluvial fans, serve as the main pathways for water to recharge aquifers in the valley (Mower, 1965).

The paleotopography of the Tertiary Oak City Formation is mostly buried by valley-fill sediments. This may influence the presence and flow of groundwater in certain areas. In some locations, this formation provides small amounts of water to wells, likely where the material is less compact and coarser. The Oak City Formation is found at shallower depths closer to the mountains relative to the depths at center of the valley, which explains why there are few successful irrigation wells in this formation on the valley's east side. Wells drilled in the Oak City Formation show hydraulic connection with the valley-fill along the foothills of the Pahvant Range. However, no aquifer tests have been performed in this formation and its hydraulic properties are not well constrained.

The lacustrine layers of gravel and sand form the confining layers within the valley-fill aquifer. The confined parts of the aquifer are the primary groundwater sources in Pahvant Valley. Artesian pressure is found immediately east of the exposed Quaternary basaltic volcanic rocks in the center of the valley, starting about six miles west of the Pahvant Range, where the aquifers are interspersed with lacustrine clay beds. Multiple clay beds divide the valley fill into several linked, confined aquifers that spread westward in finger-like extensions. Coarse-sediment zones are thickest close to the mountains and thin toward the valley. Near the mountains, particularly around the apex of the alluvial fans, coarse deposits are often at or near the surface. However, just a short distance west from the mountains, the top layers of the surface consist of fine sand, silt, and clay. Aquifer tests indicate transmissivity values between 2000 to 40,000 feet squared per day (ft^2/day) (Mower, 1965) from wells completed in areas with higher artesian pressure located in the Flowell area. Other aquifer tests performed in the unconfined valley-fill aquifer upgradient near the towns of Fillmore and Meadow suggest transmissivity is likely between 1200 to 3000 ft^2/day (Wall Engineering, 2010) in the central part of the alluvial fan.

The volcanic aquifer throughout Pahvant Valley generally shares similar water-bearing characteristics. The basalt in this region consists of some of the youngest lava flows in Utah—the Ice Springs flow is only about 800 years old (Johnsen et al., 2010). Basalt flows in the Pahvant Valley volcanic aquifer generally have fractures, brecciated layers, and a blocky structure that significantly increase its permeability (Miller, 2000). As a result, the wells drilled into this rock type in Pahvant Valley typically produce large amounts of water. Although other types of volcanic rocks such as rhyolites and ash deposits are also present in Pahvant Valley, we chose to group all volcanic rocks into one aquifer based on geographic and hydrogeologic characteristics using one name, the volcanic aquifer. Though aquifer characteristics such as transmissivity, storativity, porosity, and permeability within the volcanic aquifer vary, the geochemical signatures of water samples are relatively similar. An aquifer test using volcanic aquifer wells in the Flowell district ([(C-21-5)7cdd-2; (C-21-5)7cdd-3]) indicates that the aquifer has transmissivity as high as 3 million ft^2/day, attributed primarily to fracture flow (Mower, 1965)! Storativity from the same test was 0.06 (Mower, 1965).

Groundwater

Livingston and Maxey (1944) studied artesian groundwater leakage in the Flowell area in an effort to understand the hydraulic gradient between confining units as well as transmissivity through the water-bearing sand and gravel beds. Mower (1965, 1967) worked in Pahvant Valley throughout the 1960s, and produced several reports characterizing the hydrologic conditions of Pahvant Valley. Mower's work helped us better conceptualize the valley's aquifers, groundwater chemistry, water budget, and flow paths.

Recharge to the valley-fill aquifer occurs directly on the alluvial fans by infiltration of stream flow, snowmelt, and precipitation. A small amount of recharge to the valley-fill is also possibly subsurface flow from Paleozoic and Mesozoic bedrock of the Canyon Mountains and Pahvant Range, but this amount has not been quantified and is assumed negligible (Mower, 1965). Recharge to the volcanic aquifer occurs directly on the exposed volcanic rocks by infiltration of snowmelt and precipitation and by subsurface flow from the valley-fill aquifer. Clear Lake, Hatton Hot Spring, and Meadow Hot Springs represent the primary sources of discharge from the valley. Mundorff (1970) estimated discharge from Meadow Hot Springs of 60 gallons per minute (gpm), however no measurable discharge as overland flow from Meadow Hot Springs has been reported since.

Groundwater flows through the valley fill from the mountain front toward the valley floor into the volcanic aquifer and then to the major discharge area of Clear Lake. The mean discharge to Clear Lake between 1960 and 2021 was 15,555 acre-feet per water year (ac-ft/wy) (Utah Division of Water Rights, 2023). From the early 1990s to 2023, flows recorded at Clear Lake have declined by approximately 555 ac-ft/yr. As of summer 2022, the measurable discharge to Clear Lake ceased, leaving all but the area immediately adjacent to the spring head dry for the first time in recorded history. Measurable discharge

returned to the Clear Lake Parshall flume in late winter 2023, flowing until early summer 2023 when flows again declined to unmeasurable levels.

Surface Water

Surface water draining into and out of Pahvant Valley falls primarily as snowfall at high elevations in the Pahvant Range and Canyon Mountains. Those high elevation regions begin to release snowmelt water in late spring with runoff peaking sometime in mid to late May. Surface water has historically been put to use by diversion into canals and pipelines along the mountain front.

Most mountain streams draining into Pahvant Valley flow seasonally from spring through early summer or are lost to seepage once the stream enters the alluvial fan. Only a few streams flow year-round, the water of which is captured and used within the valley. In 1916, the Central Utah Canal began conveying water from the Sevier River into Pahvant Valley (Enright, 1987). The Central Utah Canal stopped delivering water to Pahvant Valley at the end of the 1988 water year (Greg Greathouse, Central Utah Water Company, verbal communication, January 2024).

Currently none of the perennial streams draining into Pahvant Valley are gaged or measured in any capacity. Of these perennial streams only Chalk Creek east of Fillmore (period of record [POR]: 1944 to 1971), Meadow Creek east of Meadow (POR: 1965 to 1975), and Corn Creek east of Kanosh (POR: 1965 to 1975) have historical measurements by the U.S. Geological Survey (2024). Canal and irrigation companies record periodic flow estimates during the irrigation season at select diversion locations along Corn, Meadow, and Chalk Creeks, but these records are neither continuous nor comprehensive enough for statistical analysis.

METHODS

To achieve the objectives outlined in the Purpose and Scope, we undertook a comprehensive set of tasks, including compiling existing well data, aquifer test results, and groundwater chemistry information. We measured water levels in wells and created various maps, such as a potentiometric surface map, depth-to-water maps, and change-over-time maps for the valley-fill aquifer. Well discharge and total yearly depletion were measured and estimated, and surface and groundwater samples were collected to analyze general chemistry, environmental tracers, and stable isotopes. Our team delineated the hydrostratigraphy of the valley fill and fractured bedrock units, producing three cross sections, and developed a groundwater flow path estimate. We assessed storativity and its changes over time in the valley-fill aquifer using Interferometric Synthetic Aperture Radar (InSAR) analysis. Additionally, we compiled, measured, and modeled stream flows for all watersheds draining into Pahvant Valley, mapped water-right place-of-use locations, and refined consumptive use estimates.

Change in Storage

The specific storage coefficient (S_s) represents the amount of water drained from a compressed aquifer per unit decline in hydraulic head and unit volume of the aquifer. It is calculated using a formula incorporating factors such as water density, gravitational acceleration, aquifer compressibility, porosity, and compressibility of water. Additionally, the dimensionless storage coefficient (S) characterizes the volume of water drained per unit decline in hydraulic head and unit area of the aquifer, providing insight into the overall storage capacity of the aquifer.

The storage properties of aquifers determine their subsidence response to groundwater pumping. Storage coefficients can be split into inelastic or elastic components, based on the comparison between effective stress and preconsolidation stress. Effective stress is the actual stress experienced by the aquifer skeleton (solid matrix), calculated as the difference between total stress and pore water pressure. Preconsolidation stress is the maximum effective stress that an aquifer or confining unit has experienced, typically due to the weight of overlying sediments. If effective stress exceeds the preconsolidation stress, the aquifer undergoes inelastic (permanent) deformation, potentially leading to significant and irreversible compaction. Elastic storage relates to the reversible deformation of the aquifer matrix and the water it contains. When the hydraulic head in an aquifer is altered, such as through pumping, the aquifer matrix compresses or expands elastically. This deformation is directly proportional to the change in hydraulic head, as captured by linear regression measurements between elastic vertical deformations and hydraulic head changes. Elastic behavior is governed by the material's bulk modulus of elasticity, a measure of the material's ability to resist deformation under load. Inelastic storage involves more permanent deformations, where the changes in volume do not fully recover upon ceasing the pumping. This occurs when effective stress exceeds the preconsolidation stress of the aquifer materials. Preconsolidation stress is the maximum historical stress that a sediment layer has experienced. Exceeding this stress during groundwater extraction can lead to aquifer compaction that is irreversible, contributing to subsidence. This inelastic behavior is largely influenced by the compressibility of the aquifer materials, which is a measure of the volume change per unit pressure change. Compressibility itself is a critical factor in understanding both elastic and inelastic storage. It not only affects the magnitude of storage coefficients but also impacts how the aquifer will respond to long-term stress changes, such as those induced by sustained groundwater pumping. In regions where aquifers are highly compressible, significant subsidence can occur, leading to permanent changes in the landscape and potential damage to infrastructure.

Water Rights and Well Data

With many water right filings, especially applications to appropriate or change applications, proof of the amount of water being used is established via measurement of the source of diversion. This information is recorded in the Proof of Beneficial Use also commonly called "Proof" by the Utah Division of Water Rights (DWRi). Many of these Proofs include measurements via a flow meter, but some of these proofs use estimates based on sprinkler configuration. Due to changes over time of the pump motor configuration, depth to water level, irrigation configuration, and wear of the parts, the measurement taken from the proof may not be as reliable as a direct measurement taken more recently. Though the measurement provided with the proof is rarely ideal, it can be a valuable place to start. We need to know "how much" water each well is allotted and "where" that water is being applied. If we know where the water is being applied, we can compare our pumping estimates to evapotranspiration (ET) and seepage estimates for that field. This approach at estimation becomes more challenging when there are multiple users for a well or multiple sources of water for a water right. These values can provide a good check on later estimates.

Municipalities, counties, water districts, and some industrial and agricultural users provide water use information to the DWRi and the Utah Division of Water Resources (DWRe). Most of this information is water use from drinking water sources and secondary sources, but some other sources are included. We used these data if available as an additional resource for estimating water pumped in the valley.

We collected detailed information for 350 wells in Pahvant Valley. The well logs were tabulated from an existing geodatabase obtained from the DWRi. We used the schema of this database and added aquifer test data, lithology information, construction information, screened interval, depth to water, and specific capacity information if available. Because some wells were drilled prior to the establishment of record keeping by DWRi, there likely are wells in the valley that have not been accounted for by these records. These logs were reviewed and sorted to remove duplicates and those with inadequate or illegible data. Those retained were then sorted into types organized by water right number, well identification number (WIN), water right status, priority, and type of use. We then plotted the locations and associated data to assist with the characterization of basic aquifer parameters such as lithology of the subsurface and aquifer thickness.

We also compiled USGS groundwater level data for the region (U.S. Geological Survey, 2024), and summarized the data into a timeseries of average regional groundwater level changes. To make a summary of the regional average groundwater level changes, we calculated the average depth to water over the period of record of each well and subtracted the measured depth to water from mean depth to water, producing an anomaly time series for each well. The mean and median of all groundwater anomaly time series provides the average regional groundwater level anomaly, where a positive value is a general increase in regional groundwater levels, and a negative value is a general decrease in groundwater level values.

Field Measurements

To effectively estimate the change in storage in the Pahvant groundwater system, we first determined the change in groundwater levels. We determined which wells have been measured in water level campaigns for previous studies (Dennis et al., 1946; Mower, 1965; Holmes and Thiros, 1990) and which wells are currently measured by the USGS for yearly groundwater levels. Holmes and Thiros (1990) measured 212 wells during their spring 1986 groundwater level campaign. We timed our March 2022 groundwater level campaign to nearly coincide with USGS annual measurements to obtain the greatest number of well locations with optimal areal coverage. We measured 78 groundwater and spring head elevations between March 7, 2022, and March 11, 2022, from the valley-fill and volcanic aquifers using Solinst electronic water level meters alongside Hydrologic Instrumentation Facility graduated steel tapes. We also measured ground surface coordinate and elevation data at each well location, and measured height above the ground surface datum for the reference measurement point. Accuracy of groundwater level measurements for graduated steel tape and Solinst water level meters is 0.01 feet (Cunningham and Schalk, 2011; Jelinski et al., 2015). The USGS measured groundwater elevations at an additional 42 well/spring locations between March 15, 2022, and March 16, 2022. The resulting 120 groundwater elevations were tabulated and organized alongside the historical groundwater elevation measurements from 1986 to calculate groundwater change over time. The elevation point data were contoured using an iterative approach in ArcGIS Pro by creating a raster elevation surface, then using the *raster-to-contour* tool. The resulting contours were manually adjusted to fit both the available water level information and topographic constraints.

While conducting our field campaign, we visited most of the pumping wells, taking photographs of the wells and recording specific pump motor information. We compared our field observations with the DWRi well logs and abandonment records compiled earlier, generating a "point-in-time" count of existing agricultural pumping wells in Pahvant Valley. Well counts change over time due to abandonments, maintenance downtime, and the drilling of new wells. Due to limited land access and building enclosures for some wells, we did not visit every well in the region and had to rely on DWRi records to assume the well exists and is pumping.

Aquifer Properties and Storage Change Estimation

Aquifer properties describe how well the aquifer will yield water to wells and springs. We focused on understanding specific yield (S_y) and specific storage (S_s) to accurately assess groundwater storage changes in the aquifer. We compiled data from

aquifer tests performed in Mower (1965) and from Utah Division of Drinking Water drinking water source protection plans.

We estimated storativity using the equation:

$$S = S_y + (S_s * b) \quad (1)$$

where:

S = storativity
S_y = specific yield
S_s = specific storage
b = aquifer thickness

We based S_y and S_s on published values for aquifer materials from Johnson (1967) and Domenico (1972) and b from well drillers' logs. To estimate change in storage, we must know if the aquifer is confined or unconfined, and we must be able to estimate the storage properties of the aquifer material. Every time a public supply well is drilled, an aquifer test is required. We compiled aquifer test data from drinking water source protection plans, (Diedre Beck, Utah Division of Drinking Water, written communication, August 2021). Also, drillers sometimes perform a short-term test (i.e., specific capacity test) after drilling a new well. We compiled data from drillers' logs and public supply records to find all available aquifer property data. We used data compiled from the well log examination to interpolate and estimate aquifer properties. We combined this interpolation with the water level change map to calculate the change in storage for the area. Of the 120 wells measured in the 2022 water level campaign, 102 were data points measured for the 1986 Holmes and Thiros (1990) potentiometric surface map (Appendix A). We used the 1986 data points to interpolate groundwater elevations throughout Pahvant Valley in 1986. For the groundwater level change map, we interpolated water level changes in wells that were measured in 1986 and remeasured in 2022.

We divided the valley into areas based on their current confinement and lithology, and applied distributions of the storage parameters for each region in calculations of aquifer storage change. As the groundwater level changes in an aquifer, areas in the aquifer can transition from confined to unconfined. Once the potentiometric surface in a confined aquifer falls below the top of the confining layer, the aquifer can transition to unconfined, taking water from gravity drainage of the aquifer instead of the elastic deformation of the aquifer skeleton. We used geologic maps (Hintze and Davis, 2005; Hintze et al., 2008) to constrain the area of the aquifers, as well as descriptions from previous work (Mower, 1965; Holmes and Thiros, 1990).

To accommodate changes in confinement over time, we created two maps that delineate the area of confinement. One map delineates the area of confinement during the period of highest average groundwater levels for the region. The maximum confinement delineation is based on the distribution of flowing wells in 1986 and 1987 (U.S. Geological Survey, 2024), and the recharge-discharge areas mapped by Snyder (1998). The minimum confinement delineation is based on the water level campaign and phreatophyte map from this study and represents the conditions of confinement in 2022.

To determine the storage change for each year, we downloaded all USGS groundwater levels for the study area from the NWIS database (U.S. Geological Survey, 2024). We filtered the groundwater levels to only include measurements taken between February and May of each year from 1960 to present, and only included wells with 30 or more measurements over their record. For each well, we aggregated the data to only include one measurement for each year by taking the mean value of all measurements in the February to May time period. Most wells only had measurements for March or April. The resulting dataset had data from 411 wells, spanning from 1960 to 2024.

We used the iterative imputation in Scikit-Learn, a python machine learning library, to fill in gaps in the groundwater level record for each well. This approach iteratively regresses the available well data against data from other columns to help fill in gaps in a well record. We used a Bayesian Ridge fitting approach to perform the iterative regression. To improve the accuracy of the imputation, we included yearly records from well pumping (U.S. Geological Survey, 2021) and yearly data from the flow of Clear Lake Spring.

Once the gaps were filled, we spatially interpolated the groundwater levels for each year using linear interpolation between points. We extrapolated beyond the convex hull of the point coverage to ensure that the interpolated area included all of the delineated aquifer zones. We conducted zonal statistics of each polygon for each year, calculating the average water level for each delineated zone.

Using the average groundwater level over time and the relative percentage of confinement for each aquifer area for the two extreme times (1986 and 2022), we estimated how the relative confinement area changed over time for each delineated zone. We used the average water level and relative percent confinement for 2022 and 1986 and generated a linear equation based on those two points, where groundwater level was the independent variable and percent confinement was the dependent variable. We applied the linear equation to each zone over each year, generating a percentage confinement over time. The basalt aquifer and Oak City Formation aquifer did not have any significant confinement. The Kanosh area's confinement did not change significantly over time, based on our mapping.

For each valley-fill region, we multiplied the percent confinement by the total area to determine the confined area. The unconfined area was calculated by subtracting confined area from the total area. We then iteratively multiplied the

groundwater level change by the distribution of the storage values by the confined and unconfined areas to determine the total change in groundwater volume for each region over time.

We compared the results produced by the yearly approach to results from the two most recent detailed water level campaigns (1986 and 2022). We used a similar approach to calculate groundwater storage changes based on groundwater level changes from 1986 to 2022.

Subsidence Analysis

Interferometric Synthetic Aperture Radar (InSAR) is a remote sensing technique used to measure ground surface deformation with high precision. It combines the principles of radar interferometry and synthetic aperture radar (SAR) to create detailed maps of surface displacement. SAR uses a moving radar antenna to act as a larger antenna aperture, enabling the acquisition of high-resolution images. Interferometry involves comparing the phase (alignment) of radar signals from two or more images taken at different times. The interference patterns show deformation. By analyzing the phase differences between SAR images, InSAR can quantify ground deformation, such as subsidence, uplift, or horizontal motion. The results are presented as color-coded interference fringes, where each fringe corresponds to a specific amount of deformation.

We used InSAR data from the Alaska Satellite Facility (ASF), which provides preprocessing and creation of short baseline subsets (SBAS) of InSAR data. SBAS uses a type of InSAR analysis to minimize atmospheric effects on ground deformation measurements. InSAR is sensitive to changes in the atmosphere leading to errors in the observed interferometric phase. Atmospheric errors are greater with longer baselines due to separation between the radar antennas during image acquisition. The SBAS approach selects short baselines to reduce the influence of atmospheric effects. We downloaded and processed SBAS subsets from ASF. We used Miami InSAR time-series software in Python (MintPy) to process the downloaded SBAS data (Yunjun et al., 2019). MintPy stacks multiple interferograms to average out atmospheric noise and extract ground deformation.

Evapotranspiration and Spring Discharge

OpenET

To derive estimates of crop and phreatophyte evaporation, we used data from OpenET (Melton et al., 2021). OpenET is a data product that combines multiple peer-reviewed models of evapotranspiration (ET) estimates into one platform. OpenET leverages Google Earth Engine to automate these models and run them for the western continental United States. They produce ET estimates based on measurements from different bands, including visible and thermal bands, of captures from Landsat satellites. Data are available at yearly, monthly, and daily timescales. Because the data are made using Landsat captures, the estimates are available as raster outputs, providing area-wide coverage, with a cell size (resolution) of 30 meters. Each Landsat satellite typically passes over a spot in Utah every 16 days. There are currently two active Landsat satellites, Landsat 8 and Landsat 9. Their paths are offset, so that image acquisition of a location occurs every eight days. However, if clouds cover the location of interest, evapotranspiration cannot be estimated with the image. To fill in gaps between acquisitions, OpenET scientists use GRIDMET (Abatzoglou, 2013), a gridded climate dataset that is based on meteorological station observations. Using meteorological parameters from GRIDMET, they produce values of reference evapotranspiration, which can be scaled and calibrated to the estimates of evapotranspiration from the satellite captures.

OpenET currently incorporates six peer-reviewed and established models for estimating evapotranspiration (Table 1), as well as an ensemble value that combines results from all of the models. Five of these models are based on full or simplified implementations of the surface energy balance (SEB) approach. The SEB approach uses energy accounting to estimate the amount of energy used during evaporation. The SIMs model (Table 1) uses additional crop type and surface reflectance information for its estimates (Melton et al., 2012; Pereira et al., 2020). Previous studies indicate that SSEBop (Senay et al., 2013a; Senay, 2018) and eeMETRIC (Allen et al., 2005; Allen et al., 2007; Allen et al., 2011) both perform well in Utah (Allen et al., 2022; Huntington et al., 2022). The Upper Colorado River Commission has selected eeMETRIC as its preferred model for representing the Upper Colorado River basin, including Utah. Because we can independently run SSEBop as a validation point for historical ET, we chose SSEBop as our preferred method in this study. OpenET currently recommends using their ensemble value, but whether or not the ensemble value is more accurate in Utah than SSEBop or eeMETRIC is currently not well defined.

By subtracting 90% of gridded monthly precipitation from monthly ET values, we can estimate the net ET (Chow, 1964; Stamm, 1967). In regions like Pahvant Valley, where ET generally exceeds precipitation, net ET is the amount of water evapotranspired beyond the amount made available by precipitation. This approach assumes that all soil-water exchanges occurred within a monthly timespan. When ET is in excess of precipitation, then an alternative source of water must be present, which could include applied irrigation water, shallow groundwater, stored soil water, or error from one of the input datasets.

Clear Lake

Spring flow at Clear Lake WMA has been measured by the DWR and DWRi since 1952 (Lynn Zubeck, personal communication, November 13, 2023; Appendix B). We obtained these data, reviewed them, and used linear regression and Mann-Kendall analysis to ascertain any significant trends

Table 1. *Models used by the OpenET group that are used in calculating the ensemble values.*

Model	Version	Model Name	Primary References
ALEXI/DisALEXI	0.0.32	Atmosphere-Land Exchange Inverse / Disaggregation of the Atmosphere-Land Exchange Inverse	Anderson et al., 2007; Anderson et al., 2018
eeMETRIC	0.20.26	Google Earth Engine implementation of the Mapping Evapotranspiration at high Resolution with Internalized Calibration model	Allen et al., 2005; Allen et al., 2007; Allen et al., 2011
geeSEBAL	0.2.2	Google Earth Engine implementation of the Surface Energy Balance Algorithm for Land	Bastiaanssen et al., 1998; Laipelt et al., 2021
PT-JPL	0.2.1	Priestley-Taylor Jet Propulsion Laboratory	Fisher et al., 2008
SSEBop	0.2.6	Operational Simplified Surface Energy Balance	Senay et al., 2013a; Senay et al., 2013b; Senay et al., 2018
SIMS	0.1.0	Satellite Irrigation Management Support	Melton et al., 2012; Pereira et al., 2020

in spring discharge over time. We visited the Parshall flume where flow into Clear Lake is measured, installed a temporary pressure transducer, and validated the estimated flow at the flume using a Hach FH950 portable current velocity meter. We also collected water quality, radiogenic isotope, and stable isotope samples for laboratory analysis. We met with Lynn Zubeck, the manager of the Clear Lake WMA, who provided us with valuable information related to the history and operation of the WMA.

Depth to water was measured and groundwater chemistry samples were collected from a monitoring well, named the Zubeck Well, drilled approximately 1.3 miles northwest of the Clear Lake WMA ranch house in 2012 (WIN 434316). The well was drilled to a depth of 1380 feet below ground surface (bgs) through unconsolidated Quaternary- to Tertiary-age clay and clayey-silt. The well was drilled as an exploratory borehole to assess the viability of a production well to supplement spring flows into Clear Lake, but was changed to a monitoring well when yields from the well were deemed insufficient for use within the WMA. The well was constructed using flush thread 2-inch schedule-80 PVC pipe to a depth of 530 feet bgs, with an 8-inch conductor casing left in place after drilling to total depth. We measured static water level in the well on each site visit and installed and collected periodic water level data from a dedicated In-Situ Rugged Troll 100 pressure transducer.

We also estimated ET from Clear Lake Spring using OpenET data. We split the area into the spring pool and the outflow area and calculated the yearly net ET of the two areas using values from OpenET. For net ET, we subtracted the yearly precipitation from the ET.

NDVI Change Over Time

To assess changes in greenness over time for the Pahvant area, we calculated the Normalized Difference Vegetation Index (NDVI) using Google Earth Engine for 1989 to 2021 (Gorelick et al., 2017). We used surface reflectance imagery from Landsat 5/6/7/8 Collection 1 and masked out clouds, cloud shadows, and snow if present. We used the following equation to calculate NDVI:

$$NDVI = \frac{(NIR - R)}{(NIR + R)} \quad (2)$$

with NIR representing the near infrared band and R representing the red band. We then analyzed this data two ways. First, we calculated the median NDVI values for July 15th to August 31st of each year for each agricultural field in our area of interest. Next, we analyzed changes over time per pixel by running a Mann-Kendall test for each pixel using code from the Google Earth Engine Developers Community page, with small adjustments to account for small slopes. We considered trends significant at a stricter $p<0.01$ because of the high quantity of pixels used for the test. We then examined the fields that had significant amounts of change over time.

Phreatophyte Evapotranspiration

A measurable component of groundwater discharge is evapotranspiration (ET) from native vegetation. We first used OpenET, ground elevation, and our potentiometric surface map to determine the areas of shallow groundwater and phreatophytes. We then used National Wetland Inventory wetland mapping and the Utah DWRe Water Related Land Use map data layer to identify areas of phreatophytes (Figure 4). Phreatophytes are plants that depend on supplemental water from groundwater sources. They are typically either deep rooted plants or groundwater-dependent wetland species. We compared the areas of shallow groundwater and phreatophytes to historical aerial and satellite imagery to see if these areas have consistently green vegetation or commonly have standing water.

Once we delineated the areas of shallow groundwater, we conducted zonal statistics. Using the OpenET application programming interface (API), we downloaded rasters of total yearly evapotranspiration and precipitation for calendar years 2016 to 2022. To get the volume of water evapotranspiring from a mapped polygon area, we multiplied the mean

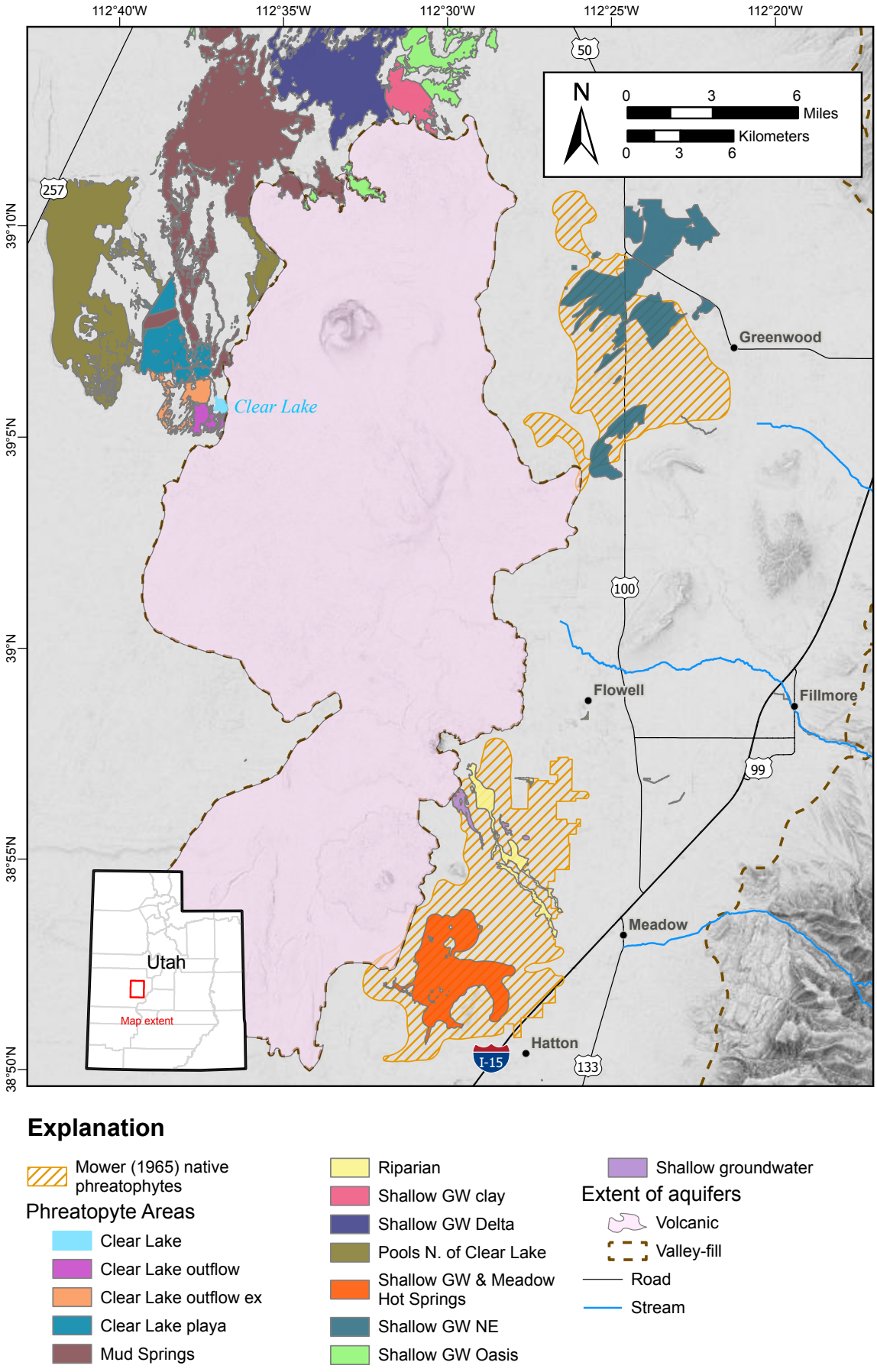

Figure 4. *Zones of phreatophytes—plants sustained by groundwater—and shallow groundwater delineated for OpenET calculations.*

evapotranspiration value in feet per year by the area of the polygon in acres, which produced a volume estimate of acre-feet per year. We used area measurements from polygons projected into the Albers equal area geographical projection, to ensure that each polygon area was accurate. OpenET reports the mean absolute error of their data product over wetlands to be 33.0% and their root mean square error to be 40.2% (Melton et al., 2021). To estimate the total amount of groundwater evaporating from an area, we use net ET, which is ET minus precipitation.

Well Depletions

Agricultural Pumping

Well withdrawals (depletions) were estimated using several methods to maximize data availability. These methods are 1) direct read of in situ totalizing flow meters, 2) recording seasonal power demand, 3) ultrasonic flow meter direct measurement, and 4) using vibration hour meters. Depletion calculations for wells equipped with in situ totalizers were accomplished by recording the number of gallons pumped over the course of the irrigation season or by recording pumping rates during the irrigation season and hours of operations recorded on the vibration hour meter.

High volume groundwater pumping is typically done using electric motors. On irrigation wells, the motor typically sits on top of the wellhead and drives a rotating shaft that turns impellers. The impellers pump water from the well to the surface via a discharge pipe. These motors range in power from ~25 to 250 horsepower, and typically have a connection voltage of 460 volts.

Some well operators choose to equip their well discharge pipe with a totalizing flow meter, which allows for the measurement of well water pumping over time. However, more than half of the observed agricultural wells were not equipped with flow meters. If a well does not have a flow meter, an alternative method is used to estimate discharge, such as using on-pipe flow meters or making estimates based on power consumption.

A non-invasive ultrasonic on-pipe flowmeter can be attached to the discharge pipe to measure the flow rate of water coming out of the well. However, for the ultrasonic flow meter to work correctly, the well discharge pipe must have adequate straight length (runout) to allow for somewhat laminar flow, and the inside and outside pipe walls must be relatively smooth to properly transmit ultrasonic signals.

To estimate discharge using power consumption, the rate of consumption is acquired either by obtaining historical power records or by directly reading power meters located in the field. Power meter values are recorded in early spring, prior to irrigation season, then recorded again in late fall after irrigation season has concluded. Horsepower determines the amount of power needed. Pumping time, power, energy, and rate are all calculated to estimate total pumping from wells (Hurr and Litke, 1989).

Water Use Calculations

Monte Carlo Model: Using data from the well depletion estimates and Monte Carlo simulations, we estimated the distribution of total pumping for the region for calendar year 2022. The Monte Carlo model iteratively multiplies randomly selected values from the fitted distributions of pumping duration and the rates of pumping to produce a modeled distribution of total agricultural groundwater pumping. Monte Carlo models are useful for estimating groundwater pumping because they can handle uncertainty and variability in complex systems. Groundwater systems are influenced by numerous uncertain factors, such as aquifer properties, pumping durations, and pumping rates, all of which can vary widely. Monte Carlo models manage these uncertainties by running multiple simulations with varying inputs drawn from probability distributions, thus generating a range of possible outcomes and helping to understand the variability in groundwater pumping estimates. Unlike deterministic models that provide a single outcome, Monte Carlo simulations produce a distribution of possible outcomes, enabling probabilistic analysis. Additionally, Monte Carlo models are valuable for sensitivity analysis, identifying which variables have the most significant impact on groundwater pumping estimates. This analysis helps focus monitoring and data collection efforts on the most influential factors and improves model accuracy by refining critical inputs.

We compiled all available irrigation pumping rate and pumping duration data and fit distributions to it. We then used iterative random samples from those distributions to calculate the distribution of total irrigation pumping. For irrigation pumping rate data, we combined our field measurements with those reported by operators and water right proof records (where a flow meter was used). For duration, we combined measurements recorded by vibration sensors with calculations of duration based on total measured flow and flow rates of the wells. We then fit distribution curves to each dataset and randomly selected 5000 samples from each distribution, multiplying the randomly selected duration by the randomly selected rate to produce a distribution of total irrigation pumping.

We used a similar approach for domestic and stock well discharge. We applied realistic distributions of pumping rates for domestic wells and stock wells. We multiplied the number of total wells in the valley by samples from the pumping rate distributions. Domestic wells that watered turf (less than 50 gpm) and stock areas (ranches and similar operations) were lumped into the domestic well count. Wells that solely watered stock areas were counted as stock wells. Municipalities report water use to the DWRi. We used this data to determine municipal water use.

Consumptive Use: We compared the pumping distribution with consumptive use rates, which were calculated using OpenET and Google Earth Engine (GEE). Using the water-related-land-use (WRLU) GIS file developed by the DWRe and the place-of-use GIS file developed by the DWRi, we attributed each field with respective potential water sources, irrigation type, and irrigation region. We downloaded monthly raster OpenET SSEBop evapotranspiration data aggregated by water year (October 1 to September 30) using GEE. We calculated 90% of GRIDMET precipitation aggregated over the same period to get effective precipitation (Chow, 1964; Stamm, 1967), then subtracted it from actual ET to calculate the net ET of the agricultural fields. The net ET is the water that should be evapotranspiring primarily from applied irrigation water. We used the water year to account for water carried forward from antecedent soil moisture and snowmelt. Groundwater pumping should equal the amount of net ET plus the amount of applied water infiltration minus the estimated surface water diverted for irrigation. We segmented the irrigated area of Pahvant Valley into 24 different areas based on water use, canal distribution, and designated groundwater districts. We used these areas for comparison because field shapes and distribution have changed over time. For investigating long-term changes, we assumed that all of areas 20, 17, 11, and 9 (Figure 3) are irrigated by surface water and all other areas are irrigated with groundwater.

Groundwater pumping should equal the amount of consumptive use plus the amount of applied water infiltration minus the estimated surface water applied for irrigation.

$$Q_{gw} = (ET - P * 0.9) + I_{irr} - S_{irr} \quad (3)$$

$$I_{irr} = I_{eff} \times (ET - P) \quad (4)$$

where:

Q_{gw} = groundwater pumping
ET = evapotranspiration
P = precipitation
I_{irr} = infiltration
I_{eff} = infiltration percentage
S_{irr} = irrigation water from surface sources

Infiltration is estimated by multiplying the consumptive use (ET - P) by a percentage of expected infiltration. For a well with a known pumping rate, infiltration percentage is pumping minus net evapotranspiration over net evapotranspiration ($I_{eff} = [Q_{gw} - ET]/ET$). Infiltration percentage can vary from negative values to greater than one. Negative values indicate that more water is evaporating than being applied, meaning that the crops get their water from another source, typically shallow groundwater or antecedent soil moisture. If the value is greater than one, then more water is infiltrating than being consumed (evapotranspired) by the crops. For our study, we assumed that infiltration percentage has a normal distribution, with an average value of 40% and a standard deviation of 20%. This assumption is based on observed distributions in fields in Castledale, Utah, as well as measurements of infiltration in similar agricultural settings. The 95% confidence interval for this distribution is 0% to 100%. OpenET reports mean absolute error for their models over croplands as 16.6% and root mean square error as 21.3% (Melton et al., 2021). We multiplied 1000 randomly selected values from the infiltration percentage distribution with the estimate of consumptive use for the valley, added the consumptive use value, and then subtracted the estimated surface irrigation. This calculation provided an independent check of our pumping data.

Changes in Water Use

Using SSEBop (Senay, 2018; Senay et al., 2020) scripts made available by Open-ET (https://github.com/Open-ET/openet-ssebop), we estimated monthly ET for the agricultural area of Pahvant Valley from 2000 to 2021, generating rasters that cover the agricultural parts of the study area. We examined how ET changed over time for each active irrigation polygon in the WRLU 2021 file. We calculated the agricultural season ET by summing the monthly rasters from April to October, the months when irrigation is typically occurring. We subtracted the year 2000 total from the year 2021 total to estimate ET changes from 2000 to 2021. We summarized the raster using polygon areas that represent active irrigation and agriculture in the valley and the water rights groundwater districts. This area encompasses both current and past irrigated areas and does not rely on the exact WRLU estimates for comparison.

Chemistry

Sampling

We collected and compiled samples for groundwater chemistry analysis to determine the connections between precipitation, streams, groundwater, and the valley-fill and volcanic aquifers of the valley. Samples were collected for major ion and trace element chemistry, stable isotopes deuterium (^{2}H) and oxygen-18 (^{18}O), and radioactive isotopes carbon-14 and tritium (^{3}H). We compiled historical water quality data from multiple agencies, including the Utah Department of Food and Agriculture, the Utah Department of Environmental Quality, the USGS, and the United States Department of Agriculture. To enhance data clarity, we reviewed and edited the information to ensure adequate geospatial coverage and eliminated redundancies. The sampling effort covered four major streams, two precipitation sites, two springs, and three wells distributed across Pahvant Valley to address geographical gaps that had insufficient data for thorough analysis.

Our precipitation sampling strategy involved monthly collections during the summer and fall and quarterly collections during the winter and spring when the sites were accessible. The two sample sites represent the two primary aquifers in the basin—the valley-fill and volcanic aquifers (Figure 5). Precipitation samplers consisted of a 2.5-gallon HDPE carboy, containing approximately 16 ounces of mineral oil to prevent evaporation, connected to a funnel and enclosed within a 30-gallon garbage can with an inverted lid to aid in the collection of rain and snowmelt (Ingraham and Taylor, 1991; Scholl et al., 1996). When present snowmelt was also collected at the two precipitation sites. Precipitation and snow samples were collected between May 2022 and October 2023, and a total of 10 samples were collected.

We collected stream samples from four sites in the Pahvant Valley catchment, including Corn Creek, Meadow Creek, Chalk Creek, and Pioneer Creek. We also sampled four wells and three springs from 2022 to 2023. Spring samples were collected at the point of issuance, and stream samples were collected from clear flowing water (i.e., not from eddies or stagnant pools).

Samples for major ion concentration analyses were collected in clean bottles supplied by the laboratory; those for anions and general chemistry were not filtered, and those for cations were filtered using a peristaltic pump and 0.45 µm filters. Samples for stable isotope composition analysis were

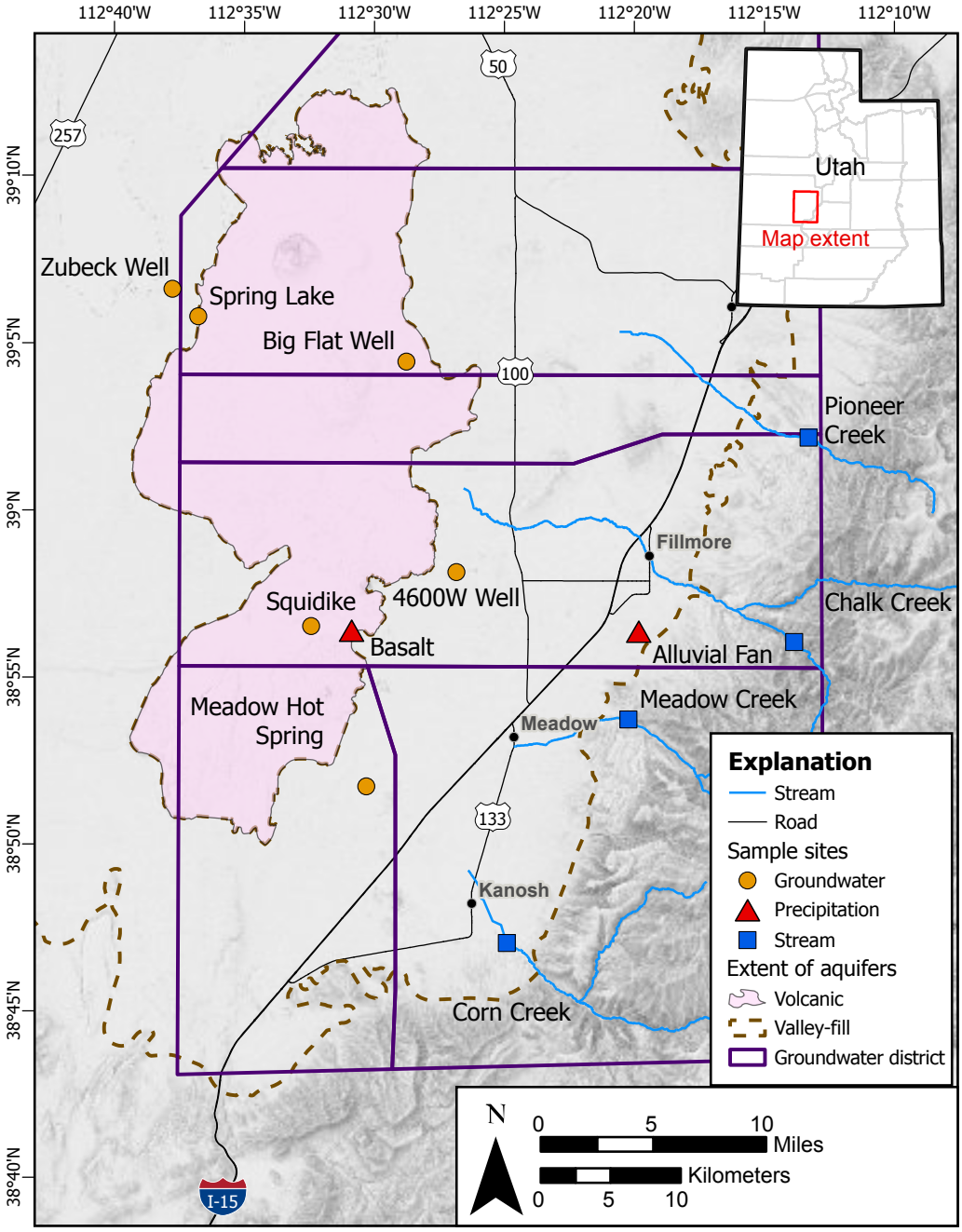

Figure 5. *Location of water chemistry samples collected during this study.*

filtered using 0.45 µm disc filters attached to a syringe, and then placed into 10-ml crimp-cap and/or snap-lid vials leaving no head space. Samples for radioactive isotope analyses were collected in 1 liter amber plastic bottles, rinsed for several volumes by the flowing sample water and sealed with minimal headspace. Samples for major solute concentrations were submitted to the Utah Public Health Laboratory; samples for stable isotope compositions were submitted to the University of Utah Department of Geology and Geophysics Stable Isotope Ratio Facility for Environmental Research (SIRFER) laboratory; samples for tritium analyses were submitted to the University of Utah Department of Geology and Geophysics Dissolved and Noble Gas Laboratory; and samples for carbon-14 analysis were submitted to the University of Georgia Accelerator Mass Spectrometry (AMS) facility.

Age Dating

Tritium is a radioactive isotope of hydrogen with two neutrons and one proton in its nucleus and is naturally occurring in the upper atmosphere. In a laboratory setting, the concentration of tritium (^3H) in water samples is measured in Tritium Units (TU), where one TU corresponds to one tritium atom per 10^{18} hydrogen atoms. Typically, the natural background level of tritium in the atmosphere is around 5-10 TU, although this can vary due to factors like nuclear testing or releases from nuclear facilities (Clark and Fritz, 1997). During the 1950s and 1960s, thermonuclear bomb testing increased the concentration of atmospheric tritium concentrations to nearly 4000 TU in the northern hemisphere. Tritium has a half-life of 12.4 years and decays into a daughter isotope of helium-3. Tritium concentrations were measured using the tritium-^3He ingrowth method (Solomon and Cook, 2000).

Carbon-14 (^{14}C) is a naturally occurring radioactive isotope of carbon that has a half-life of about 5730 years, which allows the determination of groundwater residence times of up to 40,000 years (Kalin, 2000). Carbon-14 data are expressed as percent modern carbon (pmC) relative to A.D. 1950 levels, based on the National Bureau of Standards oxalic acid standard. Carbon-13 (^{13}C) is a naturally occurring stable isotope of carbon that is used to evaluate chemical reactions involving carbon (Clark and Fritz, 1997). Carbon-13 is expressed as an isotopic ratio ($^{13}C/^{12}C$), reported as delta (δ) values in units of parts per thousand (per mill or ‰) relative to the Vienna Peedee Belemnite (VPDB) standard. The $\delta^{13}C$ ratio in groundwater depends upon numerous factors, which include the type of vegetation in the recharge area, whether carbonate (and the $\delta^{13}C$ compositions of those minerals) is dissolved or precipitated during recharge, and whether the system is open or closed.

Carbon-14 is produced naturally in the upper atmosphere by a cosmic ray reaction with nitrogen. Atmospheric testing of nuclear weapons also produced elevated ^{14}C, so in some instances values greater than 100 pmC can occur in groundwater. Carbon-14 is not part of the water molecule, so ^{14}C activities are affected by chemical reactions between the aquifer material and the dissolved constituents in the water. Chemical reactions can either add or remove carbon; therefore, knowledge of chemical reactions that occur during recharge and transport through the aquifer are necessary for estimating the initial activity (A_o) of ^{14}C. Age calculations require estimates of some chemical parameters during recharge and model calculations of reactions during groundwater transport. A_o is the initial, non-decayed ^{14}C composition of the groundwater and must be determined to calculate ^{14}C ages. In the absence of subsurface reactions, A_o is assumed to be 100 pmC. However, this assumption is rarely valid due to the common presence of carbonate minerals and elevated CO_2 concentrations in the soil. Many models account for geochemical reactions and gas exchanges to determine A_o (Ingerson and Pearson, 1964; Mook, 1972; Tamers, 1975; Fontes and Garnier, 1979; Han and Plummer, 2013). We calculated A_o using the revised Fontes and Garnier model of Han and Plummer (2013), which models isotopic exchange controlled by soil gas CO_2 in the unsaturated zone and carbonate minerals in the saturated zone. We assumed end members of radiocarbon activity and $\delta^{13}C$ ratios to be 100 pmC and -21.8 ± 1.4‰, respectively for soil gas CO_2 (Hart, 2009), and 0 pmC and 0‰ for carbonate minerals, respectively. Groundwater age is calculated by:

$$t = \tau \ln (A_o/A) \quad (5)$$

where:

- t = groundwater age (years)
- τ = 8267, a constant equal to ^{14}C half-life (5730 years) ÷ ln 2
- A_o = calculated initial ^{14}C activity (pmC)
- A = measured ^{14}C activity (pmC)

Clustering Analysis

We used k-means clustering analysis and multivariate cluster analysis—both statistical techniques used to identify groups, or clusters, of similar objects or cases based on multiple variables simultaneously—to discriminate between how many unique sources of groundwater may be present in Pahvant Valley. For the analysis, we used sites which contained chemistry laboratory analysis for bicarbonate, calcium, chloride, magnesium, potassium, sodium, specific conductance, and sulfate. We used the k-means elbow method as an initial assessment of the number of potential clusters.

Next, we leveraged the multivariate cluster analysis tool in ESRI ArcGIS Pro to map these clusters and determine if they are spatially viable. The resultant cluster analysis was used to map regions where similarities in water chemistry were present, helping to characterize the variations in groundwater chemistry, its locations, and identify the

number of clusters, or for the use of this study, the number of potential groundwater sources contributing to the aquifers within Pahvant Valley.

To assess the groundwater quality laboratory results and water quality parameters within each groundwater district we utilized a geospatial statistical tool built into ESRI ArcGIS Pro called *Summarize Within* that tabulates all sampling points and their associated data within each respective polygon. We then used the *Summarize Within* tool to calculate statistics of the water quality sampling points located within each groundwater district.

Flow Measurements of Surface Water in Pahvant Valley

Surface water flows into the valley primarily from watersheds within the Pahvant Range and Canyon Mountains. Chalk Creek, Meadow Creek, Corn Creek, and Pioneer Creek (Figure 6) have some of the most significant discharges from the Pahvant Range, but all have either no or limited periods of record documenting accurate stream flow measurements. The principal streams contributing surface water inflow into Pahvant Valley are Chalk Creek, Corn Creek, and Meadow Creek. These streams account for approximately 46% of total surface water contribution to the valley. Chalk Creek (stream gage no. 10232500), Meadow Creek (stream gage no. 10233000), and Corn Creek (stream gage no. 10233500) were measured by the USGS starting in the mid-1940s and ending in the mid-1970s (Table 2). Chalk Creek Irrigation Company provided us with records of peak flows, approximate dates, and estimated durations. Their records indicate "Special highs" which are flows that exceed 35 cubic feet per second (cfs) and "General highs," which are flows that go above 80 cfs. At the time of this study Corn Creek Irrigation Company, Meadow Creek Irrigation and Canal Company, and Holden Irrigation Company did not have available records of streamflow captured by their diversions and had not reported diversions to the DWRi.

Due to the paucity of current streamflow data, we leveraged the USGS StreamStats web product to model flows for all streams draining into Pahvant Valley, including numerous smaller seasonal and ephemeral streams that contribute lesser amounts of individual surface water flows. These smaller streams are also ungaged with no historical records available. To estimate the contribution of these smaller streams, we used StreamStats to perform volumetric and statistical analysis for these watersheds. StreamStats uses regional regression equations and watershed parameters to estimate flow statistics of a given point along a stream (Ries et al., 2017). The StreamStats model can be run through a browser on any internet-connected computer, and the USGS has recently added web-service capabilities for scripted modeling. We ran the StreamStats model for 21 watersheds along the western slope of the Pahvant Range (Figure 6).

RESULTS AND DISCUSSION

Change in Storage

Introduction

Parameters to estimate changes in groundwater storage include change in groundwater level, extent of the aquifer(s), and aquifer storativity. The aquifer storativity is a combination of specific storage and specific yield. In confined aquifers, specific yield is negligible and specific storage is the defining measure of aquifer storage. Specific storage typically varies from 1 x 10^{-6} (1/ft) to 1 x 10^{-2} (1/ft). Specific yield is generally orders of magnitude greater than specific storage, ranging from 0.01 to 0.5 and, therefore, typically defines the storage of unconfined aquifers (Johnson, 1967; Lv et al., 2021). Because the storage properties vary so much, we have to discern which parts of the aquifer are confined and unconfined and determine how those areas change with changing groundwater levels.

Water Level Change and Potentiometric Map

Groundwater movement across an interconnected aquifer system is controlled by relative head conditions that can be visualized using a potentiometric map. We generated a potentiometric surface map using the 120 measurements taken during the spring of 2022 UGS and USGS groundwater level campaigns (Figure 7).

For this potentiometric surface, we assumed that groundwater is largely interconnected across the near-surface aquifers (including the volcanic, Oak City Formation, and the unconsolidated valley-fill aquifers) (Figure 7). Wells are generally distributed unevenly throughout the valley and are grouped according to population density and agricultural land use. Along the western slope of the Pahvant Range, groundwater elevations were measured within the unconfined valley-fill aquifer, which is well connected. Moving westward into the valley floor, groundwater elevations were measured from a variety of unconfined, confined, and highly fractured volcanic aquifers. As such, potentiometric contours are generalized in areas of sparse data or hydrogeologic uncertainty. Error in the potentiometric surface map is driven by data density and areas along the axis of Pahvant Valley where numerous measurements have an assumed error of less than 25 feet. Areas with few direct measurements, particularly areas of upland bedrock, could have error up to 100 feet or greater.

Comparison Between Field Campaigns: The maximum groundwater level decline observed from spring 1986 to spring 2022 was in the eastern part of the study area, where groundwater levels in the McCornick District had the most decline. The maximum observed groundwater decline from 1986 to 2022 was 163 feet in USGS monitoring well site no.

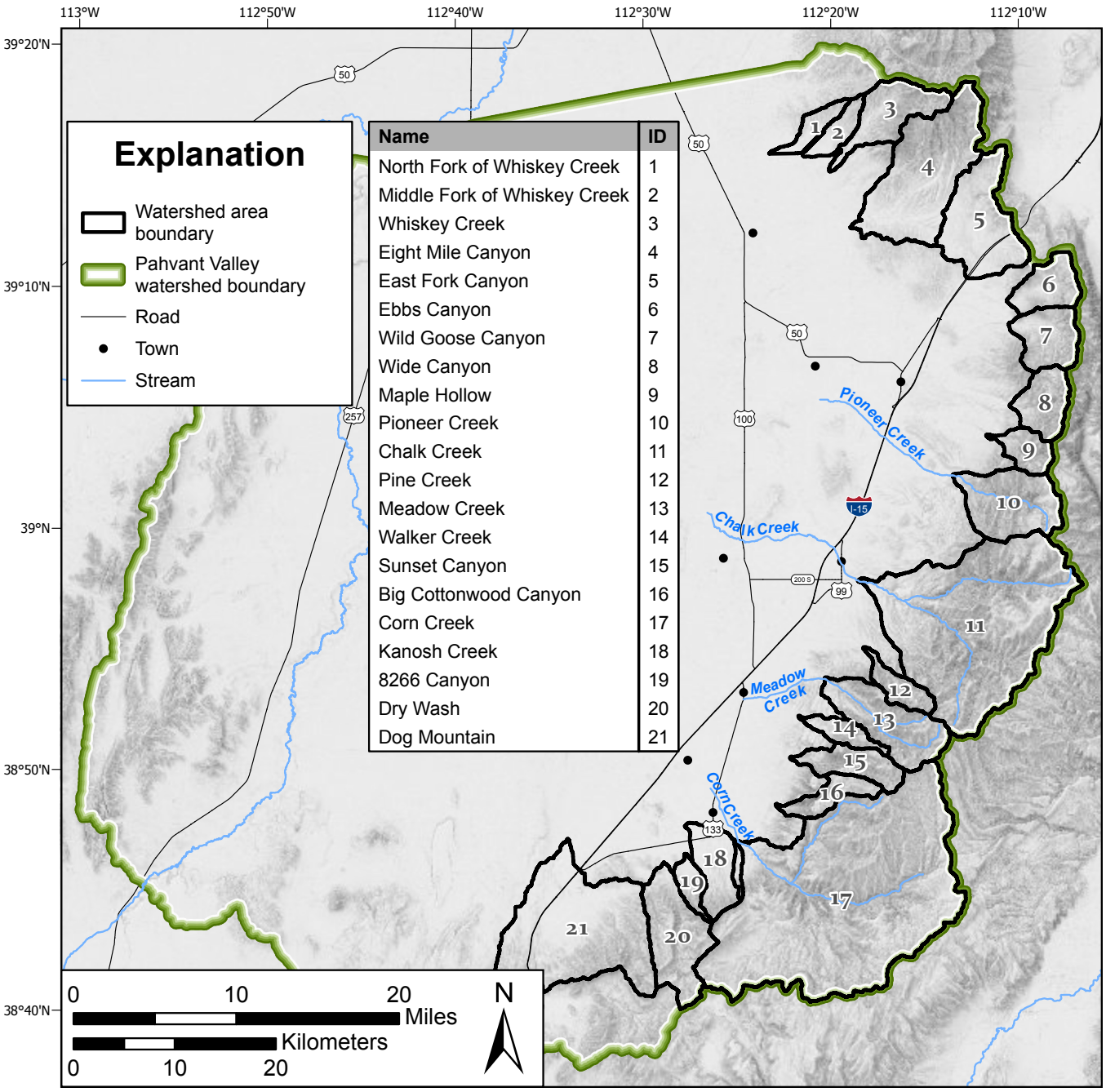

Figure 6. *Significant watersheds of the Canyon Mountains and Pahvant Range that contribute surface water to Pahvant Valley (Hydrologic Unit Code [HUC] 16030005).*

Table 2. *Flow statistics from existing USGS streamflow measurements.*

			Flow Statistics by Water Year					Daily Flow Statistics							
Creek Name	USGS ID	Period of Record	Avg (ac-ft)	Min (ac-ft)	Min Yr	Max (ac-ft)	Max Yr	1st Peak flow	Last Peak flow	Avg. (cfs)	Med. (cfs)	SD (cfs)	Max (cfs)	Max Date	Avg. Base (cfs)
Corn	10233500	8/1/1965–9/29/1975	12,877	4778	1972	26,676	1973	3/28	5/23	17.6	7.9	28.6	317	4/29/1973	7
Meadow	10233000	8/1/1965–9/29/1975	4636	2228	1972	8418	1973	4/2	5/22	6.9	2.9	10.5	117	5/13/1973	1
Chalk	10232500	3/1/1944–9/29/1971	21,969	9274	1959	44,184	1952	4/27	6/3	31.4	13	48.3	477	5/4/1952	10

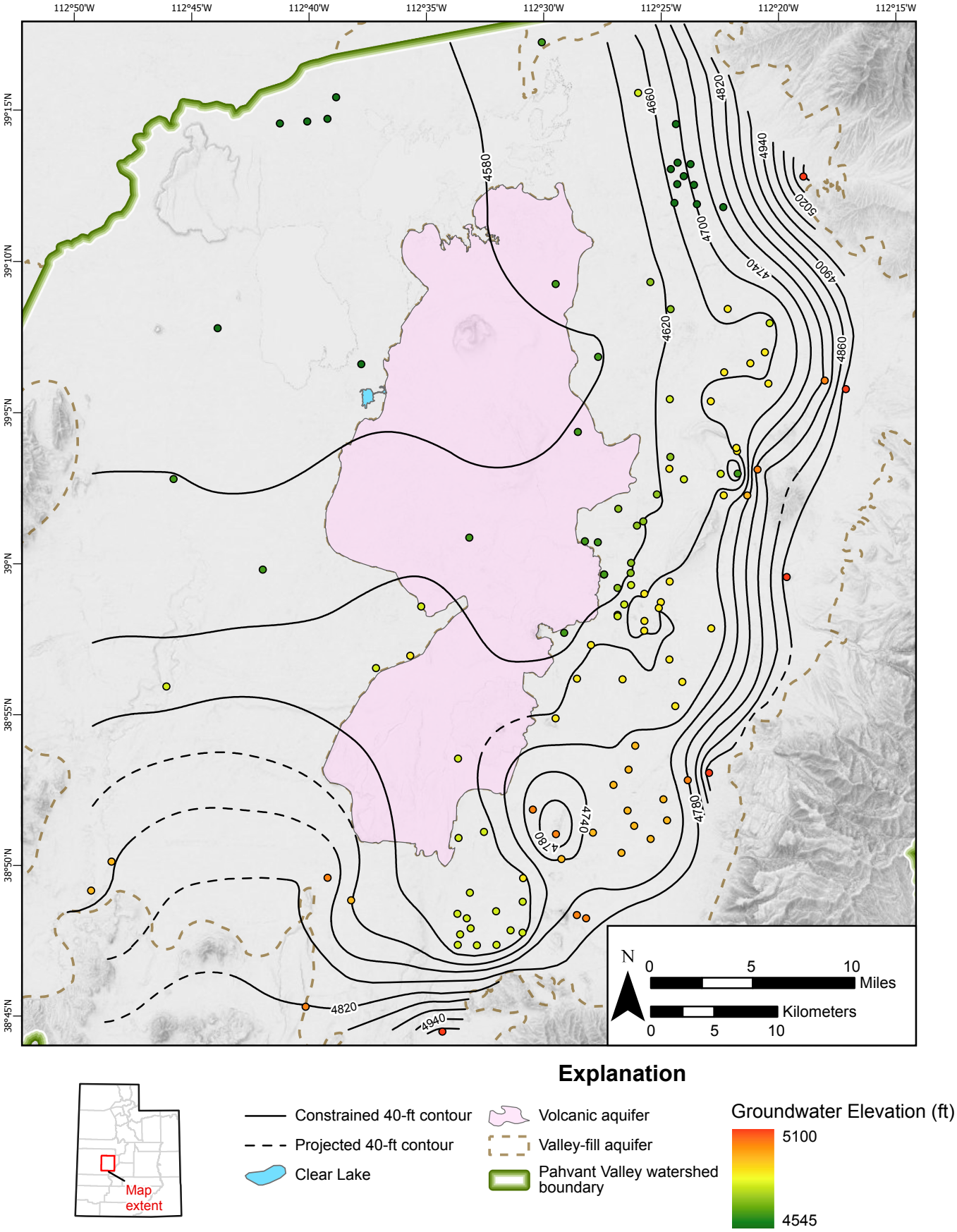

Figure 7. *Potentiometric surface map of Pahvant Valley showing 40-foot contour intervals, and individual water level measurement locations.*

391313112234201 located in McCornick. Non-agricultural areas to the west of the volcanic aquifer and in the foothills of the mountains to the east had little to no change in groundwater elevations, though some areas in the southwest part of the study area had a slight (<10 ft) increase in groundwater level (Figure 8). Where available, we interpolated groundwater level change measured in individual wells instead of comparing two potentiometric surface maps. This method reduces errors introduced from differences in elevation measurement and projection.

Our results indicate that discontinued seepage from the Central Utah Canal reduced groundwater recharge, contributing to groundwater elevations declines of 1 foot per year on average. Groundwater levels in USGS well site no. 391522112253401 (Figure 9) is an example of this documented decline.

USGS well site no. 385844112245801 which has the longest measurement record in the study area (1929 to present) shows a steady rate of decline over the period of measure (0.92 ft/yr), and went dry during the study. In response to

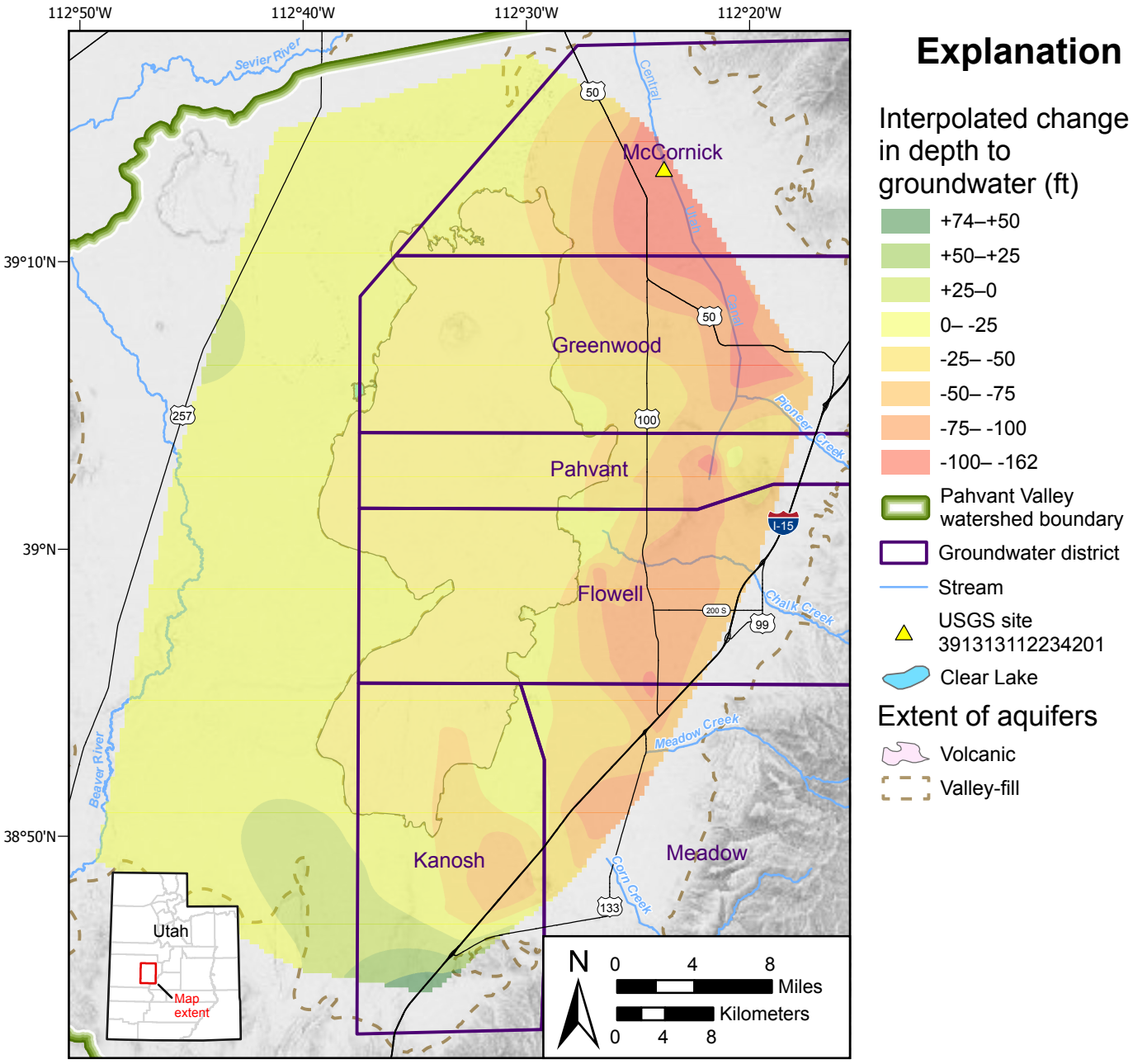

Figure 8. *Interpolated groundwater level changes recorded in the Pahvant region from 1986 to 2022. Regions in red, orange, and yellow depict declines in groundwater elevations since the mid 1980s, whereas areas shaded in light green to dark green had increases in groundwater elevations.*

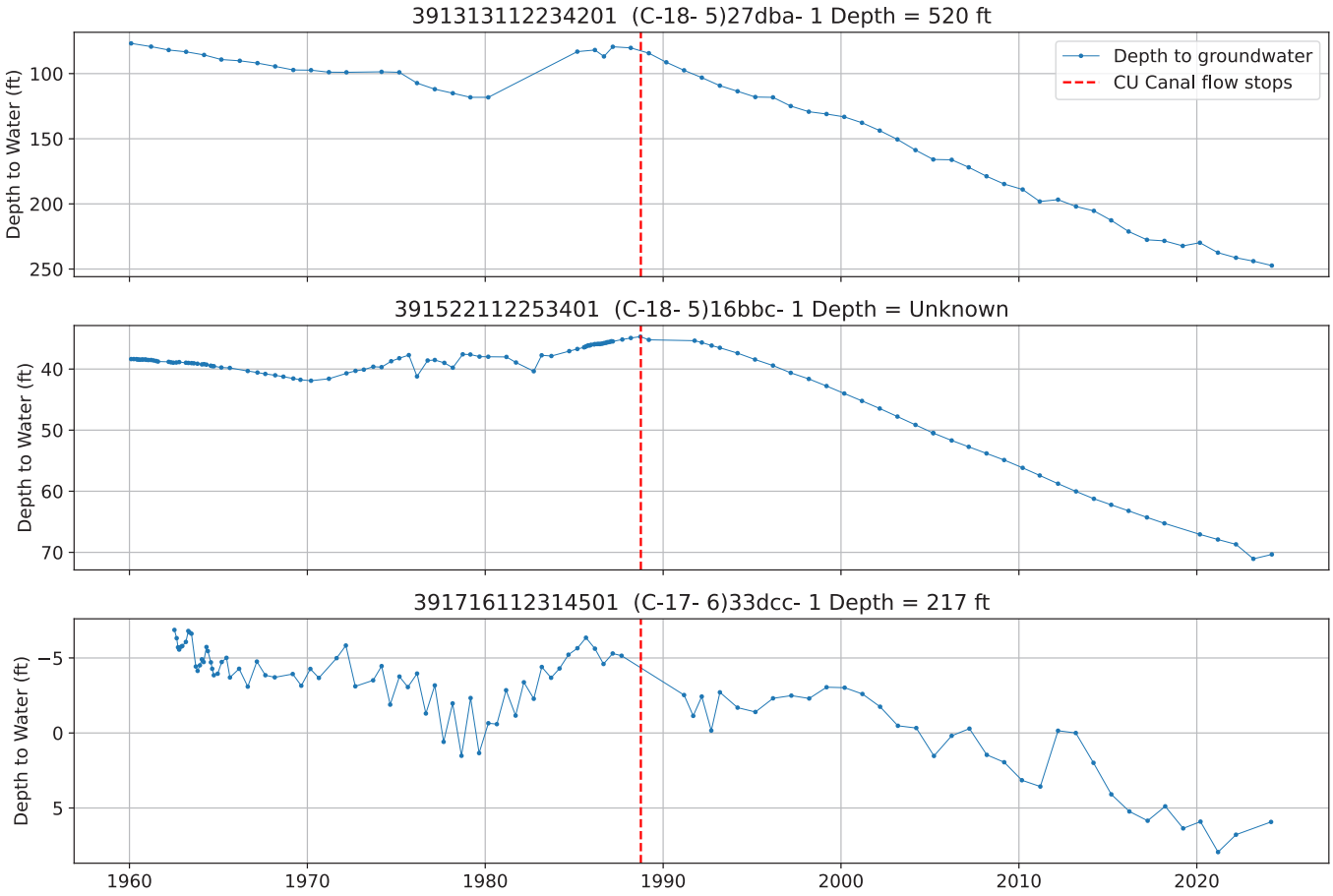

Figure 9. *Hydrographs showing consistent groundwater elevation declines following the cessation of water delivery by the Central Utah Canal.*

the wetter than average conditions in the 2023 water year, water level in the well rose more than 5 feet, and may have additional increases in response to that year, but overall, the groundwater level is declining.

We documented basin-wide changes in groundwater levels (Figures 8 and 10). The largest declines in groundwater elevation were between 150 to 160 feet and coincided with wells located near the now decommissioned Central Utah Canal. The mean decline in groundwater elevation measured throughout the study area was 26 feet. The southernmost well shown on Figure 8, well (C-24- 6) 7bad- 1, recorded an increase of 79 feet; this well appears to be an outlier relative to all the other measured wells, and these observed changes may be due to measurement error, or changes in the well since the last measurement occurred.

Year-to-Year Comparison: Year-to-year comparisons using gap-filled USGS (2024) data resulted in similar change observations as observed in the 1986 to 2022 comparison. For this comparison, we summarized water-level changes using zonal statistics. Based on year-to-year analyses, average regional groundwater levels aligned with the 1986 to 2022 groundwater level changes. Peak groundwater levels occurred in 1985 for Flowell and Pahvant, 1987 for McCornick, Kanosh, and Meadow, and 1989 for Greenwood. All average groundwater levels exhibited generally linear downward trends from 1900 to present, with small spikes during the higher water years (1999, 2011, 2019). McCornick had the most rapid declines in groundwater of about 2 feet per year. The next highest average rate of decline is 0.8 feet per year in Meadow. The average total groundwater level decline in McCornick was 74 feet.

Hydrostratigraphy and Lithologic Profiles

The Tertiary Oak City Formation is more prevalent than expected in the Greenwood groundwater district (Figures 11 and 12; cross-section A-A'). The Oak City Formation outcrops at the surface near the mountains and gradually deepens beneath alluvial deposits to the west. Unlike many Basin and Range valleys in Utah, there are no valley-bounding normal faults on the eastern edge of Pahvant Valley, limiting valley-fill basin thickness in this area. Valley-fill sediments are as deep as 300 feet in the McCornick area. The volcanic aquifer is not present in the well logs we examined in the Greenwood groundwater district. Several layers in well logs were identified as the Oak City Formation because they had clay and fine-grained materials, which could be ash layers or finer depositional sequences in this formation.

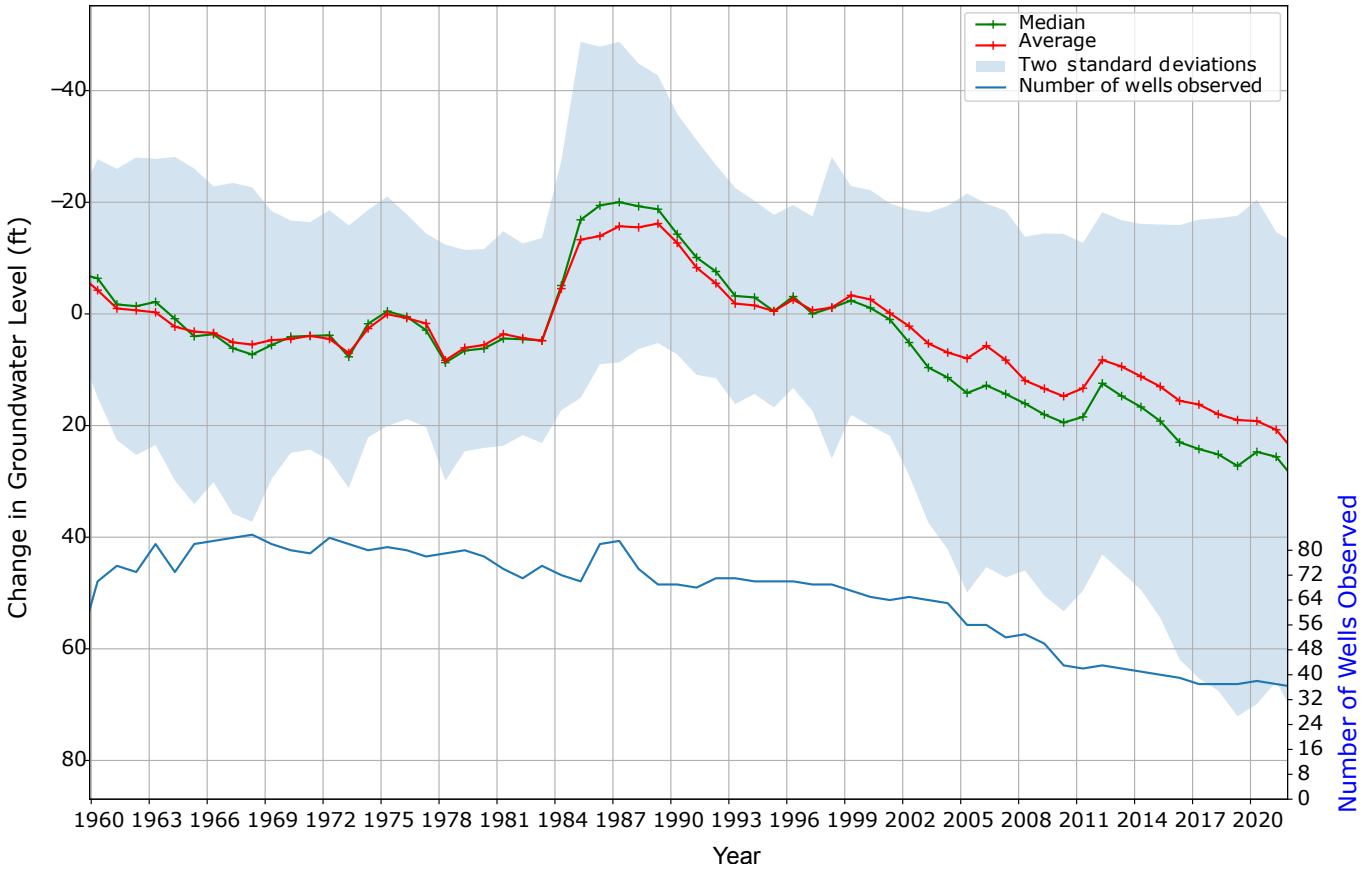

Figure 10. *Average groundwater level changes over time for Pahvant Valley unconsolidated valley fill. Source data from wells monitored by the USGS (U.S. Geological Survey, 2024).*

The Flowell and Pahvant groundwater districts cross-section (Figures 11 and 12; cross-section B-B') reveals several key features significant to the region. The section shows undifferentiated valley-fill deposits, which are typical of alluvial and fluvial sediments that have accumulated in the valley. The Oak City Formation is present, though there are uncertainties due to paleotopography, and the exact boundaries or characteristics of this formation are not well-defined in this area. There is a notable connection between the valley-fill aquifer and the volcanic aquifer in this cross section.

The southernmost cross section, in the Meadow and Kanosh groundwater districts, shows a combination of Oak City Formation and the volcanic aquifer, with a relatively thin (~100 ft thick) veneer of primarily unconfined valley-fill material on top of the more consolidated units (Figures 11 and 12; cross-section C-C'). The basalt extends far to the southeast in this region, which is supported by well logs, magnetic anomaly, and gravity surveys (Hardwick, 2013).

Aquifer Areas: The area of pressurized confinement changes with the potentiometric surface. As groundwater levels decline, the potentiometric surface drops below the top of the confining layers and the source of groundwater storage transitions from the specific storage to specific yield. While the clay confining layer will still be present, the groundwater level will be below the level of that layer, causing the aquifer to be considered "unconfined" for the sake of storage calculations. Mapping of recharge and discharge areas primarily relies on the distribution of thick clay layers and the hydrologic gradient. Both of these factors can remain relatively stable as groundwater levels drop, and a significant drop could be required to change the recharge and discharge conditions. Recharge and discharge areas in the region have not changed significantly since Snyder (1998) mapped them. The areas of exposed volcanic rock are recharge areas. North, east, and west of the volcanic aquifer is a discharge area that includes Clear Lake and the surrounding region. Secondary recharge occurs around Meadow and west of Fillmore and McCornick. Despite recharge and discharge areas not changing significantly, the area of confinement has changed (Figure 13), which modifies the calculation of aquifer storage over time.

Interpretation: In alluvial sediments like those in Pahvant Valley, where deposition has been uneven and lenticular, extrapolating individual layers between well logs is problematic. Nevertheless, each well log in these profiles reveals zones where coarse sediments are predominant.

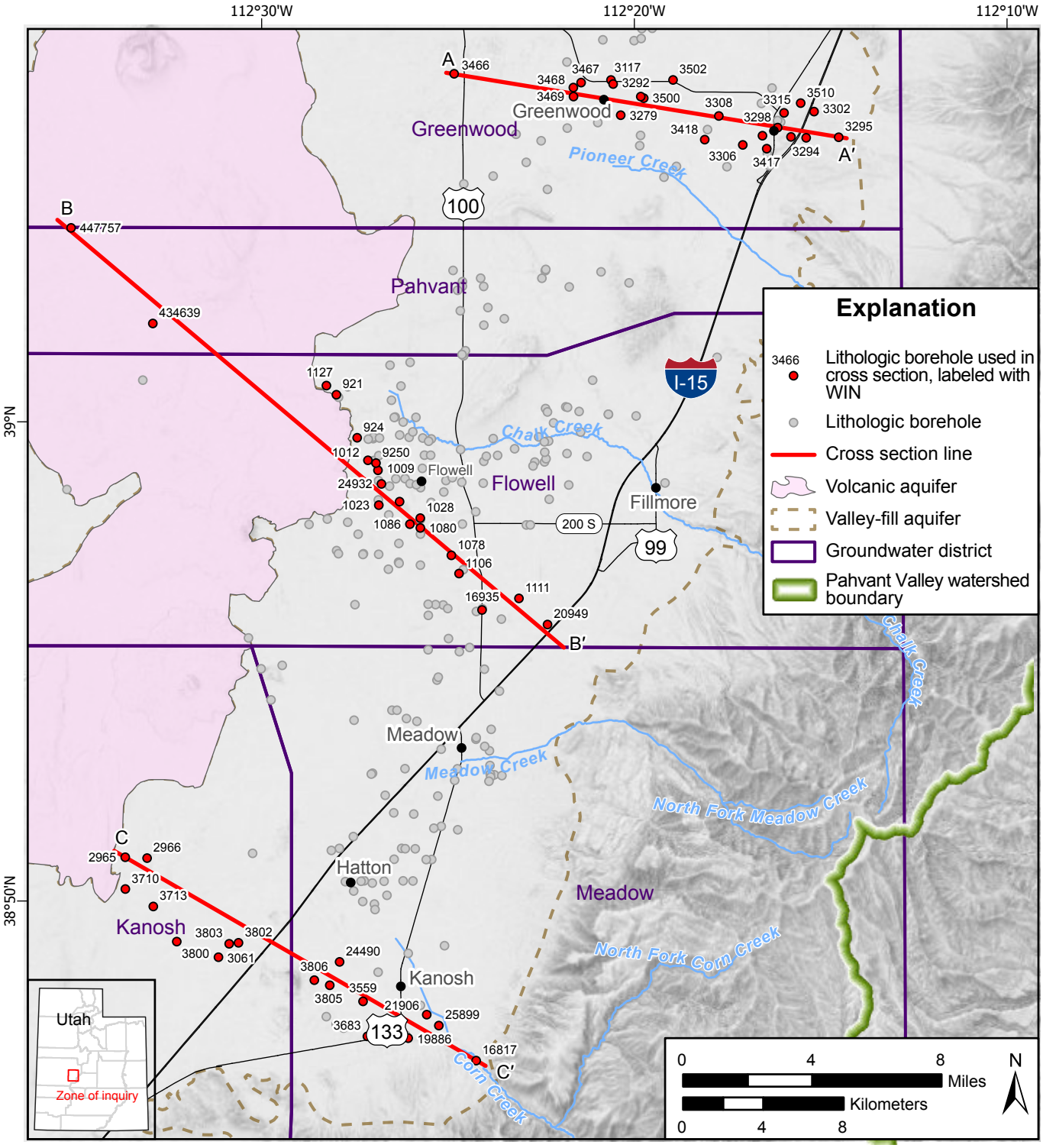

Figure 11. *Location of cross sections and lithologic boreholes shown on Figure 12. Lithologic boreholes are labeled with WIN.*

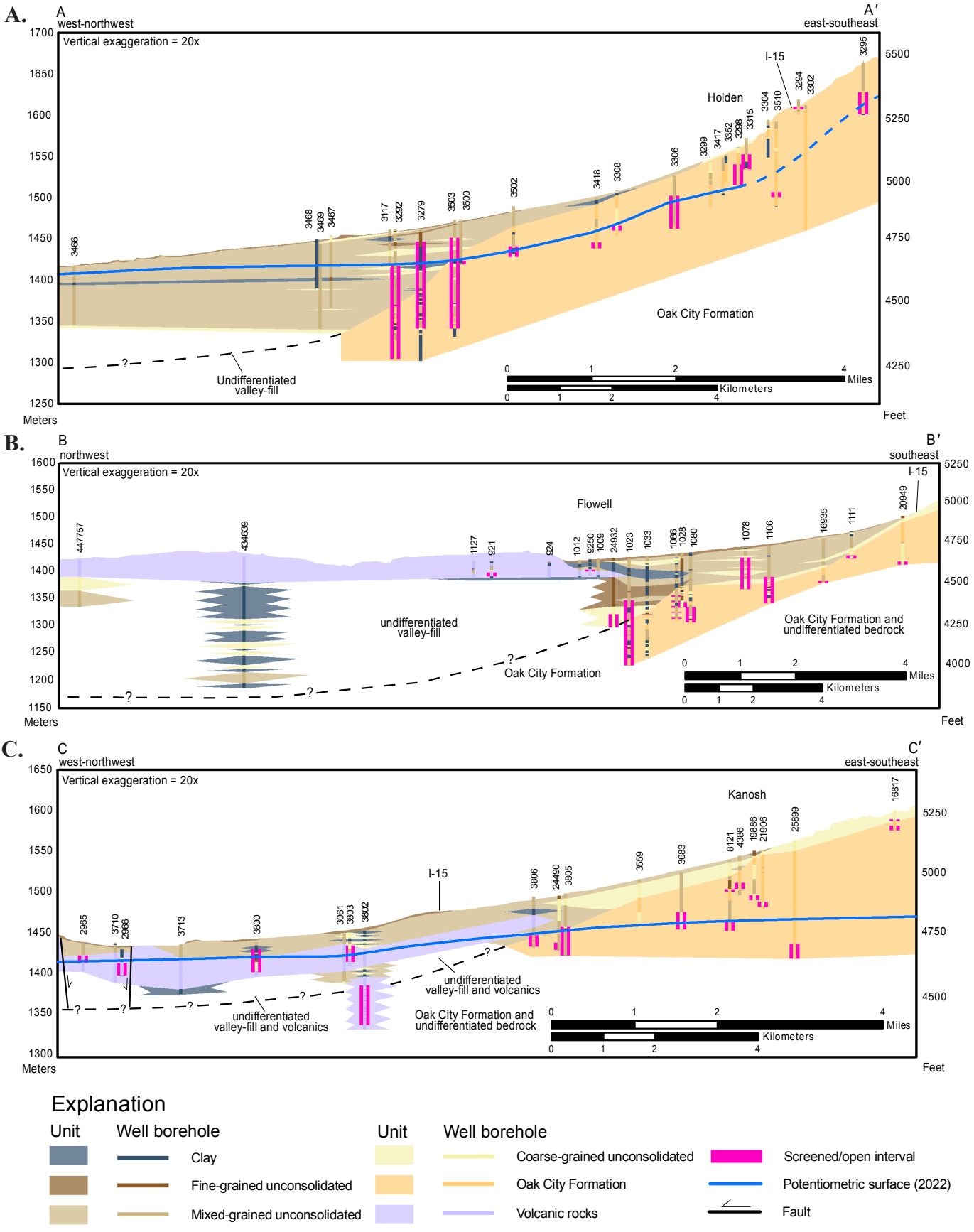

Figure 12. *Schematic geologic cross sections. See Figure 11 for cross section locations. Potentiometric surface from spring 2022. Boreholes labeled with WIN.* ***A)*** *Cross section A-A' in the Holden/Greenwood area.* ***B)*** *Cross section B-B' in the Fillmore/Flowell area. C) Cross section C-C' in the Kanosh area.*

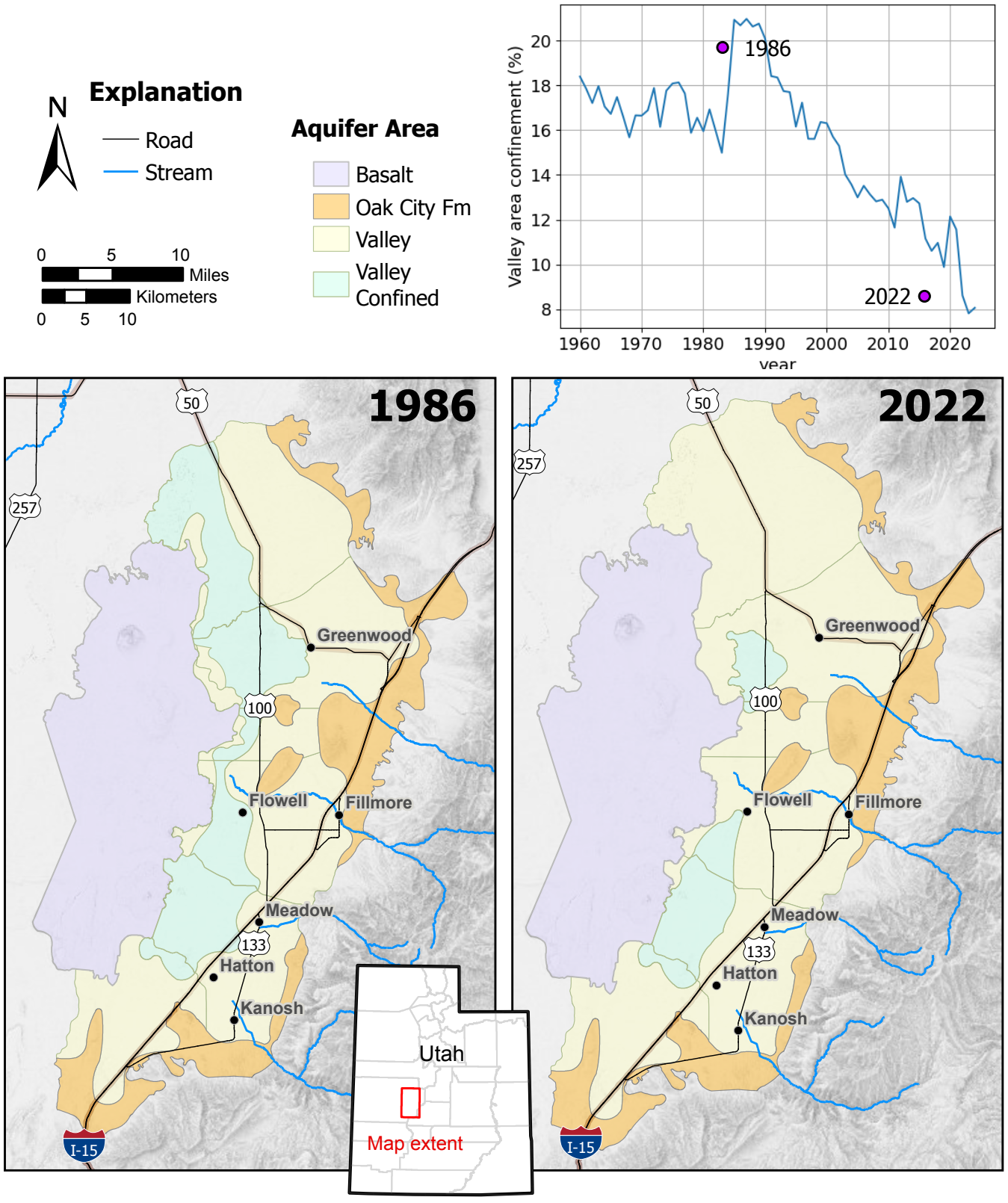

Figure 13. *Aquifer areas and coverage of confinement during 1986 (modified from Holmes and Thiros, 1990), and 2022. Inset graph shows approximate change of relative confinement over time.*

Although the Oak City Formation has a significant number of wells completed in it, it has variable aquifer properties. This unit is generally described in local drillers' logs as a semi-consolidated to a well-consolidated conglomerate, with clay units that seem fairly contiguous and can be correlated across several well records. Due to its consolidation and clay units, the Oak City Formation likely contributes little to the storage of the greater primary aquifer system.

Aquifer Property Estimates

For the sake of storage change estimation, we divided the valley-fill aquifer into four separate hydrogeologic units: basalt, unconfined valley fill, confined valley fill, and Oak City Formation. The unconsolidated sediments of Pahvant Valley have intervening and fairly contiguous clay layers, allowing for confining conditions and flowing wells in some parts of the valley. As groundwater levels change, so does the area of the aquifer that is confined and unconfined. Once groundwater head drops below the bottom of a confining clay layer, that part of the aquifer is "unconfined" in the sense that water extracted is from draining pore spaces (specific yield) and not from the elastic and inelastic compressibility of the aquifer (specific storage). Also, if the aquifer compresses over time from dewatering, storage values will decline. As groundwater level drops, the area of the unconfined aquifer grows. The storativity value is orders of magnitude higher for unconfined regions.

In 1960, the USGS conducted five multi-well aquifer tests in Pahvant Valley, including one test in the volcanic aquifer (Mower, 1965). They determined the storativity of the confined and unconfined valley-fill aquifers to be 2.5 x 10^{-4} to 1.6 x 10^{-3} and 0.1 to 0.25, respectively. The aquifer test in the volcanic aquifer yielded a storativity value of 0.06 (Mower, 1965). Using these values, we generated lognormal distributions of storativity for each aquifer (Figure 14).

The valley-fill aquifers are directly connected to the volcanic aquifer, as basalt flows contained within the volcanic aquifer interfinger with valley-fill sediments. Discharge from Clear Lake Spring, which emanates from the Ice Springs basalt, has been statistically related to groundwater levels in the valley-fill aquifer (Mower, 1967).

Subsidence

InSAR measurements and physical evidence suggest that Pahvant Valley has experienced land subsidence. Using InSAR data, we created a ground deformation map of the valley (Figure 15), discussed below. Additionally, we observed that four

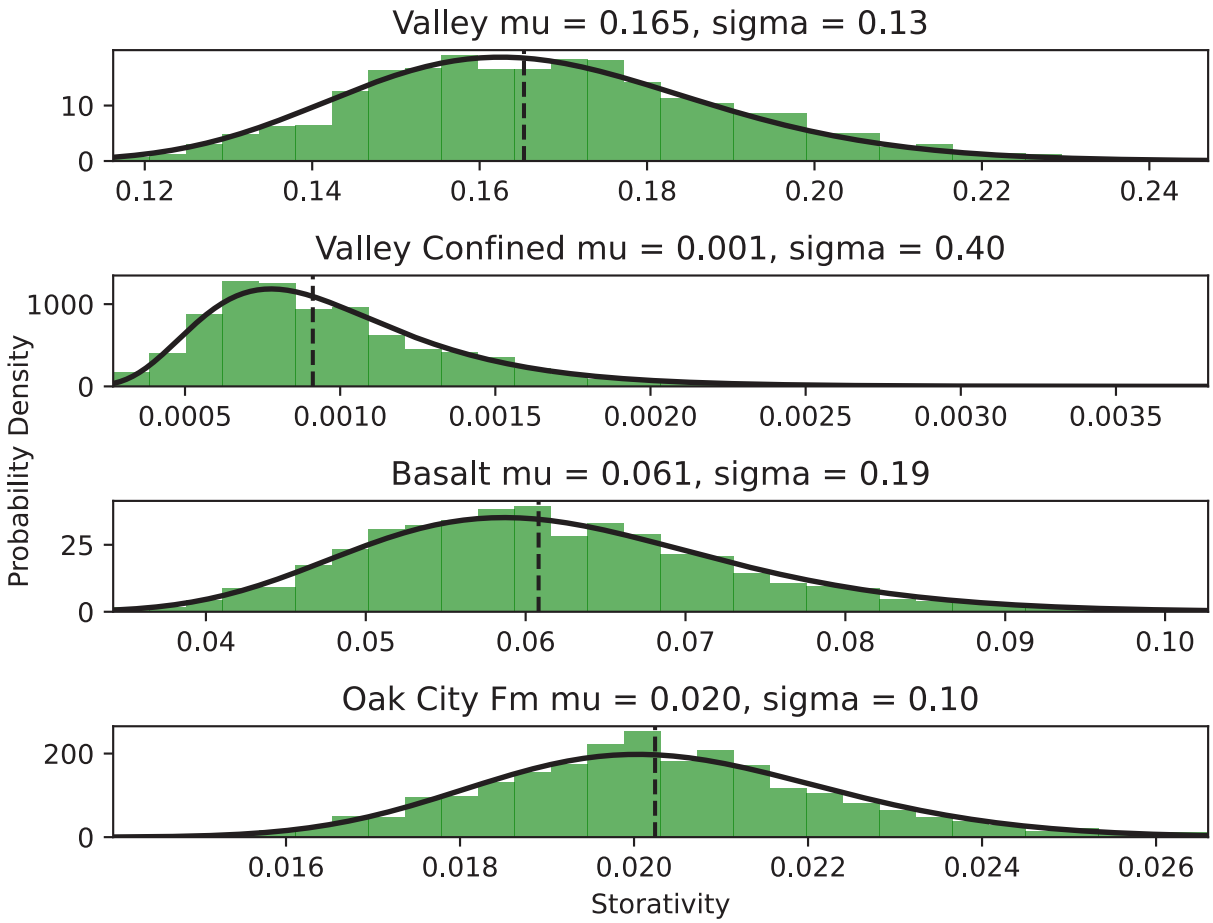

Figure 14. *Estimated distributions of aquifer storage properties.*

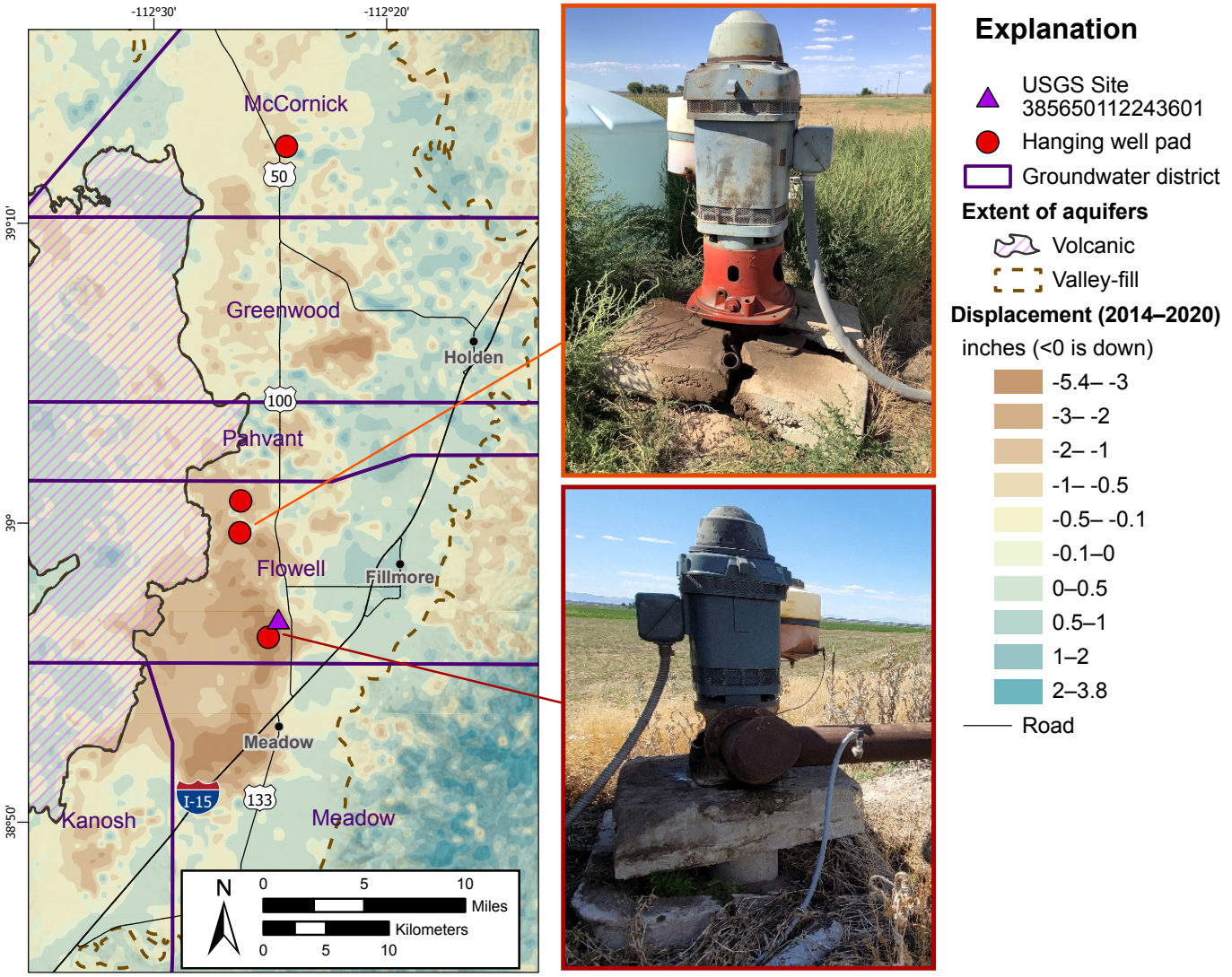

Figure 15. *Vertical ground displacement based on InSAR analysis. The photos show examples of hanging well pads in the Flowell area.*

wells in the valley have notable "hanging" well pads, where the ground around the pad has subsided relative to the well. The subsidence has caused the concrete around the casing to "float" above the ground because it is only supported by the well casing (Figure 15). These pads were floating between 4 and 8 inches above the land surface.

From 2014 to 2022, measurable amounts of subsidence have been detected using InSAR analysis. Maximum measured subsidence was 5 inches in the Meadow area. Meadow also had the highest average subsidence for the area, at 0.89 inches, with the Flowell district having average total subsidence of 0.69 inches (Table 3). The Pahvant groundwater district has the least subsidence. Additional historical InSAR data could be compiled to extend the temporal range of measurement to years before 2014. Long-term assessment of subsidence was not part of the original scope of this study.

InSAR satellites measure the ground at an angle (not straight down), and phase differences in repeat passes are used to detect ground deformation. These phase differences can be distorted with large amounts of relief, for example, in mountainous areas. Although a digital elevation model is used to remove these elevation effects during post-processing, the elevations are sometimes not detailed enough to remove all decorrelation artifacts. Correlation values are similar to a correlation coefficient, where values closer to 1 represent better correlated data. Despite these limitations, correlation was greater than 0.7 throughout the valley surface, which can be considered fairly representative. Decorrelation and standard deviation of velocities are higher in mountainous areas.

Time series data produced from InSAR analysis indicate change in the rate of deformation over time. We examined time series data of multiple locations, including the Flowell area, which has relatively high deformation and a long groundwater-level record. At the Flowell well location, the rate of subsidence varied between 2017 and 2022, averaging 0.21 feet per year, and the changes in deformation are correlative to groundwater level changes (Figure 16).

Table 3. *Zonal statistics of vertical ground deformation in the Pahvant Valley unconsolidated aquifer, summarized by groundwater district. See Figure 15 for a map of these data.*

District	Subsidence 2014-2020 (inches)					
	Area (acres)	Max	Min	Mean	Std	Median
Meadow	32,865	-5.37	1.03	-0.89	1.21	-0.30
McCornick	12,417	-1.14	1.39	-0.17	0.42	-0.20
Greenwood	31,197	-3.94	1.38	-0.21	0.88	-0.01
Pahvant	18,656	-1.99	1.39	0.00	0.65	0.14
Flowell	49,483	-4.41	1.01	-0.69	1.08	-0.33
Kanosh	15,073	-2.28	0.86	-0.34	0.52	-0.18
Hatton	12,417	-1.14	1.39	-0.17	0.42	-0.20

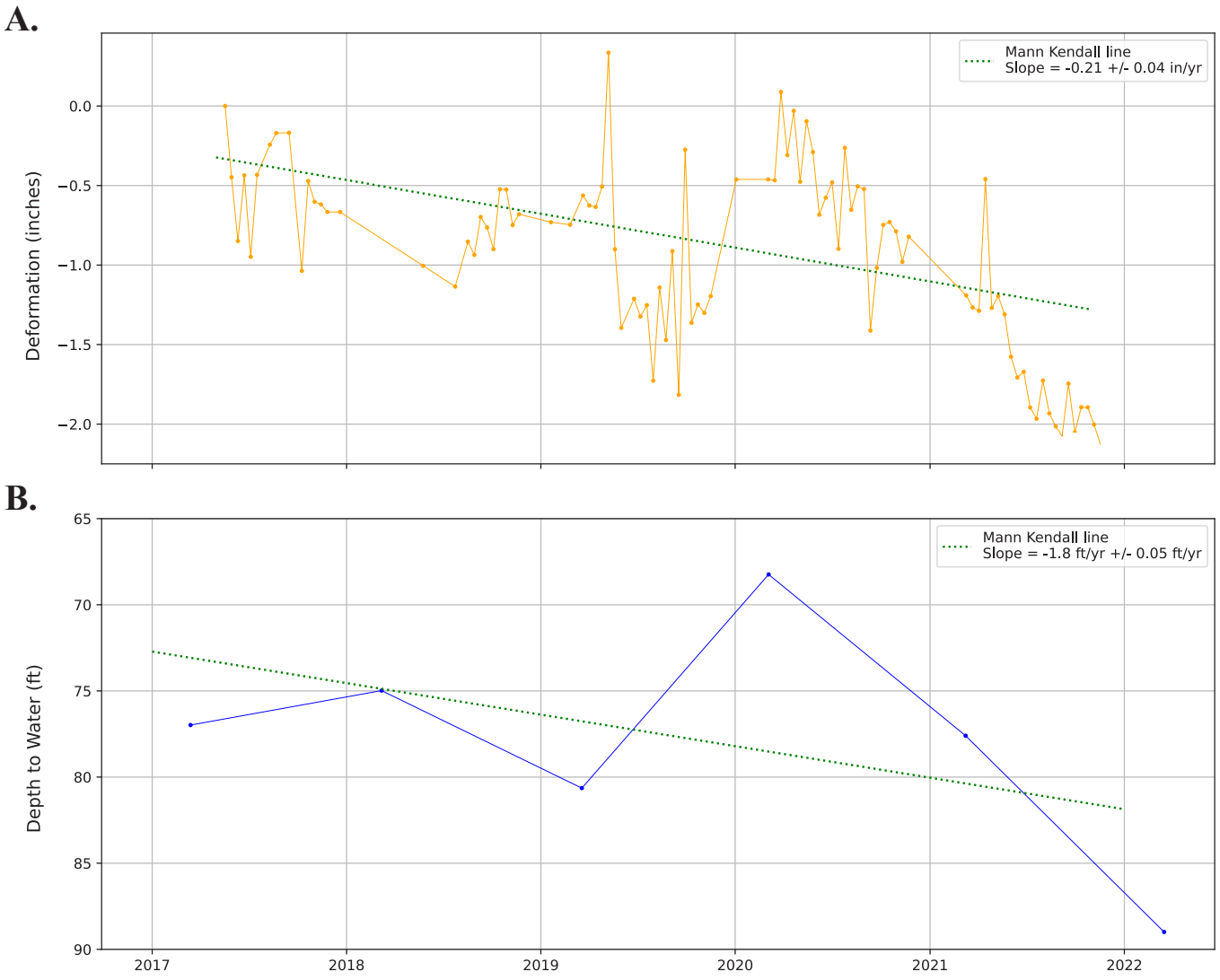

Figure 16. *Time series of **A)** ground deformation based on InSAR analysis (negative values are down) and **B)** groundwater levels at USGS well 385650112243601 (U.S. Geological Survey, 2024). See Figure 15 for the well location.*

Earth fissures are commonly associated with subsidence. We looked for earth fissures both in the field and using lidar but found no well-developed fissures. Earth fissures form from differential compaction, commonly caused by contrasting thicknesses of clay between two areas. In Pahvant Valley, the transition of sediment and clay thickness could be gradual, reducing the occurrence of earth fissures.

Discharge

Wells

Based on DWRi records and field observations, Pahvant Valley had 259 active wells in 2022 (Table 4). This count does not include domestic wells that irrigate turfgrass yards, only agricultural irrigation wells. Based on our accounting, agricultural pumping makes up more than 98% of groundwater pumping in this region (Table 4).

The number of days between April 1 and October 31, the period over which irrigation diversion from wells is allowed by water right, is 213. However, alfalfa farmers generally water less frequently early in the season and discontinue watering two to four times per year to allow the alfalfa time to dry out in the field and then be cut. Even if a farmer watered prior to or beyond the allotted irrigation dates, watering more than 213 days is improbable. Irrigation pumping duration data from Pahvant have a normal distribution. The 95th percentile ranged from 65.7 days to 175.4 days, with a mean and standard deviation of 119.7 days and 27.7 days, respectively. The measured data had a minimum pumping duration of 46 days and a maximum pumping duration of 171 days (Table 5).

In 2022, observed pumping rates ranged from 200 to 5000 gallons per minute (gpm) (Table 5). Pumping rates are constrained by realistic factors. To operate an irrigation system, a well must pump at a minimum of approximately 100 gpm. The limitations of the aquifer system and electric motor restrict the pumping rate to no more than 9000 gpm. The distribution of pumping rates is logarithmic, with many values around 1000 gpm and a few measurements near 4000 gpm. We recorded pumping rate data from 45 irrigation-well inline flow meters, which showed a lognormal distribution with a 95% confidence interval between 77 and 3312 gpm. The median rate was 836 gpm, with the minimum and maximum measured rates of 10 gpm and 4403 gpm, respectively (Table 5). The geometric mean of the 45 measurements is 722 gpm. Some error is likely associated with this estimate, as many irrigation pumps in the valley have variable rate drives that allow for a change in pumping rates to regulate system pressure. However, repeat visits to these sites indicated small variations (<100 gpm) in the pumping rate over time.

Using data from the well depletion estimates and Monte Carlo simulations, we estimated the distribution of total pumping for the region for calendar year 2022. From our Monte Carlo approach, we estimated that total pumping for the valley in 2022 is 143,362 acre feet (standard deviation of 7881 acre-feet), with a 95% confidence interval between 128,209 and 159,668 acre-feet.

Based on our irrigation pumping estimates, the groundwater pumping of 149,380 acre-feet reported by the USGS in 2021 (U.S. Geological Survey, 2021) is plausible. Using a Mann-Kendall analysis to determine if a significant trend exists in the USGS data, we determined that there has been a general increase in pumping since 1990 at an average rate of 1900 ac-ft/yr (Figure 17).

Consumptive Use

Changes in irrigation management over time have caused an overall increase in groundwater use in Pahvant Valley. NDVI time-series data indicate a statistically significant increase in greenness since 1984 (Figure 18). This increase is most noticeable during the mid 1990s to 2010, a time which also had a significant increase in the number of wells and pressurized pivot irrigation systems (Figure 19). The irrigation systems with supplemental groundwater allowed for denser, greener crops over the duration of the irrigation period. The NDVI time series show a transition from water-limited irrigation, where peaks and duration of greenness are limited by the availability of surface water, to continuous irrigation powered by pumping of groundwater. Crop yield and NDVI are correlative with evapotranspiration. Healthier, denser crops, with greater vegetative mass and leaf area transpire more than water-limited crops.

Table 4. *Point in time count of wells by type in Pahvant Valley and their estimated withdrawals for 2022. This count is based on assumed dominant use. Domestic wells that also irrigate turf are classified as domestic.*

Well Type	Active Wells 2022	Avg. Use (ac-ft)	Std. Dev. Use (ac-ft)	2.5%-tile (ac-ft)	97.5%-tile (ac-ft)	Relative Pumping
Irrigation	259	143,362	7881	128,990	158,390	98.46%
Stock	87	26	2	22	26	0.02%
Domestic	178	808	63	685	935	0.55%
Municipal	6	1270	30	1210	1327	0.87%
Industrial	2	137	15	106	166	0.09%

Table 5. *Pumping duration and rate measurements of agricultural irrigation wells in Pahvant Valley, 2022 calendar year.*

WIN[1]	Calculated Pump Duration (hr)	Vibration Duration (hr)	Pump rate (gpm)	Total Pumped (ac-ft)
919	2345		499	215
922		3408.9	4403	2763
924		2755.1	2462	1249
1013		2702.5	1109	552
1077	3111	3251.4	3072	1839
1124	1993		396	145
2309				263
3407		3759.3		
3497		2756.3		
3524				129
3525	3401		968	606
3528	3061		958	540
3802				721
3828				473
13660				271
13666	7216		503	668
23719		4110.5		
25266				
26844		2314.9		
35697		1111.6		
99980				1538
99988				347
99990		2704.3		
429388		3536.2		
433640		2452		
439393	2465		723	328
444873	8190		441	665

[1]Well identification number

Discrepancies between pumping estimates and the estimated quantity of consumptive use, as well as the ET fraction, indicate that there is likely inefficient application of water occurring. Although evaporative loss of wind-drifted water from spray nozzles has been minimized through low elevation spray application (LESA) and elimination of end guns for many of the pivot systems across the valley, evidence suggests that application in excess of consumptive use is occurring, resulting in deep percolation and evaporative loss from ponding of irrigation water on the soil surface. ET fraction is a ratio of the estimated evapotranspiration to the grass reference ET. The grass reference evapotranspiration is the hypothetical ET of an ideal grass in well-watered conditions. Generally, estimated actual ET should be less than the reference ET, which would make the ET fraction less than 1. If additional evaporation is occurring as the result of standing water, then the ratio will be greater than 1. This ratio can be observed on the field-scale and shows that many of the fields in western parts of the arable land in the valley have values near or above 1 (Appendix C).

The total consumptive use of the Pahvant Valley agricultural area in 2022 was 73,640 ac-ft. The amount of surface water irrigation is not well measured or delineated, but soil-water-balance models, along with sparse measurements, can provide some insight into the potential quantity of surface water irrigation. Based on the spatial distribution of functioning canal infrastructure, wells, and surface irrigation, we can assume that most of the fields in the eastern Fillmore, Pahvant, Greenwood, and Kanosh groundwater districts are predominantly irrigated with surface water (7, 9, 11, 17, 20 in Figure 3). For 2022, the SSEBop model estimated 21,527 ac-ft of consumptive use for these regions.

Based on NDVI time series analysis using GEE, we observed statistically significant increases in NDVI values from 1992 to 2021, focused in the areas of pivots. The increasing NDVI indicates increased plant density and vitality and coincides with a reported increase in crop yield for alfalfa in Millard County between 1980 and 2017, with an average increase of 0.02 tons per acre per year. In 2017, Millard County produced 333,000

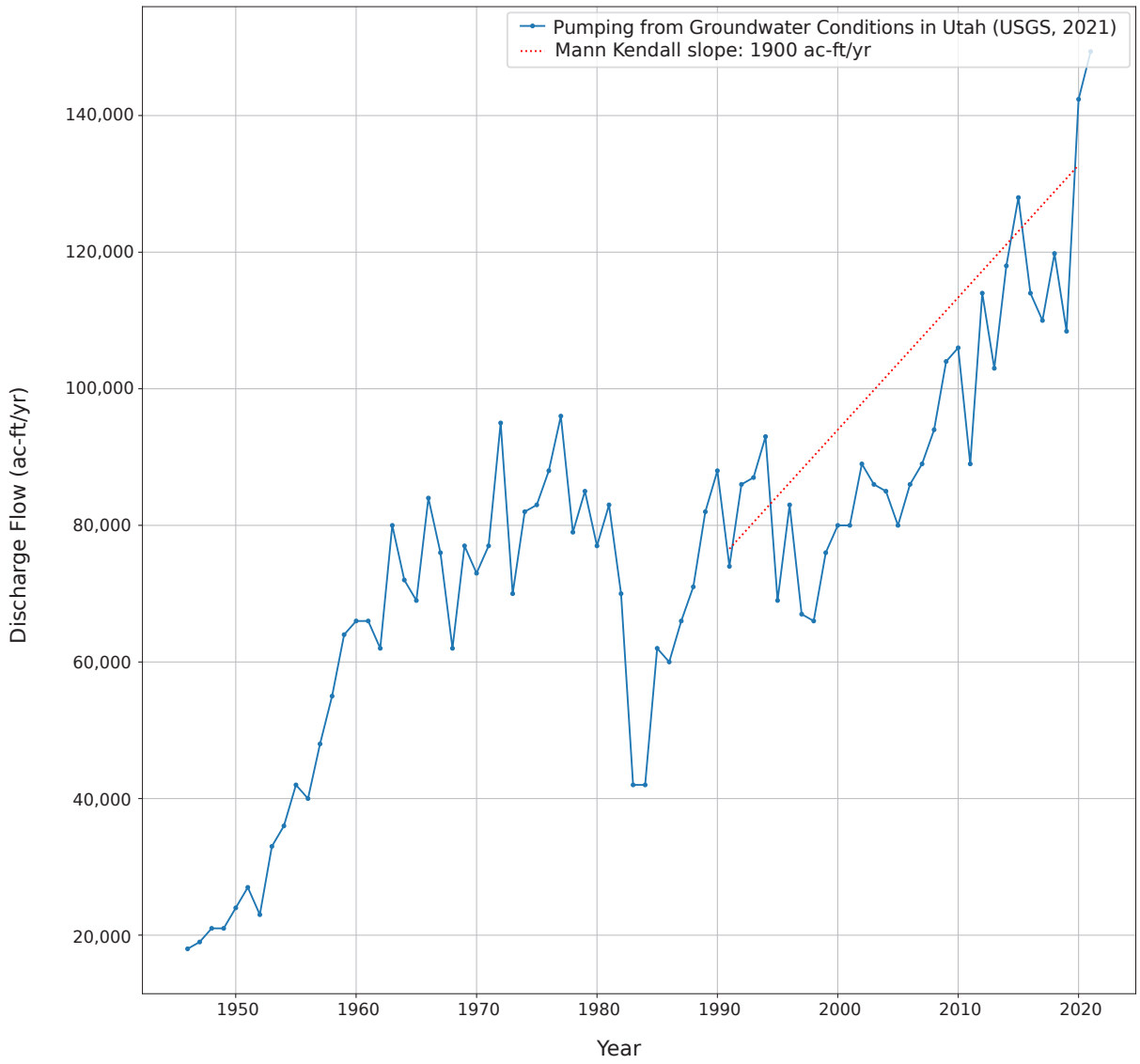

Figure 17. *Pahvant Valley groundwater pumping records over time (U.S. Geological Survey, 2024).*

tons of alfalfa (U.S. Department of Agriculture, 2023). Corn (grain) production from 1972 to 2017 increased on average 2.1 bushels per acre per year in Millard County (Figure 20).

Long-term SSEBop analysis indicates that overall consumptive water use increased from 2000 to 2021. ET increased by 23,400 ac-ft in the agricultural areas between these years, despite less precipitation in 2021 than 2000 (Figure 21; Table 6). This equates to an average increase of 1000 ac-ft/yr, which coincides with the observed increase in pumping rate (accounting for infiltration). The Kanosh District had the highest increase in estimated ET of 7700 ac-ft (Table 6). Examination of individual time series in each field showed an average ET increase of 10 inches (n = 100) in newly established fields and 1.4 inches (n = 378) in fields that were present in 2000.

Increase in ET is likely tied to changes in irrigation approach and increased use of groundwater. There appears to be a significant increase in ET and NDVI with conversion from flood irrigation to pivot irrigation. The consistent spray pattern of the pivots generates more crop yield with greener and denser crops and fewer dead areas in the fields. This increase in crop density increases consumptive use. Increases in ET can also be tied to climate change and temperature increases over time.

Based on place of use data and assumed predominant water sources for various fields, we also calculated the net ET by water source for agricultural lands. Groundwater makes up about 56% of the net ET of applied water for agricultural lands, which amounts to about 40,000 ac-ft per water year on average. Surface water makes up about 13% of the net ET in the valley (9000 ac-ft per irrigation season), the rest of the water applied (20,000 ac-ft per water year on average) is from mixed sources or was not possible to determine based on the available data (Table 7).

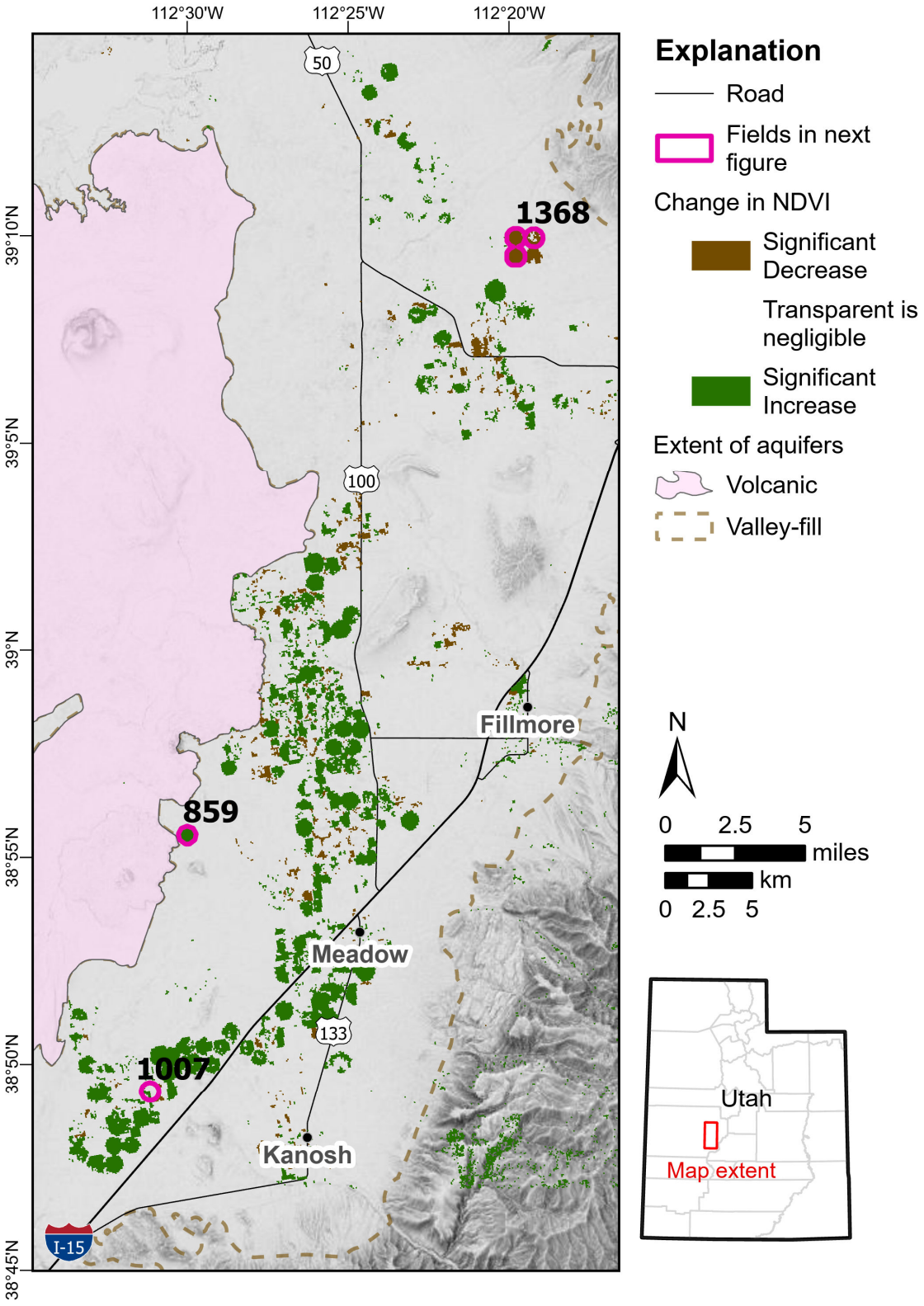

Figure 18. *Result of pixel-wise Mann-Kendall trend analysis of summer NDVI values from 1989 to 2021. Example fields are highlighted in pink and labeled with their respective field numbers and their time series are presented in Figure 19.*

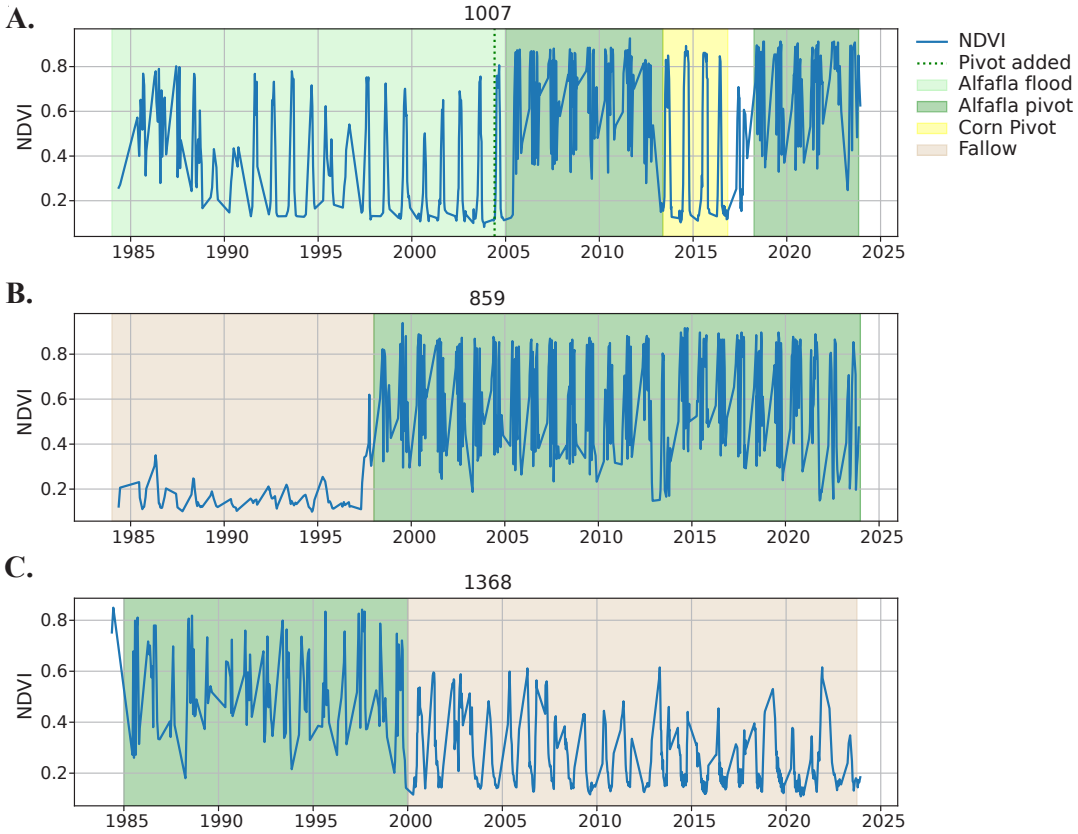

Figure 19. *NDVI changes over time in three example fields.* ***A)*** *A field with moderate increase in NDVI over time shows a transition from a lower, sparse NDVI value to a consistently high NDVI value.* ***B)*** *A field showing a marked increase in NDVI, going from bare ground to pivot irrigation.* ***C)*** *A field in an area of decreased NDVI, going from irrigated to fallowed land. See Figure 18 for locations.*

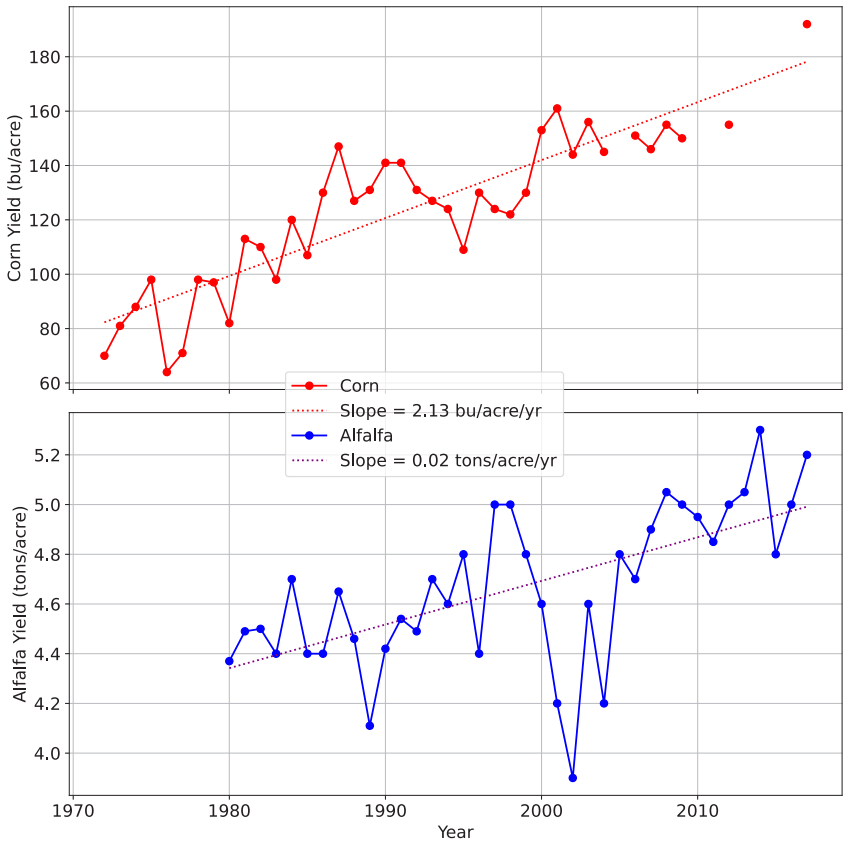

Figure 20. *Increase in agricultural production in Millard County over time. Bu = bushels.*

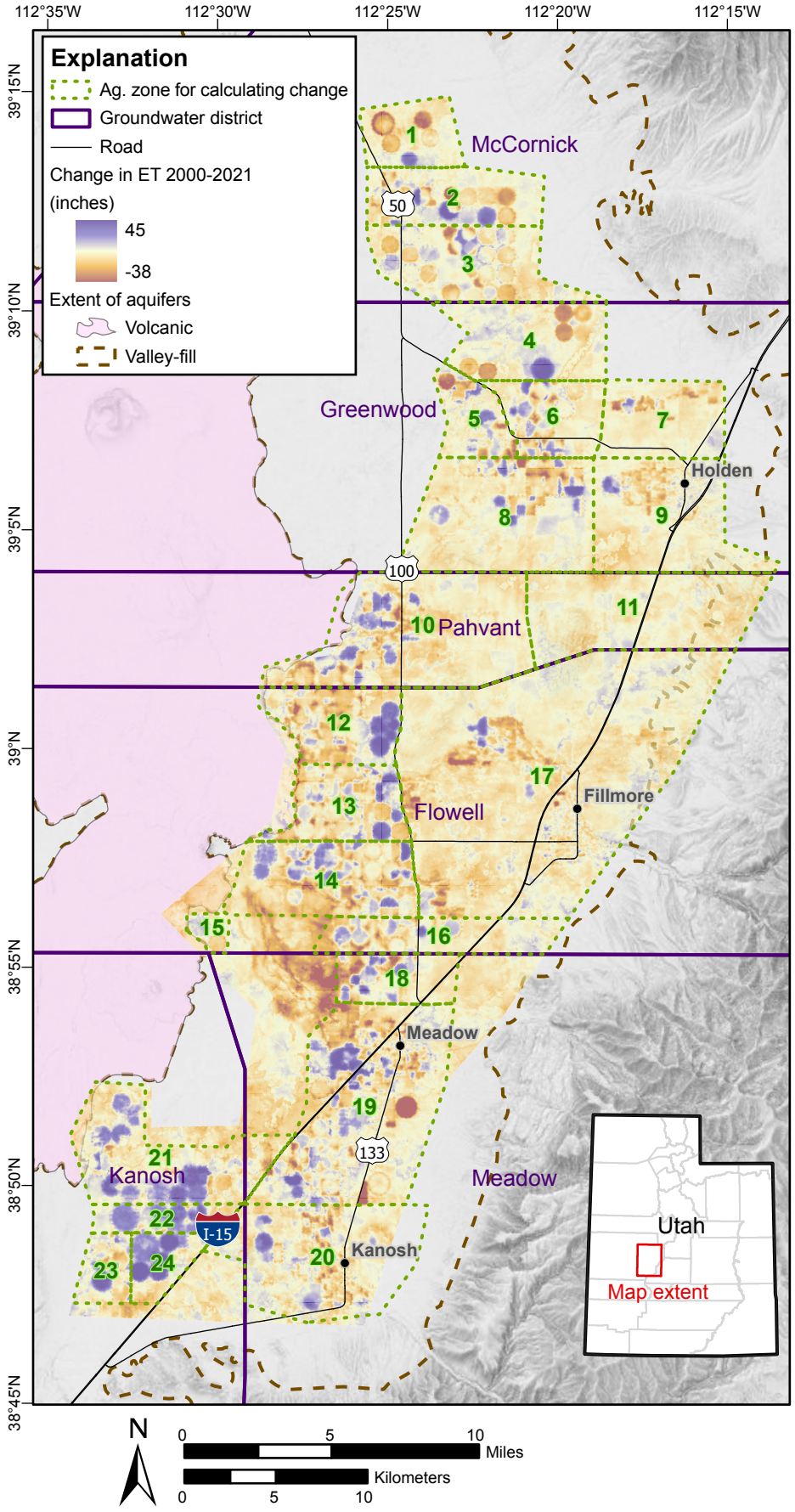

Figure 21. *Change in evapotranspiration in the arable parts of Pahvant Valley from 2000 to 2021. Groundwater districts (irrigation areas; thick dark green line) are subdivided into smaller numbered areas (dashed lines) for comparison.*

Table 6. *Change in evapotranspiration (ET) from 2000 to 2021 and estimated net evapotranspiration (ET-precipitation) during the irrigation season for each groundwater district.*

Name	Area (acres)	2000–2021 ΔET (in)	2000–2021 ΔET (acft)	2016–2022 Avg Irr ET-PPT (ac-ft/yr)
Meadow	32,171	0.7	1900	26,343
McCornick	12,776	1.7	1800	15,443
Greenwood	31,178	2.1	5400	17,814
Pahvant	18,091	1.5	2200	7029
Flowell	50,069	1.1	4400	29,043
Kanosh	15,451	6.0	7700	11,043
		Total	23,400	106,715

Table 7. *Evapotranspiration (ET) and net evapotranspiration (ET-precipitation) during the irrigation season by water source, 2016 to 2023. These data are based on a modified water related land use layer and place of uses layers.*

	Model	Water Source	Year 2014	2015	2016	2017	2018	2019	2020	2021	2022	2023	Average	Percent of Total
Water Year (Oct 1–Sept 30)	SSEBop	Groundwater	36,400	43,410	41,000	32,600	50,470	33,740	49,120	44,490	43,040	28,180	40,245	58%
		Mix	6200	7480	7400	5510	8330	5340	8990	8420	7990	5370	7103	10%
		Mix (GW likely)	8830	10,460	9560	7890	11,930	7750	11,860	11,240	10,760	7070	9735	14%
		Surface	6220	7830	9760	8690	12,700	9350	12,430	7880	8490	5300	8865	13%
		Unknown	2560	2840	2590	2300	3870	2620	3700	3330	3360	2000	2917	4%
		TOTAL	60,210	72,020	70,310	56,990	87,300	58,800	86,100	75,360	73,640	47,920	68,865	100%
	Ensemble	Groundwater	37,530	41,780	40,540	35,770	50,050	35,460	48,440	42,500	40,670	32,070	40,481	56%
		Mix	6580	7330	7370	6060	8450	5950	9170	8140	7830	6260	7314	10%
		Mix (GW likely)	9090	10,040	9450	8680	11,880	8310	11,560	10,230	10,290	7840	9737	14%
		Surface	7950	10,320	11,690	11,450	15,540	12,460	14,600	9120	10,360	8720	11,221	16%
		Unknown	2480	2830	2780	2770	3950	2790	3750	3160	3330	2460	3030	4%
		TOTAL	63,630	72,300	71,830	64,730	89,870	64,970	87,520	73,150	72,480	57,350	71,783	100%
	EEMetric	Groundwater	36,460	43,350	37,300	30,300	50,330	36,150	49,040	45,510	40,520	28,740	39,770	56%
		Mix	6620	7670	7160	5160	8470	5930	9500	8760	7840	5890	7300	10%
		Mix (GW likely)	9470	10,940	9020	7490	12,490	8730	12,390	11,000	10,680	7820	10,003	14%
		Surface	9560	11,080	10,420	8850	15,720	12,950	15,270	9320	10,060	8280	11,151	16%
		Unknown	3000	3220	2700	2390	4260	3040	4090	3570	3580	2560	3241	5%
		TOTAL	65,110	76,260	66,600	54,190	91,270	66,800	90,290	78,160	72,680	53,290	71,465	100%

Water application is tied to the availability of the water source. In especially wet years, there is a surplus of surface water, and if the farm has the infrastructure and water rights, it can apply that surface water over the duration of the irrigation season. In drier years, farms may start the season by irrigating with surface water, then later supplement the surface water with groundwater pumping later in the season. Examination of multi-band satellite imagery shows that some fields remain verdant throughout the season during drier years, whereas others taper off with the availability of surface water.

In Pahvant Valley, surface water is delivered to fields using canals and ditches operated and maintained by the canal companies. If a field is beyond the service area of the canal company, it likely is watered only by groundwater. Also, discussions with producers and canal companies about their subsurface piped infrastructure, as well as newer place of use documentation, allowed us to parse out the source of diversion and water application for most of the fields in the valley.

Clear Lake

The springs that supply the ponds at Clear Lake WMA comprise a significant natural discharge point from the volcanic aquifer. The Clear Lake Spring complex consists of two main pools, Spring Lake, which is the main area of spring flow, and Clear Lake, which is a larger pool into which Spring Lake drains. Spring Lake is a kidney-shaped pool bordered on its east edge by exposed fractured basalt, where spring flow is diffuse but visible. Clear Lake Spring water is derived from infiltration

into the volcanic aquifer and water from the aquifer to the east (Mower, 1967; Holmes and Thiros, 1990). A flume separates these two pools and has been used for measurement of Spring Lake discharge since 1960. According to DWRi records, discharge declined from about 22 cfs in 2000 to about 4 cfs in 2018 and, as of fall 2023, is less than 1 cfs (Figure 22). Habitat for the Utah conservation species least chub (*Iotichthys phlegethontis*), a fish native to the Clear Lake outflow area (Bailey et al., 2006), declined significantly during this time. The DWR has expressed interest in replacing the existing flume at Clear Lake Spring to ensure more accurate flow records.

Based on cross correlation of yearly precipitation and spring flow data, there is a lag between increases in precipitation and increases in spring flow. Pearson's correlation coefficient, a measure of the relationship, strength, and direction between two variables, is highest having a two-year offset and a value of 0.401 (Table 8). This two-year offset implies that an increase in precipitation results in an increase in spring flow two years later. Correlations in monthly data are harder to discern, likely because this is a snow-dominant hydrologic system, and there are compounding variables such as pumping and stream flow that are also driven

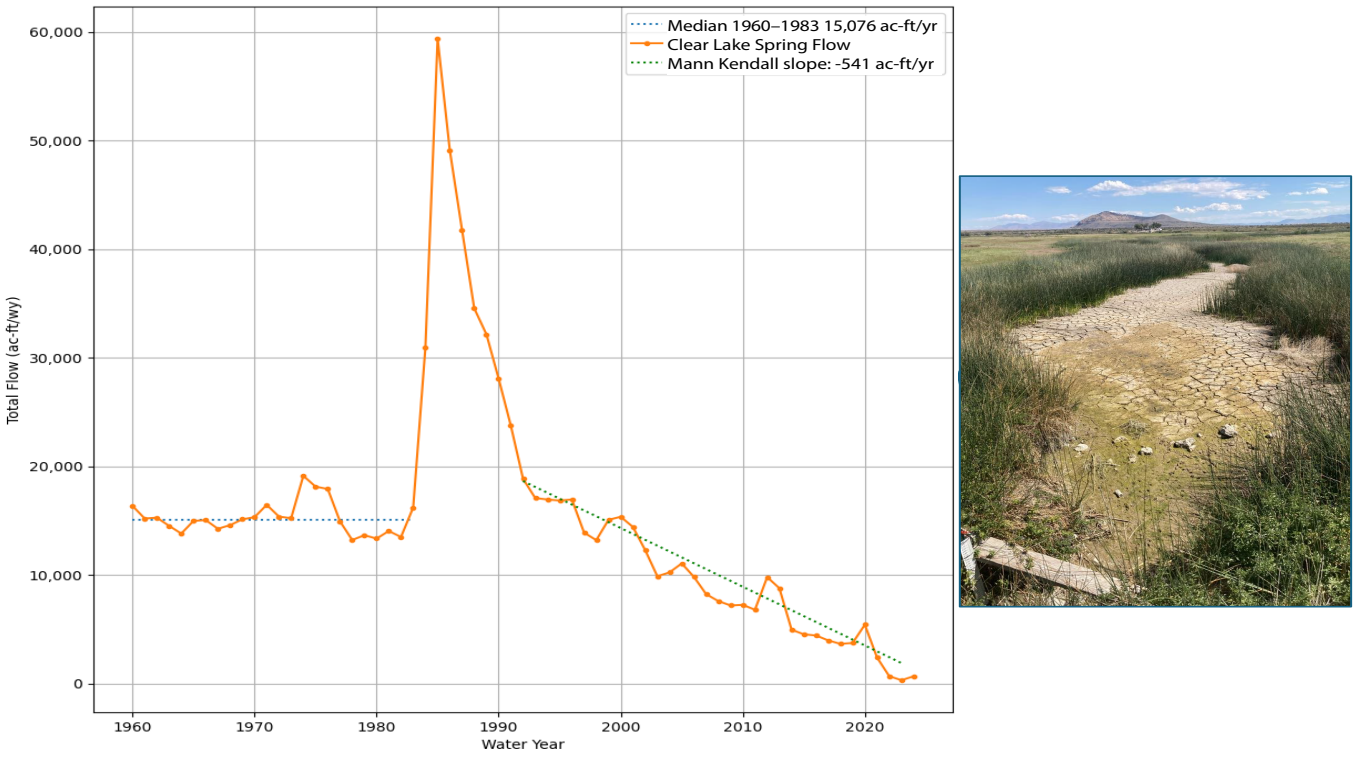

Figure 22. *Annual discharge at Spring Lake based on measurements at the Spring Lake discharge channel that connects to Clear Lake (USGS site 390540112370001). The photo was taken of the discharge channel August 30, 2022.*

Table 8. *Pearson's correlation coefficient between Clear Lake Spring flow, groundwater pumping, and Flowell precipitation. Water year is abbreviated as "wy" and calendar year is abbreviated as "cy."*

		Spring Flow (ac-ft)	
		per cy	per wy
Precipitation	cy	0.242	0.199
	wy	0.283	0.212
	wy Shift + 1	0.400	0.380
	wy Shift + 2	0.401	0.394
	wy Shift + 3	0.386	0.393
Groundwater Pumping	No shift	-0.627	-0.579
	Shift+1	-0.715	-0.696
	Shift+2	-0.718	-0.721

by snowmelt and precipitation. For example, during years where precipitation was higher than average (e.g., 1983–85), water would pool in an area labeled "the Sinks" located on the southeastern margin of the Ice Springs basalt flows. We conducted a 15-year moving average on the monthly precipitation and flow data and then aligned the peaks and troughs of the data by shifting the precipitation and conducting a cross correlation. The window of best alignment appears to be between 1 and 2 years.

Correlation between pumping and spring flow is higher than correlation between precipitation and spring flow. The highest cross correlation between yearly pumping and spring flow data is -0.72 when a two-year lag is applied to pumping. The negative correlation value indicates spring flow is inversely proportional to pumping (Figure 23). The relationship between pumping and spring flow loses significance below pumping rates of 90,000 ac-ft/yr, where other variables have more influence over spring flow below these pumping rates.

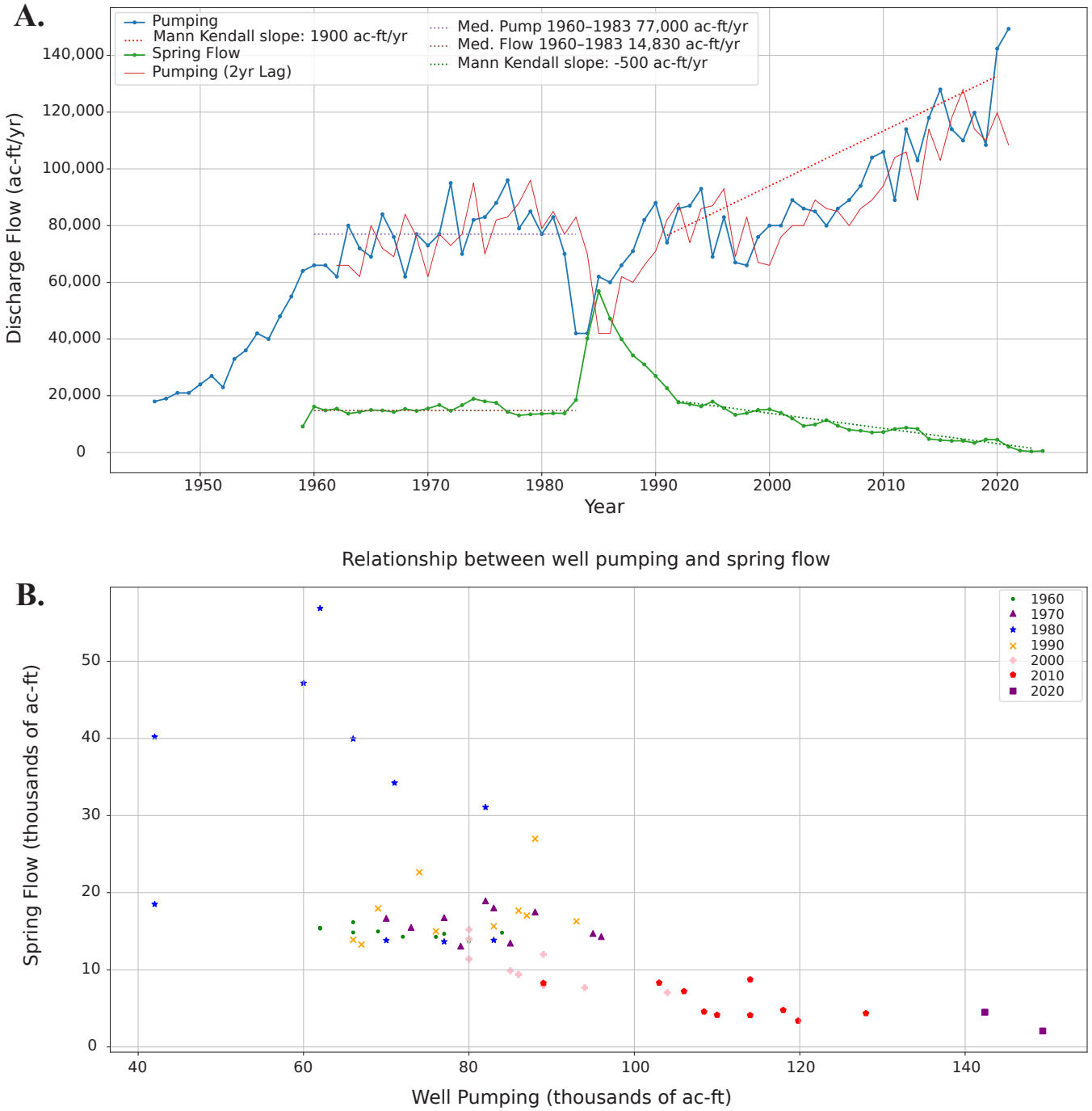

Figure 23. *Comparison between Spring Lake discharge and pumping discharge.* ***A)*** *Discharge over time for spring lake and groundwater pumping. Peaks and troughs of pumping are lagged in yearly data by about 2 years. Discharge was stable between 1960 and 1983.* ***B)*** *Relationship between pumping and discharge. No slope is apparent for the 1960s and 1970s, when pumping was between 60 and 95 thousand acre-feet (ac-ft) per year.*

The measured spring flow was relatively stable from 1960 to 1983, increased significantly in 1984 when it breached a threshold of 20,000 ac-ft per calendar year, and then receded back below that threshold in 1992 (Figure 22) and has been steadily declining since. Groundwater pumping during the 1960 to 1983 period varied between 60,000 and 95,000 ac-ft per calendar year (Figure 23). Spring flows are most stable under total pumping of <90,000 ac-ft/yr, where the relationship between spring flow and pumping is not strong (flat). Based on flow data from 1960 to 1983, the median "steady state" system spring flow is 14,830 ac-ft per calendar year, with a mean of 15,300 ac-ft and a standard deviation of 1570 ac-ft (Figure 23). Spring Lake ET was likely similar during this time, as higher pool stages are translated to flow out of the system and not a larger spring pool upstream of the gage. After 1991, the rate of spring flow recession from the early 1980s high point decreased. The spring's flow has decreased since 1992 at an average rate of about 500 ac-ft/yr (Figure 23). Spring Lake flow has been 3121 ac-ft per calendar year on average since 2018. Spring flow stopped in 2022 and the channel where the flow gage is set was dry (Figure 22).

The periodicity and long-term trend of the spring flow has changed since the big water years of the early 1980s. Prior to 1982, peak spring flow occurred in March or April and had a median of around 23 cfs. After 1995, peak spring flow occurred in May and had a median of around 20 cfs. The shift in peak in the more modern setting could be a clue to an increased influence from pumping on the spring flow, as pumping increased by about 1900 ac-ft/yr from 1991 to present (Figure 23). Due to the ongoing decline in the spring flow, there is also more variability in the flow records since the highs of the 1980s.

The spring system is a mix of water that has directly infiltrated into the volcanic aquifer, and the groundwater of the unconsolidated valley-fill material in Pahvant Valley. Mower (1967) indicated that 60% (9000 ac-ft/yr) of the spring flow was from the valley-fill aquifer and 20% (3000 ac-ft/yr) from the volcanic aquifer from 1960 to 1964. As groundwater elevation declines from increased pumping, the amount of contribution to spring flow from the valley-fill aquifer will decrease. If the decline of groundwater head continues in the valley-fill aquifer, the hydraulic gradient will reverse, taking away water that infiltrates into the volcanics that would normally flow to the spring. Additionally, several irrigation wells are screened directly to the volcanic aquifer. Mower (1967) showed that their activity is more closely related to spring flow. Evidence for this includes delayed peak flow in the spring season.

Based on OpenET estimates, Clear Lake pool net ET was about 70 ac-ft/yr on average over the last 7 years (Table 9). Contribution of precipitation upstream of the spring gage is about 48 ac-ft/year. The net ET of Clear Lake (downstream from the spring gage) should be higher than the flow measured at the Spring Lake outflow channel because

Table 9. *Estimated net evapotranspiration (evapotranspiration minus precipitation) of phreatophytes, springs, and wetlands from 2016 to 2023 in acre-feet per calendar year. Negative values equal net recharge or runoff (precipitation in excess of evapotranspiration). Positive values are assumed to indicate groundwater contribution to evapotranspiration.*

	Water Year										
Description	**2014**	**2015**	**2016**	**2017**	**2018**	**2019**	**2020**	**2021**	**2022**	**2023**	**Average**
Clear Lake	80	80	70	60	100	20	100	90	90	30	72
Clear Lake Outflow	710	690	560	550	780	260	810	590	390	80	542
Clear Lake Outflow Ex	660	560	460	360	600	60	790	480	100	-130	394
Pools N. of Clear Lake	-110	-130	-510	-830	-10	-1570	170	-160	-760	-980	-489
Clear Lake Combined[1]	**1450**	**1330**	**1090**	**970**	**1480**	**340**	**1870**	**1160**	**580**	**110**	**1038**
Playa West of Clear Lake	1390	1490	-1420	1050	6120	-4200	4700	4390	1230	-1140	1361
Riparian	-100	20	70	-20	160	60	320	0	-80	-310	12
Shallow GW Clay	-240	-30	-420	-460	270	-710	70	-190	-310	-480	-250
Shallow GW Delta	-380	770	-1420	-830	3970	-3080	1250	480	-810	-1090	-114
Shallow GW Hot Spring	950	1970	1460	1040	3340	370	2340	2290	2390	310	1646
Shallow GW NE	-1320	-730	-870	-1550	270	-1330	300	-360	-400	-2710	-870
Shallow GW Oasis	20	380	-320	-650	1280	-1200	480	-10	-430	-250	-70
Shallow Groundwater	-70	-40	-10	-40	50	-80	0	10	50	-30	-16
Meadow Spring Pools	40	70	60	40	100	20	80	80	80	30	60
Water	80	150	160	120	190	120	200	160	180	90	145
TOTAL[1]	**2540**	**4690**	**2840**	**2170**	**11,110**	**910**	**6910**	**4180**	**3280**	**540**	**3917**

[1]Positive values only are summed.

there is no surface water outflow from Clear Lake, yet it is considerably lower. For example, in the calendar year 2020, the total spring flow was measured at 4505 ac-ft (Appendix B). However, the net ET for the entire Clear Lake region was 1870 ac-ft (Table 9). All water passing through the channel should be evapotranspiring, so it should be accounted for by the remotely sensed estimates. OpenET has a mean absolute error of 33% for open water and wetlands (Melton et al., 2021), and the closest measurement of precipitation in the western part of Pahvant Valley is in Delta, so it is possible that the remotely sensed estimates are underrepresenting the actual groundwater evapotranspiration at this location. Some of the unaccounted-for water could have flowed into the playa area west of Clear Lake, which had a positive net ET that year and could account for the discrepancy (Table 9).

Other Springs and Shallow Groundwater

Shallow groundwater and phreatophytes cover a smaller area than reported in previous studies (Mower, 1965). Groundwater is shallowest near Meadow Hot Springs and immediately west of Greenwood (Figure 4). The area north of the volcanics and immediately south of Delta show signs of moisture, but based on negative consumptive use data, this moisture is more likely a combination of excess irrigation water ponding on impermeable material (Table 9). Most of the ET occurred in the shallow groundwater zone surrounding the Meadow Hot Springs area (Table 9).

Based on the respective drinking water source protection plans for the towns of Fillmore, Meadow, and Holden, there are four public water supply springs that are within the boundaries of the valley-fill aquifer. The towns' supplemental drinking water sources are various springs issuing from bedrock in the Pahvant Range. The total reported municipal spring flow in 2022 was 907 ac-ft/yr.

Groundwater Budget

Groundwater recharge should balance the change in groundwater storage and all discharge from the aquifer. The following equation summarizes the water budget residual approach to estimate recharge:

$$\text{Recharge} = \text{Discharge}_{\text{wells}} + \text{Discharge}_{\text{springs}} + \text{Discharge}_{\text{ET}} + \Delta\text{Storage} \quad (6)$$

Where the sum of discharge of wells, springs, evapotranspiration from groundwater (phreatophyte zones), and storage changes equals the amount of recharge the aquifer receives. Based on this approach, we estimate the recharge for 2022 was 68,878 acre-feet (standard deviation of 9775 acre-feet) (Table 10). From 1987 to 2022, the aquifers in this valley had been draining (negative change in storage, Table 11) at an average rate of 29,600 ac-ft per year. Since 1960, cumulative groundwater storage change is a loss of approximately 1.2 million acre-feet. From 1987 to 2022, only 7 of the 32 years have had positive changes in groundwater storage and these groundwater storage increases were the result of above-average precipitation. Using our storage change estimates with OpenET data (Melton et al., 2021) and groundwater pumping values (U.S. Geological Survey, 2021), we can derive longer-term groundwater recharge estimates (Table 11). Based on these estimates, average annual groundwater recharge from 2016 to 2022 was 90,600 ac-ft (Table 11). Due to how they are calculated, the recharge and groundwater storage change estimates are closely correlated by a linear relationship, allowing for a rough calculation of recharge from 1960 to 2022 (Table 12).

Groundwater Chemistry and Environmental Tracer Data

Introduction

Groundwater and surface water have unique chemical characteristics indicative of their points of recharge, geologic units encountered, and length of time from recharge to discharge. These characteristics can be used to discern provenance, groundwater flow paths, approximate ages, and the relationship between surface water and groundwater. Groundwater samples from throughout the Pahvant Valley display differentiated chemical characteristics indicative of these sources of recharge and flow paths through the subsurface. Groundwater sampling points located outside of the groundwater district boundaries generally lie to the west, and they are located within the Black Rock Desert and grouped separately due to distinct geochemical and geophysical characteristics.

Groundwater Temperature

Groundwater temperature across Pahvant Valley varied from 1.7° to 40.5°C (Figure 24). The mean groundwater temperature for the valley is 15.2°C. The calculated geometric mean for groundwater temperature in the valley, excluding the values from Meadow and Hatton Hot Springs, is 15.1°C. Groundwater temperatures are coolest in the Greenwood district and west-central part of the basin. The warmest measured temperatures occur in the south-central part of the valley and are connected to the Meadow and Hatton Hot Springs geothermal field having measured temperatures up to 40.5°C. The mean temperature for each district is 15.9°C for Kanosh, 14.1°C for Meadow, 14.8°C for Flowell, 17.7°C for Pahvant, 15.8°C for Greenwood, and 18.3°C for McCornick.

Total Dissolved Solids

The available water quality samples in Pahvant Valley have various reporting agencies, water sources, water types, analyte suites, analysis methods, and span a wide range of time. One common analyte among these various sources is total dissolved solids (TDS) concentration reported in milligrams

Table 10. *Summary of discharge values in 2022 calculated for Pahvant Valley.*

Category	Description	Mean (ac-ft)	Std. Dev (ac-ft/yr)
Wells	Irrigation Wells	143,362	7881
	Stock Wells	26	2
	Domestic Wells	808	63
	Municipal Wells	1270	30
	Industrial Wells	137	15
	Total Wells	**145,603**	**7880**
Springs and Shallow Groundwater	Groundwater ET (includes Clear Lake Flow)	3917	1567
	Other Valley Springs	907	100
	Total Groundwater ET and Springs	4824	1663
	Total Discharge	**150,427**	**8056**
	Change In Storage	**-81,549**	**5539**
	Recharge	**68,878**	**9775**

Table 11. *Estimated groundwater discharge values from 2016 to 2022 for Pahvant Valley. These discharge values, with the exception of 2022, are based on OpenET data (Melton et al., 2021) and USGS well pumping estimates (U.S. Geological Survey, 2021).*

Year	Discharge	Storage	Recharge	Pahvant Range Precip
2016	117,981	-36,560	81,422	383,755
2017	113,451	4670	118,120	418,641
2018	131,941	-68,493	63,448	468,556
2019	110,699	83,764	194,463	372,218
2020	150,415	-71,810	78,605	505,999
2021	154,574	-124,475	30,099	287,133
2022	149,790	-81,549	68,241	384,477
AVG	**132,693**	**-42,065**	**90,628**	**402,968**
Med	**131,941**	**-68,493**	**78,605**	

per liter (mg/L). Using TDS data, we differentiated between groundwater sampled from wells, surface water sampled from streams, and spring water sources. Figure 25 shows the distribution of TDS concentration as broken out by water type. Spring water TDS ranged from 212 to 4960 mg/L with a mean of 1520 mg/L, although concentrations are trimodally distributed with the majority of TDS concentrations less than 400 mg/L. Surface water TDS ranged from 128 to 582 mg/L and had a mean of 232 mg/L. Groundwater TDS ranged from 63 to 11,450 mg/L with a mean of 1684 mg/L. By plotting TDS concentrations spatially, we are able to see distinctions between the uplands and lowlands of Pahvant Valley's various discharge points (Figure 26). In general, TDS in groundwater increases from east to west, and from north to south, as groundwater flows from recharge locations within and along the mountain fronts to discharge points to the west (Figure 26).

Holmes and Thiros (1990) analyzed water quality changes over time, concluding that seepage of irrigation water to the unconfined aquifer within the Kanosh district led to an increase in TDS due to evaporative concentration of dissolved salts in applied irrigation water. Additionally, deeper wells in the Kanosh area and springs issuing from the valley floor west of the main agricultural center of Kanosh record higher TDS than the valley-fill aquifer mean. Two apparent factors are influencing higher TDS in Kanosh: 1) recycled irrigation water and 2) groundwater flowing from the Black Rock Desert.

Groundwater flowing into the Kanosh area originates from the southern Pahvant Range and Black Rock Desert. Surface water flowing from Corn Creek, which recharges the valley-fill aquifer, is almost entirely consumed within the Meadow district with lesser amounts making it to the eastern Kanosh district. Wells within the Kanosh district generally have TDS concentrations above the mean values of all other districts (Table 13). Total dissolved solid values in the Kanosh shallow aquifer are lower than the deeper groundwater in the same area. Due to its proximity to the Black Rock Desert, the Meadow and Hatton Hot Springs geothermal field, and the southern toe of the Pahvant Range, Kanosh is uniquely positioned between three groundwater sources compared to the other districts within Pahvant Valley. Unconsolidated valley-fill thicknesses in the Kanosh area range between 250 and 400 feet, below which volcanic deposits from the Black Rock volcano interfinger with Tertiary clay, silt, and sand transported by streams draining the Pahvant Range (Oviatt, 1991).

Table 12. *Estimated groundwater recharge from 1960 to 2022 based on linear relationship between groundwater storage changes and recharge from 2016 to 2022.*

Year	Change in Groundwater Storage			Estimated Recharge[1] (ac-ft)	Estimated Pumping (ac-ft)	Cumulative Storage Change (ac-ft)
	Median (ac-ft)	Mean (ac-ft)	Std. Dev. (ac-ft)			
1960	-39,293	-39,663	2557	94,887	66,000	-39,293
1961	-41,475	-41,896	2502	93,134	66,000	-80,768
1962	16,245	16,384	2134	138,883	62,000	-64,523
1963	-56,676	-57,229	3444	81,097	80,000	-121,199
1964	-20,212	-20,432	1423	109,983	72,000	-141,411
1965	26,405	26,649	2378	146,942	69,000	-115,005
1966	-50,641	-51,107	3039	85,903	84,000	-165,647
1967	-38,673	-39,028	2665	95,385	76,000	-204,320
1968	43,904	44,305	3301	160,801	62,000	-160,416
1969	8319	8394	1337	132,612	77,000	-15,2098
1970	2527	2561	1284	128,033	73,000	-14,9571
1971	30,707	30,985	2863	150,345	77,000	-118,863
1972	-83,077	-83,809	5231	60,232	95,000	-201,940
1973	96,483	97,463	6399	202,531	70,000	-105,458
1974	17,718	17,907	1468	140,079	82,000	-87,740
1975	-4996	-5042	1461	122,064	83,000	-92,736
1976	-57,088	-57,655	4404	80,763	88,000	-149,824
1977	-98,218	-99,124	5621	48,210	96,000	-248,042
1978	44,450	44,930	2683	161,292	79,000	-203,592
1979	-23,705	-23,921	1784	107,244	85,000	-227,296
1980	65,900	66,546	4699	178,261	77,000	-161,397
1981	-45,577	-45,986	2983	89,923	83,000	-206,974
1982	-18,405	-18,549	3619	111,461	70,000	-225,379
1983	156,876	158,484	9364	250,432	42,000	-68,503
1984	171,148	172,960	9816	261,796	42,000	102,646
1985	5786	5857	1539	130,619	62,000	108,432
1986	22,580	22,785	1616	143,908	60,000	131,012
1987	-26,002	-26,275	2059	105,396	66,000	105,010
1988	-6294	-6364	1894	121,026	71,000	98,716
1989	-57,931	-58,527	4061	80,078	82,000	40,785
1990	-88,920	-89,759	5072	55,561	88,000	-48,136
1991	-20,649	-20,869	1947	109,639	74,000	-68,785
1992	-53,640	-54,209	3733	83,468	86,000	-122,425
1993	-10,894	-11,003	1633	117,384	87,000	-133,318
1994	-64,772	-65,404	4140	74,680	93,000	-198,090
1995	61,101	61,717	3534	174,470	69,000	-136,989
1996	-86,803	-87,624	5270	57,237	83,000	-223,792
1997	4394	4470	1511	129,531	67,000	-219,398
1998	37,300	37,618	2914	155,552	66,000	-182,098
1999	-18,800	-18,949	2438	111,147	76,000	-200,897
2000	-47,038	-47,474	3316	88,755	80,000	-247,935
2001	-58,878	-59,456	5136	79,349	80,000	-306,813
2002	-102,392	-103,445	7074	44,818	89,000	-409,206
2003	-34,876	-35,209	2135	98,383	86,000	-444,082
2004	-35,718	-36,068	2758	97,709	85,000	-479,800

[1] Calculated based on the relationship: recharge = 0.785 * change in groundwater storage + 126,022

Table 12 Continued. *Estimated groundwater recharge from 1960 to 2022 based on linear relationship between groundwater storage changes and recharge from 2016 to 2022.*

Year	Change in Groundwater Storage			Estimated Recharge[1] (ac-ft)	Estimated Pumping (ac-ft)	Cumulative Storage Change (ac-ft)
	Median (ac-ft)	Mean (ac-ft)	Std. Dev. (ac-ft)			
2005	32,791	33,071	2227	151,983	80,000	-447,009
2006	-41,329	-41,740	2748	93,256	86,000	-488,338
2007	-47,626	-48,139	4465	88,233	89,000	-535,964
2008	-25,155	-25,421	3423	106,067	94,000	-561,118
2009	-43,823	-44,278	3329	91,264	104,000	-604,942
2010	-30,854	-31,108	3345	101,602	106,000	-635,796
2011	119,785	121,016	7507	221,019	89,000	-516,010
2012	-65,144	-65,772	4022	74,391	114,000	-581,155
2013	-24,791	-25,027	4821	106,376	103,000	-605,945
2014	-55,969	-56,477	5666	81,687	118,000	-661,915
2015	-104,865	-105,910	6447	42,883	128,000	-766,780
2016	-36,560	-36,940	2554	97,024	114,000	-803,340
2017	4670	4717	1773	129,725	110,000	-798,670
2018	-68,493	-69,151	4192	71,738	119,800	-867,163
2019	83,764	84,638	8026	192,463	108,430	-783,399
2020	-71,810	-72,533	5742	69,084	142,387	-855,209
2021	-124,475	-125,748	10,307	27,310	149,380	-979,684
2022	-81,549	-82,323	5539	61,398	145,600	-1,061,232
Sum	-1,061,232	-1,071,189	Average	112,675		
			Median	105,396		
			Std. Dev.	47,626		

[1] Calculated based on the relationship: recharge = 0.785 * change in groundwater storage + 126,022

Older irrigation wells drilled in Kanosh were completed in the shallow unconfined valley-fill aquifer containing groundwater with lower TDS concentrations. As groundwater levels declined in the area and some of the original wells in the area were replaced, well drillers reported poor water quality at deeper depths, with TDS concentrations up to 8850 mg/L (WIN 31756). The water quality was deemed unsuitable for irrigation, and the replacement wells were sometimes abandoned in favor of refurbishing the original wells in the area. Recycling of irrigation water in Kanosh can help explain local increases in TDS over time, but higher concentrations of TDS at depth indicate a separate source of groundwater, of which the chemical makeup correlates more closely with water sampled from Squidike Spring and Meadow Hot Springs.

Groundwater Types

The groundwater characteristics in Pahvant Valley exhibit geographical variations influenced by recharge sources and discharge locations. Valley-fill groundwater exhibits a distinct shift in cation trends from calcium to sodium-potassium type, whereas anion trends progress from bicarbonate to a mixed bicarbonate-chloride type (Figure 27). Orange arrows on Figure 27 show groundwater maturation from a more dilute to less dilute water type. This generally follows the conceptual groundwater flow path from mountain front to valley-fill aquifer then to volcanic aquifer, and finally to Clear Lake.

Surface water samples were collected from four different streams in the Pahvant Range during baseflow conditions in late autumn 2022 and are representative of groundwater released by rocks within the range. Surface water has a dilute calcium-magnesium-bicarbonate water type.

Groundwater in the Kanosh area and north to Squidike Spring, which is located between the Ice Springs and Tabernacle Hill basalt flows, tends to be more sodium-potassium type, evolving into a mixed type, with chloride dominating the anion composition. Along a western longitude, extending from Kanosh in the south to Clear Lake Spring in the north, cations generally exhibit a sodium-potassium type, with some transitioning into a mixed type. Anions in this region are predominantly chloride type, with some instances of a mixed type.

Water quality samples collected from the Black Rock region of the study area and the region west of the mapped volcanic aquifer (Figure 26) group separately from the valley-fill and volcanic aquifer water samples. Black Rock samples are of sodium-chloride type. The Black Rock anions plot closely

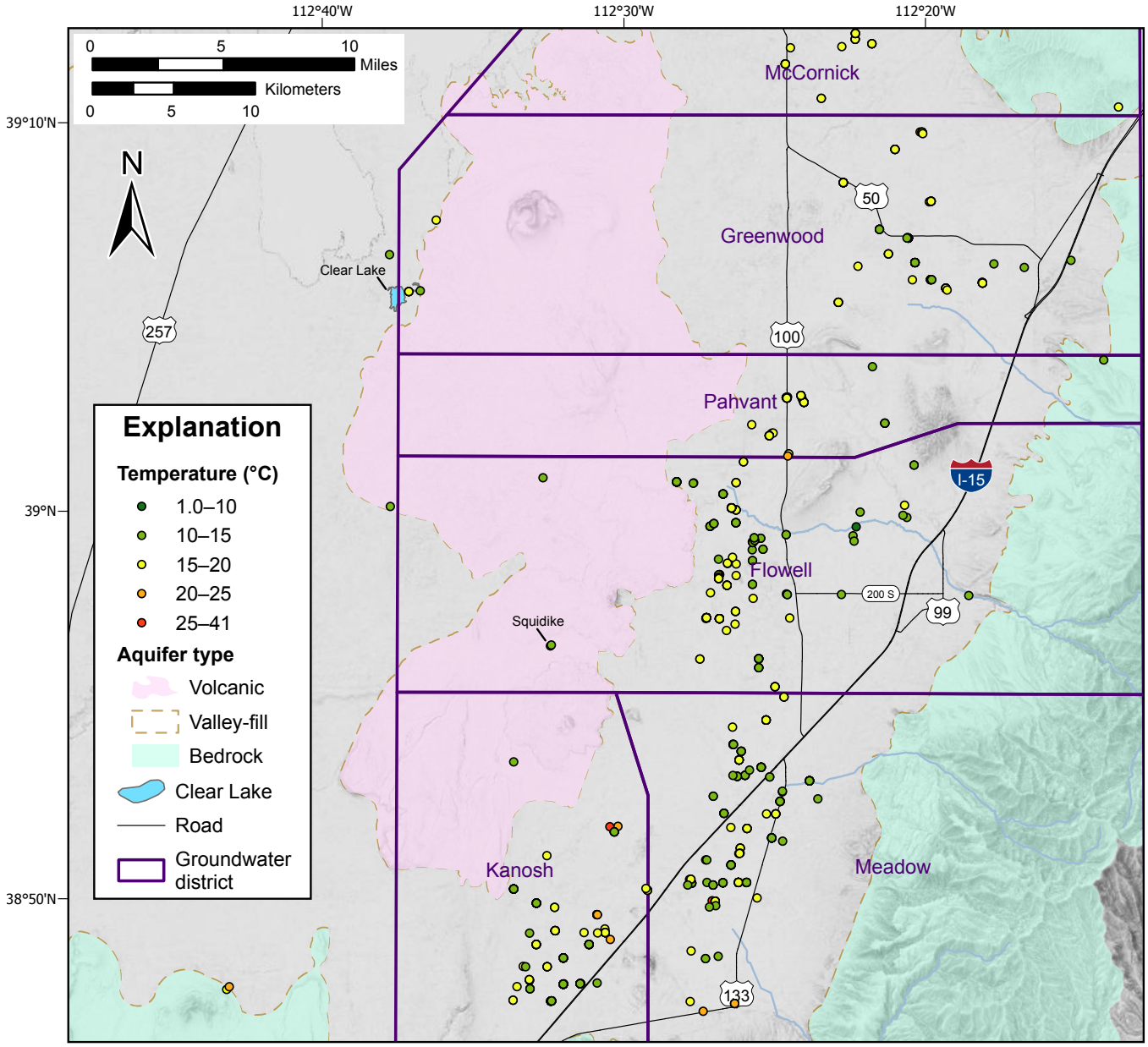

Figure 24. *Groundwater temperatures throughout the Pahvant study area. See Appendix D for data.*

with those of the Meadow Hot Springs, volcanic, Clear Lake, and with a small number of valley-fill water samples. The Black Rock cations plot separately from these other sources, and when viewed within the piper triangle matrix, their distinct grouping indicates a separate groundwater flow path from the Black Rock Desert into Pahvant Valley.

Multivariate cluster analysis allows for a statistically significant quantification of groundwater without the bias of pre-determined geographic or other delineations. We used multivariate cluster analysis to identify three separate groupings of water chemistry types (Figure 28). The analysis showed a relatively homogenous groundwater type along the piedmont of the Pahvant Range, the largest singular recharge region within the study area. Sampling points downgradient of the range should exhibit chemical characteristic similarities, which our analysis confirms.

Two unique water types exist in the southern region of the study area. As groundwater flows downgradient, mixing is noted until discharge at Clear Lake. Cluster types 1 and 2 are distributed in the southern and west-central part of the valley within the Hatton and Kanosh areas. They are chemically differentiated primarily by their chloride and sodium (mg/L) concentrations. Cluster type 1 groundwater is derived from a shallower aquifer system that receives recharge from the unconfined valley-fill aquifer, which is composed of interbedded and unconsolidated sediments with thin and infrequent volcanic lenses. Groundwater from cluster type 2 comes from a deeper aquifer unit that has a higher percentage of volcanics, likely longer groundwater residence times, and lesser quantities of dilute recharge waters. Cross-section C-C′ on Figure 12 illustrates these two shallow and deeper aquifer systems. Wells WIN 3803, WIN 3800, WIN 2966, and WIN 2965 are

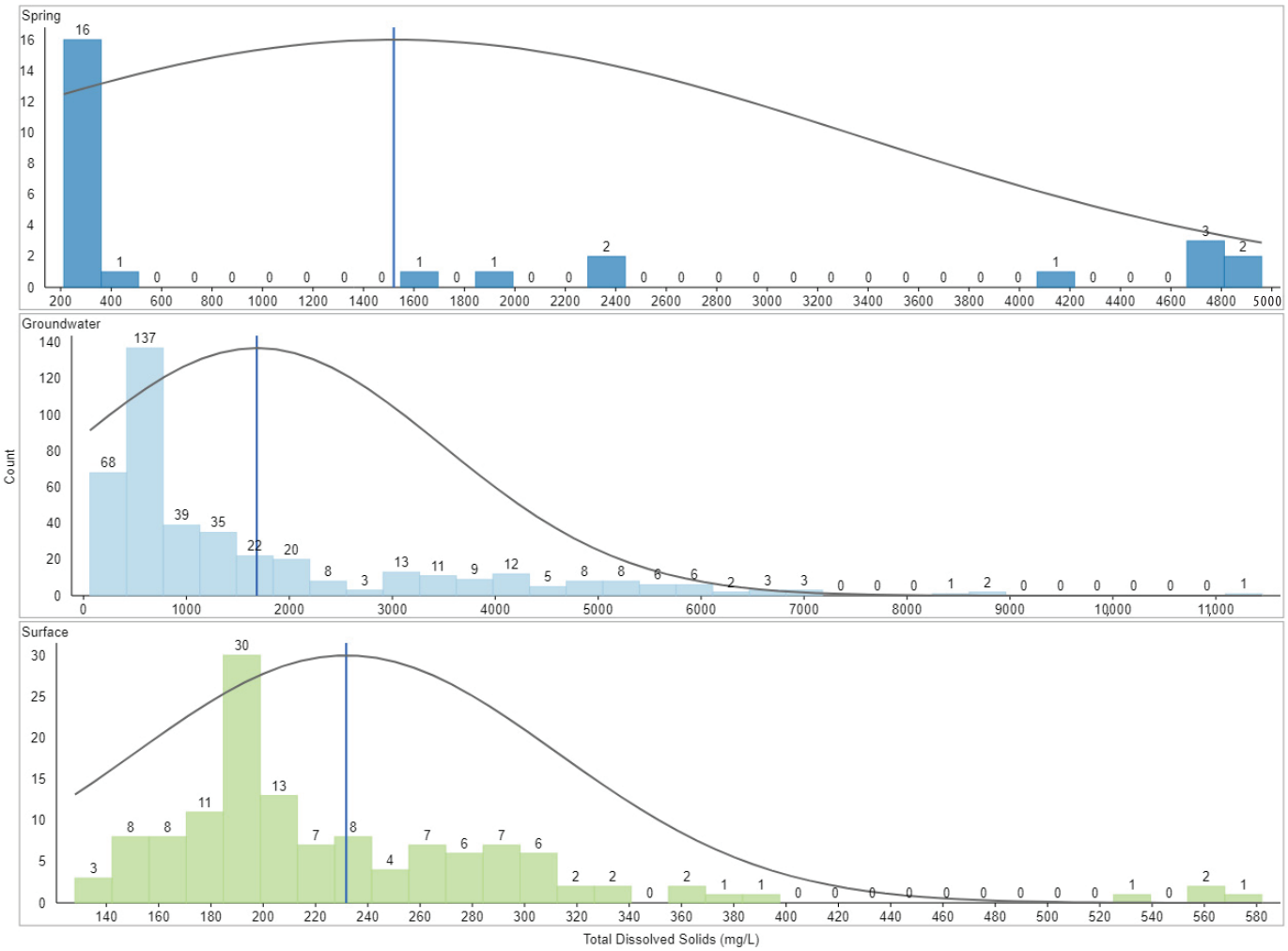

Figure 25. *Total dissolved solid concentrations grouped by water source. Normal distribution curves about the vertical mean line (dark blue) indicate values near the mean occur more frequently than values further from the mean.*

drilled and completed into the shallow aquifer within cluster type 1 in conceptual zone 2. Additionally, WIN 3802 is completed in the deeper aquifer within cluster type 2 also in conceptual zone 2. Several thin clay confining beds separate the shallow and deep aquifers. The lateral extent of these confining units is not well constrained, but they likely extend westward into the main region of the volcanic aquifer.

Stable Isotopes

Stable isotopes deuterium (^{2}H) and oxygen-18 (^{18}O) laboratory results are reported (Figure 29) in ratios of $^{2}H/^{1}H$ and $^{18}O/^{16}O$ in delta notation (δ) as per mill (‰) against the standard reference of Vienna Standard Mean Ocean Water (Gonfiantini, 1978). The ratio values were plotted and compared against a local meteoric water line (LMWL). The LMWL was calculated using linear regression for the total number of precipitation samples. Stable isotope ratios from groundwater, precipitation, and surface water vary widely from -164.35‰ to -36.50‰ $\delta^{2}H$ and -21.66‰ to -4.60‰ $\delta^{18}O$ across Pahvant Valley and area mountains (Figure 29). Springs typically fall right of the LMWL indicating enrichment (i.e., less negative ratios) due to evaporation from typical groundwater. Considering likely evaporative influences and one standard deviation laboratory uncertainty of 0.6‰ $\delta^{2}H$ and 0.1‰ $\delta^{18}O$, most of the surface water and groundwater samples have indistinguishable isotope ratios. Some groundwater is more enriched than surface water. Evaporation in spring samples is logical because many of the samples had to be collected in open pools that were actively evaporating, including Meadow Hot Springs and Clear Lake Spring. The Clear Lake best fit line on Figure 29 plots along a discrete evaporative line for Clear Lake samples. The Clear Lake best fit line intercepts the LMWL at values slightly less negative than most of the agricultural groundwater well samples. Because Clear Lake is the regional discharge point, and not all wells in the study area could be sampled for stable isotopes, we consider this best fit line to be representative of a more evaporated signal. Sampling limitations at Clear Lake only allowed for sampling from the evaporating spring pool. The hot springs show horizontal offset in $\delta^{18}O$ from the LMWL. This offset is potentially due to an increased rate of isotopic exchange with silicate rock at higher temperatures, a well-documented effect in thermal springs (Diamond, 2022). Because the observed deviation is close to LMWL, we did not

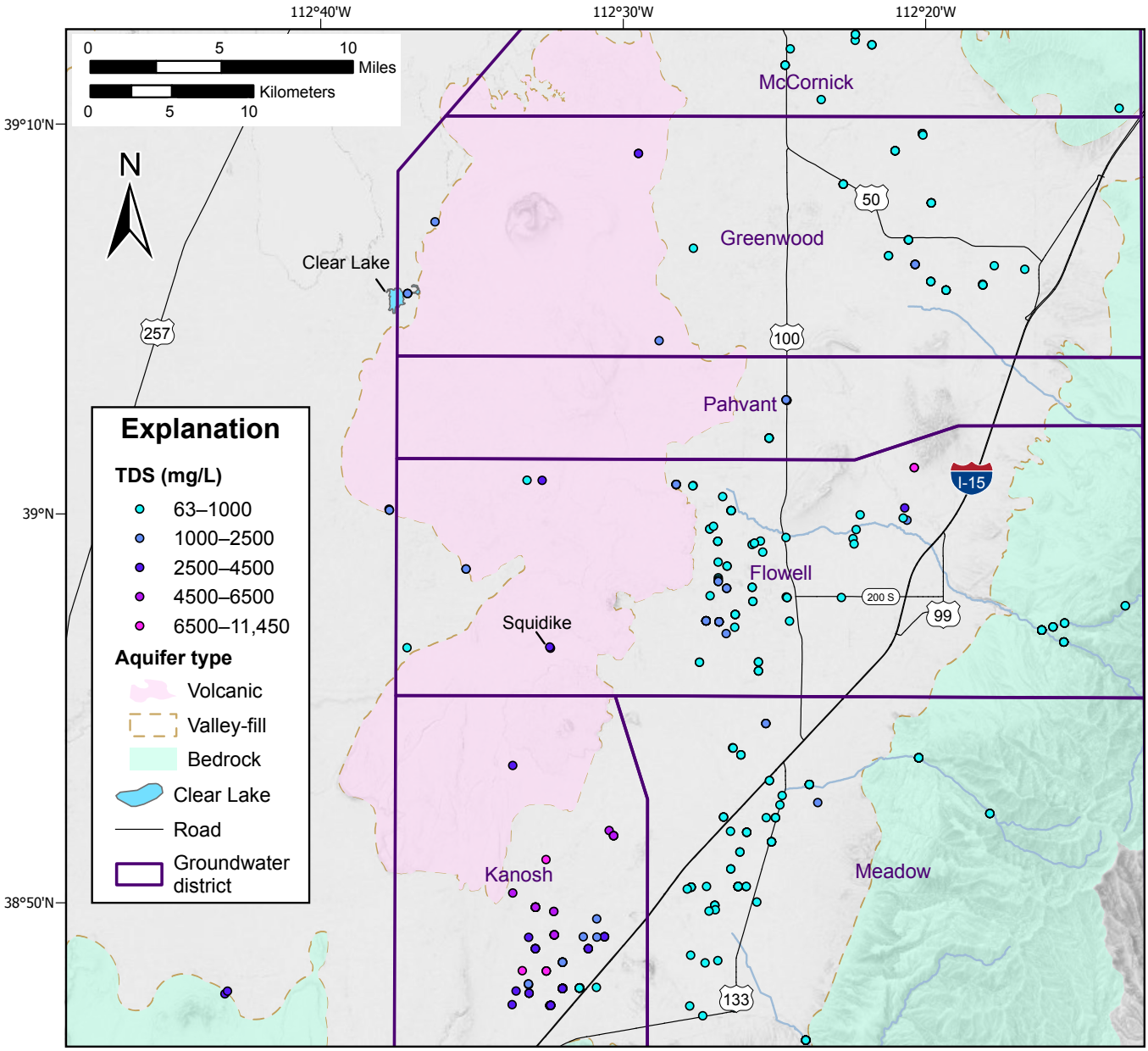

Figure 26. *Total dissolved solid concentrations of water quality samples plotted by location.*

Table 13. *Total dissolved solids (TDS) concentration statistics of groundwater districts in Pahvant Valley.*

Groundwater district	Mean TDS (mg/L)	Minimum TDS (mg/L)	Maximum TDS (mg/L)	Number of samples
Meadow	496	128	6970	311
McCornick	411	63	562	30
Greenwood	781	263	3064	136
Pahvant	999	683	1443	53
Flowell	759	136	11,450	340
Kanosh	3484	469	8850	210

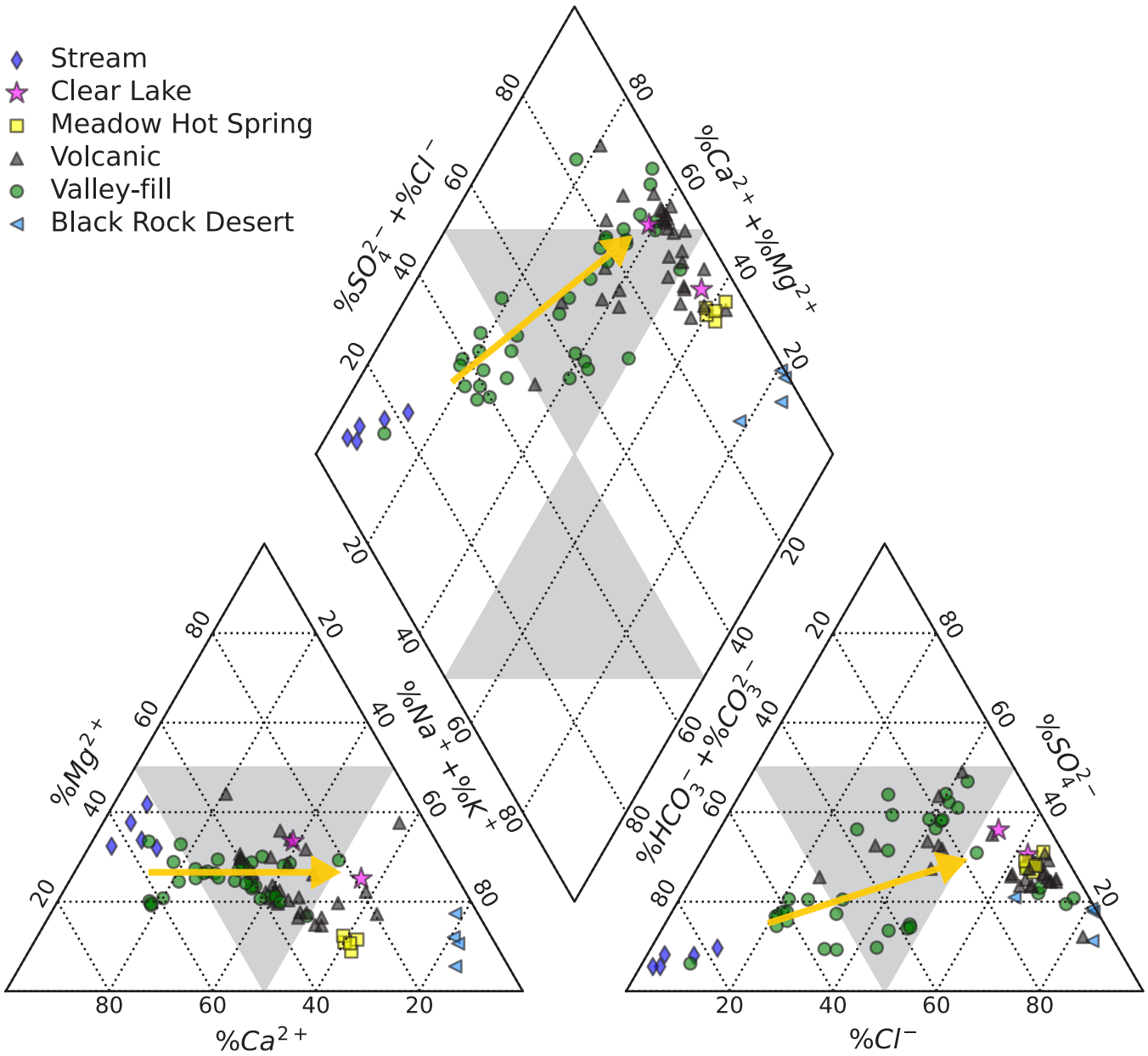

Figure 27. *Piper diagram of general chemistry of water quality samples collected in Pahvant Valley classifying water types to visualize the chemical composition of water samples. The left and right triangular fields are the cations (calcium, magnesium, sodium, potassium) and anions (carbonate, bicarbonate, sulfate, chloride), respectively. Orange arrows show evolution of valley-fill water from the Pahvant Range front towards Clear Lake.*

attribute the discrepancies to natural variation. Samples fall closer to winter precipitation than to summer precipitation on the LMWL, which likely indicates snowmelt-dominated contributions to recharge and streamflow.

Stable isotope and chemical analyses indicate that stream discharge from the Pahvant Range is closely related to the pumped groundwater, and that stream flow serves as the primary source of recharge for the valley-fill aquifer. Deuterium ratios between groundwater and surface water reside within the -115 to -120‰ δ^2H range indicating similar timing of recharge (Figure 30). Additionally, stream and groundwater isotopes exhibit an evaporative signal similar to sublimated snow (Lechler and Niemi, 2012). Springs, streams, and groundwater each have ranges within ±9‰ δ^2H. Springs and streams range from -110 to -119‰ δ^2H and groundwater ranges from -114 to 123‰ δ^2H. Streams were sampled during baseflow in late November 2022 and are considered representative of groundwater discharging from rocks in the Pahvant Range. The shift towards more depleted (i.e., more negative) δ^2H ratios in groundwater could be indicative of multiple sources of recharge contributing to the valley aquifer system. Both observations support that snowmelt is the primary source of water recharging the aquifers of Pahvant Valley.

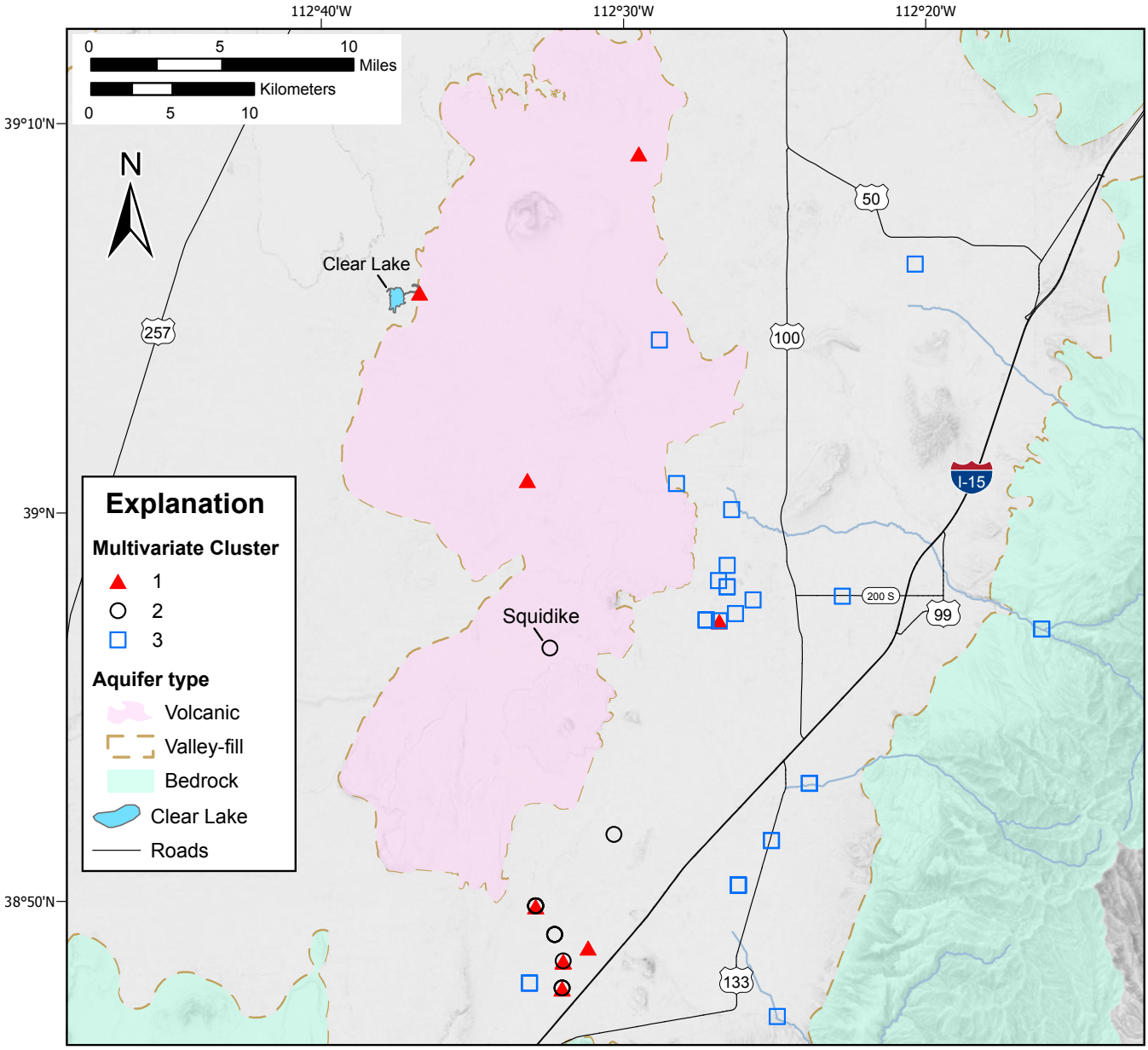

Figure 28. *K-means multivariate cluster analysis of water quality samples plotted by location showing regions of similar water chemistry.*

Radioactive Isotopes

Tritium concentrations range from 0.05 to 2.15 TU (Table 14). Samples with concentrations less than 0.5 TU have residence times (i.e., time from recharge to the water table to laboratory analysis) greater than approximately 60 years; samples having a TU value between 0.5 and 2.0 TU may contain a mixture of groundwater greater and less than 60 years in age. Samples having tritium concentrations of 2.0 TU or greater were recharged less than 60 years ago. The collection of dissolved gas samples would enable a more precise estimation of groundwater residence times from tritium concentrations. Tritium and carbon-14 results for Clear Lake and Squidike Spring indicate modern and mixed groundwater age, respectively, possibly indicating shorter residence times and thus recharge areas adjacent to those sampling points (Table 14; Figure 31).

The Zubeck well carbon-14 results suggest a premodern age and long groundwater transit times (Figure 31). This well is located down gradient of Clear Lake and the Spring Lake spring head. The well is completed at a depth of 530 feet in the terminus of the unconsolidated valley fill, in primarily silty clay and other clay deposits.

Meadow Hot Springs $\delta^{13}C$ analysis indicates a strong carbonate signal (Figure 31). Mountain groundwater recharges through the carbonate basement rocks underlying the valley-fill aquifer (Hintze et al., 2008) at an estimated depth of 1.5 to 2.5 miles below ground surface. Short strings of normal faults bisect the valley floor west of Meadow Hot Springs (Oviatt, 1991; Hintze et al., 2008) and may inhibit horizontal groundwater flow at depth. These faults then act as near vertical conduits for fluid flow for deep older groundwater.

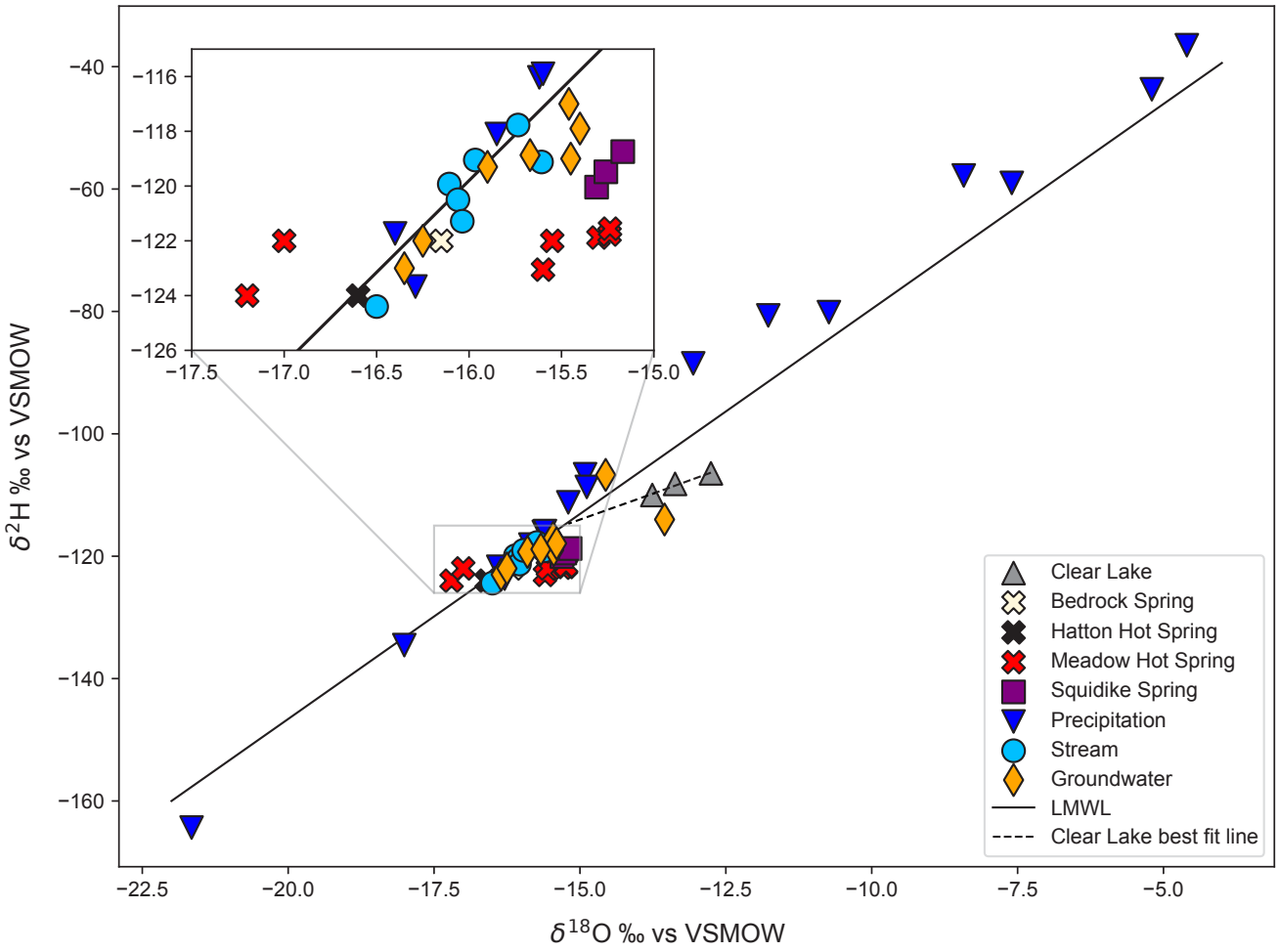

Figure 29. *Stable isotope ratios for water samples in the Pahvant region.*

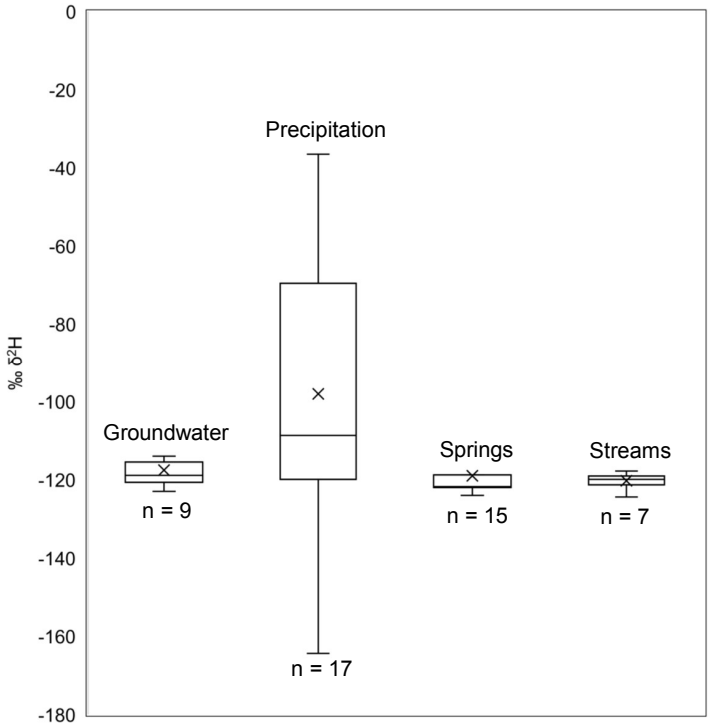

Figure 30. *Comparison of δ^2H ranges for water samples in the Pahvant region.*

Table 14. *Tritium and radiocarbon concentrations, carbon isotope ratios, and radiocarbon model age results (Fontes and Garnier, 1979).*

	Tritrium			Carbon-14					
Site Name	Sample Date	Concentration (TU)	Qualitative age	Sample Date	Concentration (pmC)	d¹³C (‰)	Uncorrected age (yr B.P.)	Fontes and Garnier correction age (yr B.P.)	Modified Fontes and Garnier correction age (yr B.P.)
Squidike Spring	4/14/2023	0.65	mixed	11/7/2022	40.08	-6.45	7340	--	*--
Meadow Hot Spring Pool 1	4/14/2023	0.05	pre-modern	11/7/2022	1.43	-0.71	34,100	--	--
Meadow Hot Spring Pool 2	4/14/2023	0.08	pre-modern	--	--	--	--	--	--
Clear Lake	4/14/2023	2.15	modern	11/8/2022	75.16	-5.73	2290	--	*--
Zubeck Well	--	--	--	11/9/2022	28.66	-11.19	10,040	30,018	4236

* Null value indicates a given model resulted in a negative age

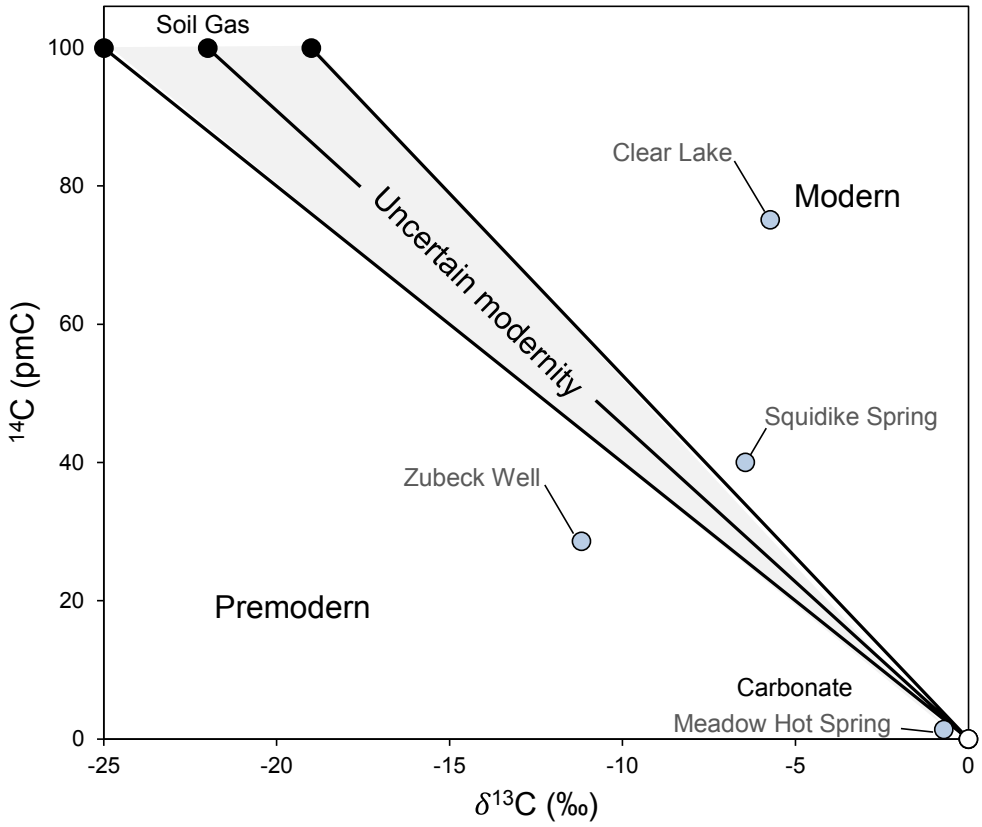

Figure 31. *Carbon isotopes in groundwater samples and simple mixing lines.*

The strong carbonate $\delta^{13}C$ signal (-0.71‰) likely indicates that the uncorrected age of 34,000 years BP is heavily biased towards older ages due to the presence of "dead" ^{14}C from water-rock reactions with carbonate rocks. Discharge at Meadow Hot Springs has likely experienced substantial dissolution/precipitation in contact with Paleozoic and Mesozoic carbonate rocks at high temperatures, replacing the original groundwater ^{14}C with radiocarbon-dead carbon from the host rocks. Noble gas radioisotope age dating would better constrain the age of groundwater discharging from Meadow Hot Springs.

CONCLUSION

Conceptual Groundwater Model

Groundwater in Pahvant Valley presents in a variety of locations, geologic conditions, hydraulic head conditions, chemistry, and flow paths. Groundwater typically flows from upland areas of higher elevation or hydraulic potential head down in elevation and areas of lower head potential. Generally, groundwater recharges within the Pahvant Range and Canyon

Mountains alluvial fans, flows towards the volcanic aquifer, and discharges to Clear Lake. Precipitation falling directly onto the volcanic aquifer contributes less, but significant amounts of recharge to the system.

Conceptual Groundwater Zones

Based on the geologic and hydrologic data presented in this report, we delineated three conceptual groundwater zones. Figure 32 shows conceptual groundwater zones that are delineated based on areas of shared hydrogeologic, geochemical, and potentiometric characteristics within the valley. These conceptual groundwater zones are closely linked, and rely on one another to buffer water quality, hydraulic gradient, and groundwater storage.

Conceptual groundwater zone 1 is delineated along the Canyon Mountains and Pahvant Range fronts (Figure 32). The principal aquifer in this zone is the valley-fill aquifer, which is continuous in extent from the southern slope of the Canyon Mountains to the southern terminus of the Pahvant Range. In this zone, the valley-fill aquifer is east of and adjacent to the Ice Springs basalt flow in the Flowell groundwater district, which contains interbedded clay, sand, and gravel layers that have historically had the highest hydraulic head to produce artesian aquifer conditions. The western boundary of conceptual groundwater zone 1 resides along the eastern edge of the volcanic aquifer, and the thick clay deposits north of the valley-fill aquifer and west of the McCornick groundwater district.

Thickness of the valley-fill aquifer within conceptual groundwater zone 1 varies throughout Pahvant Valley from tens of feet to over one thousand feet. Tertiary-age Oak City Formation is deposited overtop the overturned Paleozoic and Mesozoic rocks, which comprise much of the Pahvant Range. The Oak City Formation underlies much of the alluvial-fan deposits adjacent to the Pahvant Range. Valley-fill aquifer thicknesses increase from east to west, and from south to north. Confining units within the valley-fill aquifer in zone 1 create confined and unconfined conditions throughout the valley. Artesian conditions have been documented at wells completed within the valley-fill aquifer from the McCornick to Flowell groundwater districts, but at the time of this report no flowing wells were observed or reported. The confined part of the valley-fill aquifer in conceptual groundwater zone 1 within the Flowell groundwater district produces some of the greatest yields from wells within the study area. Farther south in the Meadow groundwater district, the valley-fill aquifer in conceptual groundwater zone 1 is unconfined with more poorly sorted alluvial deposits. Lastly, in the southernmost part of this zone in the Kanosh district, the alluvium is less thick and underlain by the Oak City Formation and volcanics of the Black Rock Desert. Several wells are completed within the Oak City Formation and volcanics (cross-section C-C′ on Figure 12) with lesser yields than those completed in the conceptual groundwater zone 1 valley-fill aquifer.

Groundwater elevations decrease from east to west from 5100 feet to 4547 feet with a mean elevation of 4668 feet above sea level. Observed groundwater level changes from 1987 to 2022 in conceptual groundwater zone 1 ranged between +1.27 to -163.7 feet. Groundwater chemistry in zone 1 contains a heterogenous mixture of magnesium bicarbonate and calcium chloride water types.

We consider conceptual groundwater zone 1 to be Pahvant Valley's largest aquifer containing areas of water quality fit for human consumption and also adequate potential yield for economic use. This zone covers a vast part of the study area, and serves the most communities, farms, and industries within the valley. In the future it will be important to record instantaneous streamflow from watersheds draining the Pahvant Range to safeguard and better understand inflows to this valuable resource.

Conceptual groundwater zone 2 is delineated along the northern extent of the Black Rock Desert located in the southern region of the Pahvant study area. The southern boundary is delineated as the topographic divide along the crest of the Black Rock Desert, the western boundary along the southeastern piedmont of the Cricket Mountains, and the northern terminus as the southern extent of Tabernacle Hill volcanics. The subsurface in zone 2 is composed of interbedded volcanic deposits and Quaternary- to Tertiary-age unconsolidated to semi-consolidated alluvial and fluvial deposits. Groundwater quality degrades with depth, and groundwater elevations decrease from south to north from 4999 feet to 4635 feet with a mean elevation of 4698 feet above sea level. Groundwater level fluctuations in conceptual groundwater zone 2 ranged from +79 feet to -79 feet with a mean change of -34.9 feet from the late 1980s until the spring of 2022. Groundwater chemistry in zone 2 is distinct with more homogeneity and less apparent mixing compared to conceptual groundwater zone 1. Groundwater in zone 2 is sodium chloride type where sodium and potassium are the predominant cations, and chloride is the dominant anion.

The upper part of the conceptual groundwater zone 2 aquifer is currently stressed. Changes in storage, the recycling of irrigation water within the shallow unconfined valley-fill aquifer, and reduced volumes of recharge due to recent drought conditions in Utah have resulted in increased TDS concentrations to the extent that groundwater usage for irrigation or livestock is not possible in select locations. Water quality degradation within zone 2 continues to be of primary concern for area water users.

Conceptual groundwater zone 3 is the volcanic aquifer that extends throughout the central region of the study area. The volcanic aquifer of zone 3 extends from just south of Tabernacle Hill to north of Pahvant Butte. It is a composition of blocky "A'ā'" lava flows, rhyolitic deposits, basalt flows, numerous cinder cones, and tuff deposits. Precipitation falling directly onto the

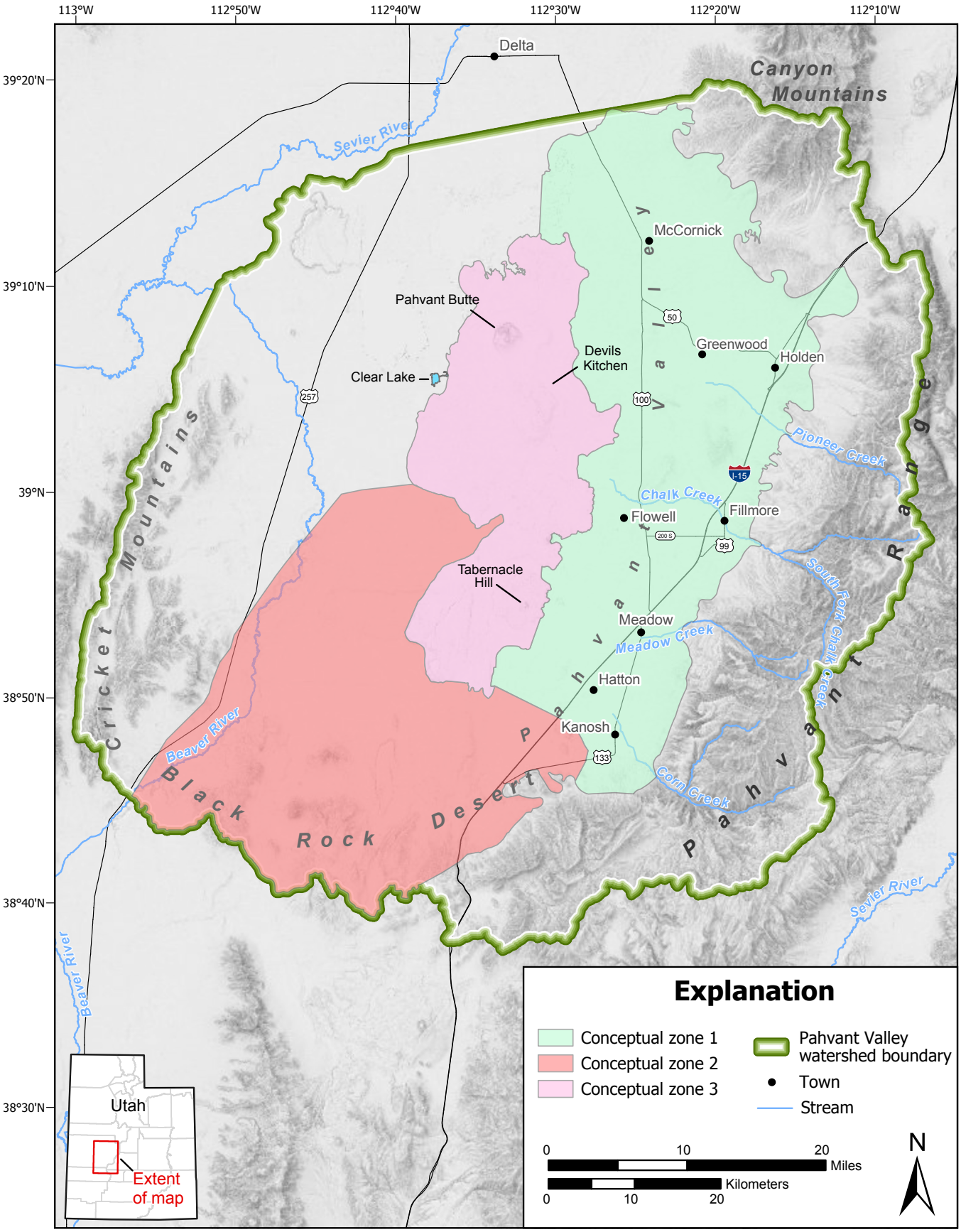

Figure 32. *Conceptual groundwater zones within Pahvant Valley that illustrate separate sources of groundwater and the possibility of groundwater mixing as groundwater flows to Clear Lake.*

volcanic aquifer infiltrates quickly and is added to the groundwater flowing into the aquifer by seepage from the valley-fill aquifer. Groundwater elevations decrease from south to north from 4821 feet to 4570 feet with a mean elevation of 4641 feet above sea level. Groundwater elevation changed between +8.3 feet to -15.6 feet with a mean decline of 4.3 feet from the late 1980s until spring of 2022. Groundwater in the volcanic aquifer in conceptual groundwater zone 3 is generally a mixture of sodium-chloride and calcium-chloride water types.

The conceptual groundwater zone 3 volcanic aquifer plays a key role in regional agriculture and the Pahvant Valley aquifer system at large. Production wells completed in the zone 3 volcanic aquifer have measured some of the highest pumping rates of any in the area. Here, the volcanic aquifer is also the sole source for spring water flowing into Clear Lake. Wells completed in the volcanic aquifer are somewhat limited geographically due to the difficulty of travel and land development over much of the area of the rocky and fractured aquifer. Although direct infiltration of precipitation plays a role in recharge to the volcanic aquifer in zone 3, the primary source of recharge is the valley-fill aquifer of conceptual groundwater zone 1. Reductions in groundwater elevations within the valley-fill aquifer regions east of the conceptual groundwater zone 3 volcanic aquifer have decreased hydraulic potential head and introduced a reversal of the historical groundwater gradient which once produced artesian conditions in western Flowell groundwater district while also buffering groundwater flowing into the conceptual groundwater zone 3 volcanic aquifer. Clear Lake flow records indicate the influence that zone 1 valley-fill aquifer pumping has on the conceptual groundwater zone 3 volcanic aquifer groundwater elevations, gradient, and discharge to Clear Lake (Figure 26).

Figure 3 shows a conceptual block diagram of Pahvant Valley and the primary aquifer systems within. Precipitation falling on the Pahvant Range infiltrates directly to bedrock or the mountain-adjacent alluvial fan of conceptual groundwater zone 1. Groundwater from the south in conceptual groundwater zone 2 generally moves northward through the volcanics of the Black Rock Desert before encountering volcanics of conceptual groundwater zone 3. Groundwater within conceptual groundwater zone 3 flows northward, eventually discharging at Clear Lake. The waters within conceptual groundwater zone 3 represents a mixture of conceptual groundwater zones 1 and 2.

Groundwater Budget and Water Use Effects

Table 12 summarizes the recharge over the past several decades, showing that years where groundwater recharge exceeds discharge are punctuated by se.veral years. Decrease in storage occurred in 42 of 62 years between 1960 and 2022 (about two-thirds of the years). Long-term estimated average recharge is higher than that displayed in Table 11, likely skewed by the anomalous recharge events of the early 1980s. Despite years where recharge exceeds discharge, cumulative loss in groundwater storage from 1960 to 2022 amounts to more than 1 million ac-ft (Table 12).

Determining the individual sources of recharge is beyond the scope of this study. Our goal was to determine the total discharge out of the groundwater system, as well as the storage changes, allowing us to estimate the total recharge as the residual. Based on our recharge-discharge map, recharge via infiltration occurs over the basalt aquifer, as well as near the alluvial fans on the eastern margin of the valley. Based on our ET data (Appendix C), infiltration from irrigation is likely occurring at the fields adjacent to the basalt aquifer. Unlined canals flowing over the valley-fill aquifer generally lose water to groundwater, as documented in the Central Utah Canal. We suspect very little water is recharging from the subsurface, but this number has not been rigorously calculated or measured.

Key findings from our study indicate that a marked increase in groundwater consumption is driven primarily by agricultural activities. Evidence includes the increase in ET from 2000 to 2021, which rose 23,400 acre-feet, equating to an average annual increase of 1000 acre-feet. The Kanosh district experienced the highest increase in estimated ET at 7700 acre-feet, reflecting the intensive agricultural practices in this area.

Our study also highlights the impact of irrigation methods on groundwater use. The transition from flood irrigation to pivot irrigation has significantly increased crop density and vitality, as indicated by the NDVI analysis. NDVI values have shown statistically significant increases from 1992 to 2021, correlating with higher crop yields. For instance, alfalfa yield in Millard County increased by an average of 0.02 tons per acre per year between 1980 and 2017, culminating in a production of 333,000 tons in 2017.

Groundwater storage changes were estimated using specific yield (S_y) and specific storage (S_s) values. The study employed data from aquifer tests and well logs to interpolate and estimate these properties, enabling an accurate assessment of storage changes. The analysis revealed that groundwater levels have been steadily declining, particularly in areas near the decommissioned Central Utah Canal, where declines of up to 160 feet were recorded. The mean decline across the study area was 25.59 feet.

Our study underscores the importance of streamflow from the Pahvant Range as a primary source of recharge for the valley-fill aquifer. Stable isotope and chemical analyses confirm that stream discharge significantly influences groundwater recharge. The correlation between pumping and spring flow is notably high, with a Pearson's correlation coefficient of -0.72 when a two-year lag is applied to pumping, indicating that decreased pumping leads to increased spring flow two years later.

Declining groundwater has caused measurable ground subsidence, which results in a permanent decline in elastic storage

capacity of the aquifer. The subsidence analysis using InSAR has identified measurable ground deformation, with maximum subsidence of 5 inches observed in the Meadow area. This subsidence is closely correlated with groundwater level changes, highlighting the impact of groundwater extraction on land stability. The Flowell district, in particular, exhibited an average subsidence rate of 0.21 feet per year between 2017 and 2022.

Additionally, pumping in excess of sustainable rates has caused Clear Lake Spring, a critical species habitat, to stop flowing.

Overall, this study highlights the critical balance between groundwater extraction and recharge, the effects of irrigation practices on water use, and the importance of continuous monitoring and management to safeguard the region's water resources. These findings underscore the need for sustainable groundwater management practices to ensure the long-term viability of both agricultural productivity and ecological health in Pahvant Valley.

ACKNOWLEDGMENTS

This study was funded by the Utah Division of Water Rights. We thank the citizens of Pahvant Valley for aiding us in data collection and for providing valuable local knowledge. We would like to thank Claire Spangenberg Kellner and Elizabeth Stimmel (UGS) for helping collect field data. We thank Lynn Zubeck of the Division of Wildlife Resources who allowed us unfettered access to the Clear Lake Wildlife Management Area, for providing the historical lens from which to view Clear Lake, for historical data, and for his camaraderie. Thanks to Keyvan Asghari, David Jones, and others at the Utah Division of Water Rights for their technical review. We thank Lucy Jordan, Hugh Hurlow, and Stephanie Carney for their insightful comments to the report.

REFERENCES

Abatzoglou, J.T., 2013, Development of gridded surface meteorological data for ecological applications and modeling: International Journal of Climatology, v. 33, no. 1, p. 121–131, https://doi.org/10.1002/joc.3413.

Allen, R.G., Pereira, L.S., Howell, T.A., and Jensen, M.E., 2011, Evapotranspiration information reporting, I—Factors governing measurement accuracy: Agricultural Water Management, v. 98, no. 6, p. 899–920, https://doi.org/10.1016/j.agwat.2010.12.015.

Allen, R., Robison, C., Hipps, L., Schroeder, M., Carlisle, J., Eckhart, D., Harrison, A., Bureau, U., Huntington, J., Pearson, C., Dunkerly, C., Melton, F., Minor, B., Volk, J., Morton, C., Schwalbe, Z., Schumacher, R., Wilson, M., Bryant, N., and Painter, J., 2022, Assessing agricultural consumptive use in the Upper Colorado River Basin Phase III Repor—November 2022: https://doi.org/10.13140/RG.2.2.28316.77444.

Allen, R.G., Tasumi, M., Morse, A., and Trezza, R., 2005, A Landsat-based energy balance and evapotranspiration model in Western US water rights regulation and planning: Irrigation and Drainage Systems, v. 19, no. 3–4, p. 251–268, https://doi.org/10.1007/s10795-005-5187-z.

Allen, R.G., Tasumi, M., and Trezza, R., 2007, Satellite-based energy balance for mapping evapotranspiration with internalized calibration (METRIC)–Model: Journal of Irrigation and Drainage Engineering, v. 133, no. 4, p. 380–394, https://doi.org/10.1061/(ASCE)0733-9437(2007)133:4(380).

Allmendinger, R.W., Sharp, J.W., Von Tish, D., Serpa, L., Brown, L., Kaufman, S., Oliver, J., and Smith, R.B., 1983, Cenozoic and Mesozoic structure of the eastern Basin and Range province, Utah, from COCORP seismic-reflection data: Geology, v. 11, no. 9, p. 532–536, https://doi.org/10.1130/0091-7613(1983)11<532:CAMSOT>2.0.CO;2.

Anderson, M. C., Norman, J. M., Mecikalski, J. R., Otkin, J. A., & Kustas, W. P. (2007). A climatological study of evapotranspiration and moisture stress across the continental United States based on thermal remote sensing: 1. Model formulation. Journal of Geophysical Research, 112(D10), https://doi.org/10.1029/2006JD007507.

Anderson, M. C., Hain, C. R., Kustas, W. P., & Cawse-Nicholson, K. (2018). Disaggregation of remotely sensed evapotranspiration estimates for field-scale precision agriculture and drought monitoring. In ECOSTRESS Science Team Workshop (California Institute of Technology, Pasadena, CA).

Bailey, C.L., Wilson, K.W., and Andersen, M.E., 2006, Conservation agreement and strategy for Columbia spotted frog (*Rana luteiventris*) in the State of Utah: Utah Division of Wildlife Resources Publication 06–01, 51 p.

Bastiaanssen, W.G.M., Menenti, M., Feddes, R.A., and Holtslag, A.A.M., 1998, A remote sensing surface energy balance algorithm for land (SEBAL), 1—Formulation: Journal of Hydrology, v. 212–213, p. 198–212, https://doi.org/10.1016/S0022-1694(98)00253-4.

Clark, I., and Fritz, P., 1997, Environmental isotopes in hydrogeology: Boca Raton, CRC Press, 328 p.

Chow, V.T., 1964, Handbook of applied hydrology: New York, McGraw Hill, 540 p.

Cuch, F.S. (editor), 2000, A History of Utah's American Indians: Logan, Utah, Utah State Division of Indian Affairs.

Cunningham, W.L., and Schalk, C.W., 2011, Groundwater technical procedures of the U.S. Geological Survey—GWPD 1–Introduction to the Groundwater Technical Procedures (Techniques and Methods 1-A1): U.S. Geological Survey, U.S. Department of the Interior, 151 p.

Currey, D.R., Atwood, G., Mabey, D.R., Roy, J.S., and Brown, K.D., 1984, Major levels of Great Salt Lake and Lake Bonneville: Utah Geological and Mineral Survey Map 73, scale 1:750,000, https://doi.org/10.34191/M-73.

Dean, P., 2023, 2023 Economic report to the Governor: Utah Economic Council, 190 p.

Dennis, P.E., Maxey, G.B., and Thomas, H.E., 1946, Ground water in Pavant Valley, Millard County, Utah: U. S. Geological Survey Technical Publication 3, 102 p.

Diamond, R.E., 2022, Stable isotope hydrology: University of Pretoria, South Africa, The Groundwater Project, 102 p.

Dittmer, D.E., Graham, L., Lundskog, C., Broderius, C., Wheeler, K.K., Fridell, R.A., Mecham, D.J., and Lawrence, K., 2019, Least Chub (*Iotichthys phlegethontis*) statewide monitoring and conservation summary 2019: Utah Division of Wildlife Resources, 36 p.

Domenico, P.A., 1972, Concepts and models in groundwater hydrology: New York, McGraw Hill, 416 p.

Enright, M., 1987, Seepage study of a 15.3-mile section of the central Utah canal, Pahvant Valley, Millard County, Utah: Utah Department of Natural Resources, Division of Water Rights Technical Publication 91, 24 p.

Feuz, R., Larsen, R., and Nelson, M., 2020, Size and scope of Millard County agriculture 2019: Utah State University Extension, 4 p.

Fisher, J.B., Tu, K.P., and Baldocchi, D.D., 2008, Global estimates of the land—atmosphere water flux based on monthly AVHRR and ISLSCP-II data, validated at 16 FLUXNET sites: Remote Sensing of Environment, v. 112, no. 3, p. 901–919, https://doi.org/10.1016/j.rse.2007.06.025.

Fontes, J.C., and Garnier, J.M., 1979, Determination of the initial ^{14}C activity of the total dissolved carbon—A review of the existing models and a new approach: Water Resources Research, v. 15, p. 399–413, https://doi.org/10.1029/WR015i002p00399.

Gonfiantini, R., 1978, Standards for stable isotope measurements in natural compounds: Nature, v. 271, no. 5645, p. 534–536.

Gorelick, N., Hancher, M., Dixon, M., Ilyushchenko, S., Thau, D., and Moore, R., 2017, Google Earth Engine—Planetary-scale geospatial analysis for everyone: Remote Sensing of Environment, v. 202, p. 18–27, https://doi.org/10.1016/j.rse.2017.06.031.

Han, L.F., and Plummer, L.N., 2013, Revision of Fontes & Garnier's model for the initial ^{14}C content of dissolved inorganic carbon used in groundwater dating: Chemical Geology, v. 351, p. 105–114, https://doi.org/10.1016/j.chemgeo.2013.05.011.

Hardwick, C.L., 2013, Geothermal resources in southwestern Utah: gravity and magnetotelluric investigations: Salt Lake City, University of Utah, M.S. thesis, 67 p.

Hart, R., 2009, Isotopic evaluation of carbon dioxide in soil gas in Utah for a more accurate input variable in groundwater age determining models: Provo, Utah, Brigham Young University, M.S. thesis, 69 p.

Hintze, L.F., and Davis, F.D., 2005, Geologic map of the Delta 30′ x 60′ quadrangle and part of the Lynndyl 30′ x 60′ quadrangle, northeast Millard County and parts of Juab, Sanpete, and Sevier Counties, Utah: Utah Geological Survey, Map 206DM, scale 1:100,000, https://doi.org/10.34191/M-206DM.

Hintze, L.F., Davis, F.D., Rowley, P.D., Cunningham, C.G., Steven, T.A., and Willis, G.C., 2008, Geologic map of the Richfield 30′ x 60′ quadrangle, southeast Millard County and parts of Beaver, Piute, and Sevier Counties, Utah: Utah Geological Survey Map 195DM, scale 1:100,000, https://doi.org/10.34191/M-195dm.

Holmes, W.F., and Thiros, S.A., 1990, Groundwater hydrology of Pahvant Valley and adjacent areas, Utah: Utah Department of Natural Resources Technical Publication 98, 73 p.

Huntington, J., Pearson, C., Minor, B. Volk, J., Morton, C., Melton, F., Allen, R., 2022 Upper Colorado River Basin OpenET intercomparison summary, 34 p., https://doi.org/10.13140/RG.2.2.21605.88808.

Hurr, R.T., and Litke, D.W., 1989, Estimating pumping time and groundwater withdrawals using energy-consumption data: U.S. Geological Survey Water-Resources Investigations Report 89–4107, 31 p., https://doi.org/10.3133/wri894107.

Ingerson, E., and Pearson, F.J., 1964, Estimation of age and rate of motion of ground water by the ^{14}C method, *in* Miyake, Y., and Koyama, T., editors, Recent researches in the fields of hydrosphere, atmosphere and nuclear chemistry: Tokyo, Editorial Committee for Sugawara Volume, Water Research Laboratory, Nagoya University, p. 263–283.

Ingraham, N.L., and Taylor, B.E., 1991, Light stable isotope systematics of large-scale hydrologic regimes in California and Nevada: Water Resources Research, v. 27, no. 1, p. 77–90, https://doi.org/10.1029/90WR01708.

Jelinski, J., Clayton, C.S., and Fulford, J.M., 2015, Accuracy testing of electric groundwater-level measurement tapes: U.S. Geological Survey Open-File Report 2014-1236, 27 p., https://doi.org/10.3133/ofr20141236.

Johnsen, R., Smith, E., and Biek, R., 2010, Subalkaline volcanism in the Black Rock Desert and Markagunt Plateau volcanic fields of south-central Utah, *in* Carney, S.M., Tabet, D.E., and Johnson, C.L., editors, Geology of south-central Utah: Salt Lake City, Utah Geological Association, v. 39, p. 109–150.

Johnson, A.I., 1967, Specific yield—Compilation of specific yield for various materials: U.S. Geological Survey Water Supply Paper 1662-D, 74 p., https://doi.org/10.3133/wsp1662D.

Kalin, R.M., 2000, Radiocarbon dating of groundwater systems, *in* Cook, P.G., and Herczeg, A.L., Environmental tracers in subsurface hydrology: Boston, Springer, p. 111-144.

Kampf, S.K., and Burges, S.J., 2007, A framework for classifying and comparing distributed hillslope and catchment hydrologic models: Water Resources Research, v. 43, 25 p. W05423, https://doi.org/10.1029/2006WR005370.

Kelsey, Venetta Bond. Life on the Black Rock Desert: A History of Clear Lake, Utah. 1992.

Laipelt, L., Kayser, R. H. B., Fleischmann, A. S., Ruhoff, A., Bastiaanssen, W., Erickson, T. A., & Melton, F. (2021). Long-term monitoring of evapotranspiration using the SEBAL algorithm and Google Earth Engine cloud computing. ISPRS Journal of Photogrammetry and Remote Sensing, 178, 81-96. https://doi.org/10.1016/j.isprsjprs.2021.05.018.

Livingston, P.P., and Maxey, G.B., 1944, Underground leakage from artesian wells in the Flowell area, near Fillmore, Utah: Utah Department of Natural Resources, Division of Water Rights Technical Publication Number 1, 36 p.

Lechler, A.R., and Niemi, N.A., 2012, The influence of snow sublimation on the isotopic composition of spring and surface waters in the southwestern United States—Implications for stable isotope–based paleoaltimetry and hydrologic studies: Geological Society of America Bulletin, v. 124, no. 3–4, p. 318–334, https://doi.org/10.1130/B30467.1.

Lv, M., Xu, Z., Yang, Z.-L., Lu, H., and Lv, M., 2021, A comprehensive review of specific yield in land surface and groundwater studies: Journal of Advances in Modeling Earth Systems, v. 13, no. 2, https://doi.org/10.1029/2020MS002270.

Lyman, E.L., and Newell, L.K., 1999, A history of Millard County—Utah centennial county history series: Salt Lake City, Utah State Historical Society and Millard County Commission, 452 p.

Lynn Zubeck, personal communication regarding spring flow records for Clear Lake, Utah, received by Greg Gavin via email, January 17, 2024.

Meinzer, O.E., 1911, Ground water in Juab, Millard, and Iron counties, Utah: U.S. Geological Survey Water-Supply Paper 277, 162 p., https://doi.org/10.3133/wsp277.

Melton, F., Huntington, J., Grimm, R., Herring, J., Hall, M., Rollison, D., Erickson, T., Allen, R., Anderson, M., Fisher, J., Kilic, A., Senay, G., Volk, J., Hain, C., Johnson, L., Ruhoff, A., Blankenau, P., Bromley, M., Carrara, W., and Anderson, R., 2021, OpenET— Filling a critical data gap in water management for the western United States: Journal of the American Water Resources Association, https://doi.org/10.1111/1752-1688.12956.

Melton, F.S., Johnson, L.F., Lund, C.P., Pierce, L.L., Michaelis, A.R., Hiatt, S.H., Guzman, A., Adhikari, D.D., Purdy, A.J., Rosevelt, C., Votava, P., Trout, T.J., Temesgen, B., Frame, K., Sheffner, E.J., and Nemani, R.R., 2012, Satellite irrigation management support with the terrestrial observation and prediction system—A framework for integration of satellite and surface observations to support improvements in agricultural water resource management: IEEE Journal of Selected Topics in Applied Earth Observations and Remote Sensing, v. 5, no. 6, p. 1709–1721, https://doi.org/10.1109/JSTARS.2012.2214474.

Miller, J.A., 2000, Ground water atlas of the United States: U.S. Geological Survey Hydrologic Atlas 730, https://doi.org/10.3133/ha730.

Mook, W.G., 1972, On the reconstruction of the initial ^{14}C content of groundwater from the chemical and isotopic composition, *in* Eighth International Conference on Radiocarbon Dating: Royal Society of New Zealand, p. 342–352.

Mower, R.W., 1965, Ground-water Resources of Pavant Valley, Utah: United States Geological Survey Water-Supply Paper 1794, 93 p., https://doi.org/10.3133/wsp1794.

Mower, R.W., 1967, Causes of fluctuations in the rate of discharge of Clear Lake Springs, Millard County, Utah: U.S. Geological Survey Water-Supply Paper 1839-E , 36 p., https://doi.org/10.3133/wsp1839E.

Mundorff, J.C., 1970, Major thermal springs of Utah: Utah Geological and Mineral Survey Water-Resources Bulletin 13, 69 p., https://doi.org/10.34191/WRB-13.

Oviatt, C.G., 1991, Quaternary geology of the Black Rock Desert, Millard County, Utah: Utah Geological Survey Special Study 73, 28 p., https://doi.org/10.34191/SS-73.

Pereira, L.S., Paredes, P., Melton, F., Johnson, L., Wang, T., López-Urrea, R., Cancela, J.J., and Allen, R.G., 2020, Prediction of crop coefficients from fraction of ground cover and height—Background and validation using ground and remote sensing data: Agricultural Water Management, v. 241, p. 106197, https://doi.org/10.1016/j.agwat.2020.106197.

Ries, K.G.I., Newson, J.K., Smith, M.J., Guthrie, J.D., Steeves, P.A., Haluska, T., Kolb, K.R., Thompson, R.F., Santoro, R.D., and Vraga, H.W., 2017, StreamStats, version 4: U.S. Geological Survey Fact Sheet 2017–3046, https://doi.org/10.3133/fs20173046.

Scholl, M.A., Ingebritsen, S.E., Janik, C.J., and Kauahikaua, J.P., 1996, Use of precipitation and groundwater isotopes to interpret regional hydrology on a tropical volcanic island—Kilauea volcano area, Hawaii: Water Resources Research, v. 32, no. 12, p. 3525–3537.

Senay, G., 2018, Satellite psychrometric formulation of the operational Simplified Surface Energy Balance (SSEBop) model for quantifying and mapping evapotranspiration: Applied Engineering in Agriculture, v. 34, p. 555–566, https://doi.org/10.13031/aea.12614.

Senay, G.B., Bohms, S., Singh, R.K., Gowda, P.H., Velpuri, N.M., Alemu, H., and Verdin, J.P., 2013a, Operational

evapotranspiration mapping using remote sensing and weather datasets—A new parameterization for the SSEB approach: Journal of the American Water Resources Association, v. 49, no. 3, p. 577–591, https://doi.org/10.1111/jawr.12057.

Senay, G., Gowda, P., Kagone, S., Howell, T., Friedrichs, M., Marek, T., and Verdin, J., 2013b, Evaluating the SSEBop approach for evapotranspiration mapping with landsat data using lysimetric observations in the semi-arid Texas High Plains: Hydrology and Earth System Sciences Discussions, v. 11, https://doi.org/10.5194/hessd-11-723-2014.

Senay, G., Kagone, S., and Velpuri, N., 2020, Operational global actual evapotranspiration– development, evaluation and dissemination: Sensors, v. 20, https://doi.org/10.3390/s20071915.

Snyder, N.P., 1998, Map of recharge and discharge areas for the principal basin-fill aquifer system Sevier Desert, Millard County, Utah: Utah Geological Survey Map 175, 11 p., 1 plate, 1 appendix, https://doi.org/10.34191/M-175.

Solomon, D.K., and Cook, P.G., 2000, ^{3}H and ^{3}He, *in* Cook, P., and Herczeg, A.L., editors, Environmental tracers in subsurface hydrology: Boston, Kluwer Academic Publishers, p. 397–424.

Stamm, G.G., 1967, Problems and procedures in determining water supply requirements for irrigation projects, *in* Hagan, R.M., Haise, H.R., Edminster, T.W., editors, Irrigation of agricultural lands: John Wiley & Sons, Ltd, p. 769–785, https://doi.org/10.2134/agronmonogr11.c45.

T. A. Steven, 1990, Geologic map of the Richfield 1 x 2 quadrangle, west-central Utah. I-1901. USGS. 1:250,000 scale.

Tamers, M.A., 1975, Validity of radiocarbon dates on groundwater: Geophysical Surveys, v. 2, no. 2, p. 217–239, https://doi.org/10.1007/BF01447909.

Thiros, S.A., and Manning, A.H., 2004, Estimation of groundwater age and recharge rates using environmental tracers: Great Basin National Park, Nevada: U.S. Geological Survey Water-Resources Investigations Report 03–4277, 84 p.

U.S. Department of Agriculture (USDA), 2023, National Agricultural Statistics Service Cropland Data Layer: Online, https://www.nass.usda.gov/Research_and_Science/Cropland/SARS1a.php, accessed August, 2024.

U.S. Geological Survey, 2024, National Water Information System (NWIS): Online, https://waterdata.usgs.gov/nwis, accessed July, 2024.

U.S. Geological Survey, 2021, Utah Groundwater Pumpage Data: Online, https://warcapps.usgs.gov/gs-water/uwsc/ugcwa/PumpageData/Data2021, accessed October 2023.

Utah Division of Water Resources, 2021, Water-related land use and data collection program: Utah Department of Natural Resources, 98 p.

Wall Engineering, 2010, Fillmore City well no. 2 and no. 3 drinking water source protection plan.: Consultants Report for the Utah Division of Drinking Water, 139 p.

Yunjun, Z., Fattahi, H., and Amelung, F., 2019, Small baseline InSAR time series analysis– Unwrapping error correction and noise reduction: Computers & Geosciences, v. 133, https://doi.org/10.1016/j.cageo.2019.104331.

Zume, J.T., and Tarhule, A.A., 2008, Simulating the impacts of groundwater pumping on stream–aquifer dynamics in semi-arid northwestern Oklahoma, USA: Hydrogeology Journal, v. 16, no. 4, p. 797–810.

APPENDICES

APPENDIX A

Depth to groundwater and groundwater elevation data

Appendix A. *Depth to groundwater and groundwater elevation data.*

UGS ID no.	USGS site no.	USGS site name	Well depth (ft)	Date measured	2022 Depth to groundwater (ft)	2022 Groundwater elevation (ft)	Date	1986 Depth to groundwater (ft)	1986 groundwater elevation (ft)	Groundwater elevation change (ft)	Ground surface elevation (ft)	Longitude	Latitude	Agency
1	390747112435101	(C-19- 8)27ddb- 1	0	3/8/2022	3.48	4575.5	3/1/1986	5.91	4573.1	-2.43	4579.006	-112.42400	39.12992	UGS
2	384722112315801	(C-23- 6)21cdd- 1	630	3/16/2022	153.27	4638.7	3/1/1986	105.63	4686.4	47.64	4792.002	-112.56100	38.78942	UGS
3	384722112333701	(C-23- 6)20ccc- 1	320	3/16/2022	118.39	4644.2	3/1/1986	93.06	4669.5	25.33	4762.591	-112.54200	38.78942	UGS
4	384743112333101	(C-23- 6)20cbb- 1	430	3/16/2022	99.08	4646.9	3/1/1986	74.58	4671.4	24.5	4745.932	-112.41200	38.79525	UGS
5	384751112312201	(C-23- 6)21add- 1	445	3/16/2022	141.84	4645.6	3/1/1986	70.98	4716.4	70.86	4787.399	-112.49200	38.79747	UGS
6	384755112330401	(C-23- 6)20bda- 1	307	3/16/2022	98.12	4639.6	3/1/1986	68.95	4668.8	29.17	4737.705	-112.41100	38.79858	UGS
7	384815112280901	(C-23- 6)13ddd- 1	250	3/16/2022	135.35	4777.1	3/1/1986	99.22	4813.2	36.13	4912.44	-112.48600	38.80414	UGS
8	384815112331401	(C-23- 6)17cdc- 1	440	3/16/2022	88.43	4644.7	3/1/1986	56.35	4676.8	32.08	4733.178	-112.41700	38.80414	UGS
9	384824112333801	(C-23- 6)18ddd- 1	382	3/16/2022	81.33	4647.4	3/1/1986	55.59	4673.1	25.74	4728.715	-112.45700	38.80664	UGS
10	384829112315901	(C-23- 6)16cda- 1	205	3/16/2022	85.43	4649.4	3/1/1986	12.77	4722	72.66	4734.817	-112.45700	38.80803	UGS
11	384848112305101	(C-23- 6)15bda- 1	415	3/16/2022	114.77	4650.4	3/1/1986	40.88	4724.3	73.89	4765.166	-112.43800	38.8133	UGS
12	384906112330601	(C-23- 6)17baa- 1	140	3/16/2022	64.89	4648.1	3/1/1986	31.45	4681.5	33.44	4712.972	-112.43800	38.81831	UGS
13	384935112305002	(C-23- 6)10bdd- 2	132	3/16/2022	99.53	4655	3/1/1986	28.92	4725.6	70.61	4754.529	-112.46200	38.82636	UGS
14	385013112291201	(C-23- 6) 2dad- 1	400	3/16/2022	62.42	4737.8	3/3/1986	46.38	4753.9	16.04	4800.27	-112.47100	38.83692	UGS
15	385053112252401	(C-22- 5)33cdd- 2	270	3/16/2022	133.9	4703.1	3/3/1986	40.23	4796.8	93.67	4837.027	-112.43400	38.84803	UGS
16	385055112333501	(C-22- 6)32ccc- 1	115	3/16/2022	66.67	4645.2	3/1/1986	37.02	4674.8	29.65	4711.842	-112.35600	38.84858	UGS
17	385107112323001	(C-22- 6)32dad- 1	400	3/16/2022	52.74	4647	3/1/1986	20.06	4679.6	32.68	4699.696	-112.42000	38.85192	UGS
18	385130112244201	(C-22- 5)33ada- 1	256	3/16/2022	158.34	4702.5	3/3/1986	66.07	4794.8	92.27	4860.845	-112.40100	38.8583	UGS
19	385453112292701	(C-22- 6)11acd- 1	61	3/16/2022	25.14	4665	3/7/1986	3.15	4687	21.99	4690.141	-112.36300	38.91469	UGS
20	385650112243601	(C-21- 5)33aad- 1	352	3/16/2022	88.99	4662.9	3/6/1986	1.66	4750.2	87.33	4751.842	-112.47600	38.94719	UGS
21	385743112290501	(C-21- 6)26aac- 1	105	3/16/2022	66.75	4598.2	3/5/1986	50.46	4614.5	16.29	4664.937	-112.41100	38.96191	UGS
22	385844112245801	(C-21- 5)21aba- 1	251	3/16/2022	69	4676.3	3/24/1986	-17.2	4762.5	86.2	4745.316	-112.28600	38.97886	UGS
23	385939112272302	(C-21- 5) 7cdd- 2	150	3/15/2022	54.99	4596.8	3/6/1986	41.33	4610.4	13.66	4651.764	-112.34100	38.99414	UGS
24	385939112272303	(C-21- 5) 7cdd- 3	150	3/15/2022	54.45	4597.3	3/6/1986	41.33	4610.4	13.12	4651.764	-112.30100	38.99414	UGS
25	385942112261502	(C-21- 5) 8cdd- 3	278	3/15/2022	70	4612.7	3/4/1986	39.69	4643	30.31	4682.686	-112.34300	38.99497	UGS
26	390002112261401	(C-21- 5) 8dbb- 2	400	3/16/2022	60.96	4617.6	3/4/1986	33.8	4644.8	27.16	4678.552	-112.36900	39.00052	UGS
27	390043112273901	(C-21- 5) 6cac- 1	90	3/15/2022	49.33	4596	3/6/1986	30.54	4614.8	18.79	4645.347	-112.40700	39.01191	UGS
28	390045112281201	(C-21- 6) 1ddb- 1	105	3/15/2022	59.78	4597.4	3/6/1986	42.1	4615.1	17.68	4657.161	-112.39600	39.01247	UGS
29	390116112255901	(C-21- 5) 5abd- 1	206	3/15/2022	33.35	4607.4	3/6/1986	11.45	4629.3	21.9	4640.766	-112.43300	39.02108	UGS
30	390216112222001	(C-20- 5)26ddd- 1	250	3/15/2022	113.86	4731.4	3/3/1986	29.06	4816.2	84.8	4845.282	-112.37200	39.03775	UGS
31	390218112250801	(C-20- 5)28cdd- 1	354	3/15/2022	42.56	4614.5	3/4/1986	-9.47	4666.6	52.03	4657.096	-112.36200	39.0383	UGS
32	390248112235901	(C-20- 5)27bda- 1	190	3/15/2022	57.41	4630.8	3/4/1986	1.35	4686.8	56.06	4688.198	-112.37400	39.04663	UGS
33	390344112214301	(C-20- 5)24bda- 1	300	3/15/2022	108.38	4664.1	3/3/1986	43.17	4729.3	65.21	4772.449	-112.36300	39.06219	UGS
34	390422112283001	(C-20- 6)13caa- 1	90	3/15/2022	66	4582.5	3/1/1986	58.39	4590.1	7.61	4648.479	-112.44800	39.07275	UGS
35	390527112243501	(C-20- 5) 9ada- 1	212	3/15/2022	17.63	4636.5	3/5/1986	-9.8	4663.9	27.43	4654.143	-112.44800	39.0908	UGS
36	390547112170501	(C-20- 4) 3dcc- 1	212	3/15/2022	77.18	4925.6	3/1/1986	23.8	4978.9	53.38	5002.749	-112.44300	39.09636	UGS
37	390558112202301	(C-20- 4) 6dbd- 1	435	3/15/2022	128	4663.8	3/3/1986	15.14	4776.7	112.86	4791.806	-112.41800	39.09941	UGS

Appendix A. *Continued.*

UGS ID no.	USGS site no.	USGS site name	Well depth (ft)	Date measured	2022 Depth to groundwater (ft)	2022 Groundwater elevation (ft)	Date	1986 Depth to groundwater (ft)	1986 groundwater elevation (ft)	Groundwater elevation change (ft)	Ground surface elevation (ft)	Longitude	Latitude	Agency
38	390604112175901	(C-20- 4) 4dab- 1	755	3/15/2022	139.7	4785.2	3/1/1986	34.08	4890.9	105.62	4924.94	-112.42900	39.10108	UGS
39	390700112203201	(C-19- 4)31dbb- 1	523	3/15/2022	139.31	4655	3/3/1986	32.42	4761.9	106.89	4794.298	-112.42900	39.11663	UGS
40	390826112220701	(C-19- 5)23dcd- 1	460	3/15/2022	104	4672.6	3/3/1986	24.75	4751.8	79.25	4776.577	-112.63000	39.14052	UGS
41	391156112242601	(C-19- 5) 3bbb- 1	186	3/15/2022	178.13	4555.4	3/1/1986	27.2	4706.3	150.93	4733.505	-112.64700	39.19889	UGS
42	391313112234201	(C-18- 5)27dba- 1	520	3/15/2022	241.32	4555.7	3/1/1986	81.88	4715.1	159.44	4797.022	-112.65400	39.22024	UGS
43	391522112253401	(C-18- 5)16bbc- 1	0	3/15/2022	68.69	4636	3/1/1986	35.92	4668.7	32.77	4704.658	-112.68700	39.25941	UGS
44	--	--	--	3/7/2022	116.18	4672.7	--	--	--	--	4788.404	-112.66800	39.0378	UGS
45	390259112214201	(C-20- 5)25abc- 1	82	3/7/2022	186.85	4585.3	3/3/1986	41.64	4729.3	145.21	4770.906	-112.76300	39.04979	UGS
46	390246112221701	(C-20- 5)26add- 1	314	3/7/2022	129.27	4640.9	3/4/1986	30.5	4738.3	98.77	4768.807	-112.70000	39.04967	UGS
47	390344112214301	(C-20- 5)24bda- 1	300	3/7/2022	109.87	4668.3	3/3/1986	43.17	4732.9	66.7	4776.058	-112.55300	39.06395	UGS
48	385816112264801	(C-21- 5)19daa- 3	650	3/7/2022	27.42	4646.2	3/5/1986	-45.5	4716.9	72.92	4671.433	-112.49200	38.97186	UGS
49	385816112264801	(C-21- 5)19daa- 3	650	3/7/2022	28.06	4643.3	3/5/1986	-45.5	4716.6	73.56	4671.093	-112.46100	38.97108	UGS
50	385839112263101	(C-21- 5)20bba- 2	480	3/7/2022	26.88	4650.9	3/5/1986	-51	4726	77.88	4675.042	-112.58700	38.97757	UGS
51	385828112245501	(C-21- 5)21aca- 1	251	3/7/2022	78.63	4658.8	3/24/1986	-17.2	4754.6	95.83	4737.443	-112.61900	38.97562	UGS
52	385752112255801	(C-21- 5)29aba- 1	406	3/8/2022	46.72	4661.1	3/5/1986	-45	4750.9	91.72	4705.947	-112.59500	38.96309	UGS
53	385806112254001	(C-21- 5)20dad- 1	293	3/8/2022	33.85	4673.1	3/5/1986	-28	4734.9	61.85	4706.948	-112.56100	38.96849	UGS
54	--	--	--	3/8/2022	25.45	4570.4	--	--	--	--	4592.592	-112.63700	39.11011	UGS
55	--	--	--	3/8/2022	9.83	4573.3	--	--	--	--	4580.468	-112.65400	39.257	UGS
56	--	--	--	3/8/2022	17.37	4572.4	--	--	--	--	4587.115	-112.66900	39.24514	UGS
57	391420112412001	(C-18- 8)24ada- 2	601	3/8/2022	6.05	4572.5	3/2/1986	-7.58	4584.7	13.63	4577.143	-112.80700	39.24261	UGS
58	--	--	--	3/8/2022	6.6	4574	--	--	--	--	4579.371	-112.82100	39.24369	UGS
59	390250112454201	(C-20- 8)28bcd- 1 Cominco Well	651	3/8/2022	36.65	4580.6	3/1/1986	33.37	4582.6	3.28	4615.93	-112.76800	39.04679	UGS
60	385948112415001	(C-21- 8)12dcc- 1	150	3/8/2022	53.25	4596.2	3/1/1986	45.19	4602.3	8.06	4647.509	-112.41000	38.99682	UGS
61	390052112323801	(C-21- 6) 5cad- 1	127	3/8/2022	51.92	4593.8	3/2/1986	42.48	4603	9.44	4645.498	-112.42400	39.01447	UGS
62	390916112292801	(C-19- 6)23aba- 1	45	3/9/2022	21.63	4592.9	3/1/1986	5.8	4607.4	15.83	4613.238	-112.50100	39.15424	UGS
63	390650112273801	(C-19- 5)31cbd- 1	375	3/9/2022	38.91	4577.8	3/2/1986	-7.1	4623.2	46.01	4616.085	-112.40600	39.11412	UGS
64	385835112350901	(C-21- 7)24acb- 1	420	3/8/2022	19.07	4634.5	3/7/1986	15.54	4638	3.53	4653.583	-112.40500	38.97647	UGS
65	385635112370601	(C-21- 7)34dab- 1	117	3/8/2022	56.01	4642.6	3/2/1986	40.45	4658.2	15.56	4698.639	-112.41000	38.94246	UGS
66	--	--	--	3/8/2022	23.41	4655	--	--	--	--	4676.936	-112.40100	38.94927	UGS
67	385332112333601	(C-22- 6)19aaa- 1	152	3/8/2022	102.34	4647.5	3/2/1986	76.43	4673.4	25.91	4749.794	-112.31600	38.89246	UGS
68	384850112381001	(C-23- 7)16ada- 1	390	3/8/2022	200.11	4699.2	3/2/1986	208.45	4690.8	-8.34	4899.271	-112.39300	38.8141	UGS
69	384931112391201	(C-23- 7) 9cbb- 1	0	3/8/2022	52.19	4768.9	3/1/1986	57.18	4762.9	-4.99	4820.041	-112.40500	38.82656	UGS
70	384519112400401	(C-24- 7) 5bca- 1	0	3/8/2022	312.2	4821.2	3/2/1986	311.22	4821.7	0.98	5132.904	-112.39100	38.75519	UGS
71	385007112482201	(C-23- 9)12aaa- 1	0	3/8/2022	30.7	4736.5	3/2/1986	24.34	4742.8	6.36	4767.169	-112.37300	38.8355	UGS
72	384909112491501	(C-23- 9)13bbb- 1	0	3/9/2022	60.31	4721.2	3/2/1986	53.48	4726.9	6.83	4780.399	-112.34000	38.81947	UGS
73	385618112460301	(C-22- 8) 5aaa- 1 Black Willow Well	134	3/9/2022	53.13	4643.6	3/2/1986	49.07	4647.6	4.06	4696.696	-112.40700	38.9323	UGS
74	--	--	--	3/9/2022	44.37	4623.2	--	--	--	--	4666.093	-112.40200	39.1404	UGS
75	--	--	--	3/9/2022	37.55	4609.7	--	--	--	--	4645.222	-112.46600	39.15531	UGS
76	391714112300301	(C-18- 6) 2bbb- 2	246	3/9/2022	1.46	4596.3	3/2/1986	-10.7	4607	12.16	4596.328	-112.47600	39.28722	USGS
77	391437112241201	(C-18- 5)22bbd- 1	480	3/9/2022	225.44	4569.8	3/1/1986	94.28	4701	131.16	4795.25	-112.38100	39.24224	USGS

Appendix A. *Continued.*

UGS ID no.	USGS site no.	USGS site name	Well depth (ft)	Date measured	2022 Depth to groundwater (ft)	2022 Groundwater elevation (ft)	Date	1986 Depth to groundwater (ft)	1986 groundwater elevation (ft)	Groundwater elevation change (ft)	Ground surface elevation (ft)	Longitude	Latitude	Agency
78	391315112241601	(C-18- 5)27cba- 1	495	3/9/2022	204.86	4553.8	3/1/1986	48.95	4708.1	155.91	4757.097	-112.44400	39.22104	USGS
79	391302112243301	(C-18- 5)28dda- 1	504	3/9/2022	190.91	4555.2	3/1/1986	37.07	4708.6	153.84	4745.717	-112.43500	39.2175	USGS
80	391246112241701	(C-18- 5)34bba- 1	502	3/9/2022	207.11	4551.5	3/1/1986	43.38	4715.2	163.73	4758.613	-112.32700	39.2136	USGS
81	--	--	--	--	103.58	5098.5	--	--	--	--	5202.069	-112.34800	39.21339	USGS
82	391234112233701	(C-18- 5)34adb- 3	512	3/9/2022	233.96	4547.8	3/1/1986	73.24	4708.3	160.72	4781.569	-112.38100	39.20879	USGS
83	391232112241701	(C-18- 5)34bca- 1	400	3/9/2022	182.67	4560.7	3/1/1986	38.4	4710.5	144.27	4748.925	-112.35300	39.20921	USGS
84	391153112232701	(C-19- 5) 3aaa- 1	550	3/9/2022	222.28	4547.1	3/1/1986	63.87	4704.7	158.41	4768.616	-112.41100	39.1982	USGS
85	391147112221901	(C-19- 5) 2aad- 1	655	3/9/2022	284.17	4546.9	3/1/1986	129.21	4701.9	154.96	4831.111	-112.42900	39.19656	USGS
86	390757112202001	(C-19- 4)30dab- 1	502	3/9/2022	161.31	4651.4	3/1/1986	57.54	4755.2	103.77	4812.736	-112.44800	39.13271	USGS
87	385511112243501	(C-22- 5)10bbb- 2	338	3/9/2022	126.6	4663.9	3/6/1986	12.1	4777.4	114.5	4789.533	-112.43800	38.92145	USGS
88	385605112240301	(C-22- 5) 3baa- 1	380	3/9/2022	125.87	4662.1	3/5/1986	36.77	4750.1	89.1	4786.852	-112.44700	38.93482	USGS
89	--	--	--	3/9/2022	8.41	4658	--	--	--	--	4664.004	-112.57200	38.95519	USGS
90	385611112284201	(C-21- 6)36cdd- 1	815	3/9/2022	9.22	4666.1	3/25/1986	-19.5	4692.9	28.72	4673.37	-112.51500	38.93658	USGS
91	385752112225301	(C-21- 5)26abb- 1	410	3/9/2022	209.05	4664.3	3/19/1986	112.91	4758.6	96.14	4871.529	-112.47700	38.96439	USGS
92	385556112263601	(C-22- 5) 5bca- 1	288	3/9/2022	31.08	4664.7	3/6/1986	-39.5	4733.3	70.58	4693.773	-112.44500	38.93625	USGS
93	385347112260402	(C-22- 5)17dbd- 1	350	--	29.58	4711.1	3/5/1986	0	4739.6	29.58	4739.553	-112.49100	38.89957	USGS
94	385933112193101	(C-21- 4)17baa- 1	140	3/10/2022	105.24	4906	3/4/1986	50.4	4960.6	54.84	5010.962	-112.46500	38.99273	USGS
95	390307112205101	(C-20- 4)30bab- 1	100	3/10/2022	32.77	4833.1	3/3/1986	24.97	4840.8	7.8	4865.73	-112.43600	39.05202	USGS
96	390523112225001	(C-20- 5)11bdd- 1	387	3/10/2022	47.75	4665.3	3/8/1986	0	4713.1	47.75	4713.099	-112.44000	39.08965	USGS
97	--	--	--	3/10/2022	116.15	4656.8	--	--	--	--	4772.974	-112.39800	39.1106	USGS
98	385923112243201	(C-21- 5)16ada- 1	109	3/10/2022	106.45	4664.8	3/4/1986	15.09	4755.6	91.36	4770.72	-112.41500	38.99022	USGS
99	385845112254001	(C-21- 5)17adc- 1	236	--	45.42	4658.6	3/4/1986	-14.6	4719.3	60.02	4704.667	-112.45100	38.98349	USGS
100	385859112264902	(C-21- 5)18dad- 2	110	3/10/2022	63.3	4604.7	3/6/1986	-43.7	4711.7	107	4667.988	-112.44000	38.9867	USGS
101	385916112261403	(C-21- 5)17bdd- 3	530	3/10/2022	33.04	4649.9	3/5/1986	-27.5	4710.2	60.54	4682.653	-112.38300	38.98828	USGS
102	390149112264701	(C-20- 5)32cbb- 1	942	3/10/2022	32.15	4607.6	3/20/1986	0	4639.8	32.15	4639.773	-112.54700	39.03036	USGS
103	384428112341701	(C-24- 6) 7bad- 1	0	3/10/2022	15.48	4999.3	3/4/1986	94.48	4919.5	-79	5014.009	-112.42900	38.74141	USGS
104	384747112305001	(C-23- 6)22caa- 1	150	3/10/2022	184.06	4650.7	3/4/1986	113.06	4721.7	71	4834.718	-112.41100	38.79618	USGS
105	384821112283201	(C-23- 6)13dcb- 1	205	3/10/2022	140.68	4761	3/1/1986	110.45	4789.8	30.23	4900.203	-112.41000	38.80592	USGS
106	385026112264001	(C-23- 5) 5cba- 1	225	3/10/2022	126.35	4707.6	3/3/1986	32.17	4801.6	94.18	4833.767	-112.37200	38.84035	USGS
107	385105112292501	(C-22- 6)35ddb- 1	0	3/10/2022	1.32	4817.6	3/1/1986	2.59	4816.3	-1.27	4818.904	-112.50800	38.8507	USGS
108	385105112280601	(C-22- 6)36dda- 2	0	3/10/2022	81.83	4708.7	3/3/1986	2.48	4786.7	79.35	4789.148	-112.46500	38.85154	USGS
109	385107112260601	(C-22- 5)32dbd- 1	182	3/10/2022	100.72	4702.2	3/4/1986	6.64	4794	94.08	4800.664	-112.43600	38.85528	USGS
110	385149112262302	(C-22- 5)29cdd- 2	380	3/10/2022	79.72	4704.1	3/3/1986	0	4784.2	79.72	4784.194	-112.44000	38.86372	USGS
111	385250112234801	(C-22- 5)22dac- 1	373	3/10/2022	136.87	4770.6	3/4/1986	71.92	4835.6	64.95	4907.52	-112.39800	38.88053	USGS
112	385200112245801	(C-22- 5)28dbd- 1	112	3/10/2022	102.22	4715.5	3/3/1986	26.89	4790.3	75.33	4817.171	-112.41500	38.86995	USGS
113	--	--	--	3/10/2022	41.77	4714.1	--	--	--	--	4754.437	-112.45100	38.8779	USGS
114	--	--	--	3/10/2022	46.4	4702.6	--	--	--	--	4748.541	-112.44000	38.88636	USGS
115	--	--	--	3/11/2022	131.1	4907.5	--	--	--	--	5037.144	-112.38300	38.88456	USGS
116	--	--	--	3/11/2022	126.34	4635	--	--	--	--	4759.719	-112.54700	38.7892	USGS
117	390116112255901	(C-21- 5) 5abd- 1	206	3/11/2022	33.03	4618.8	3/6/1986	11.45	4638.4	21.58	4649.877	-112.42900	39.02342	USGS
118	--	--	--	3/11/2022	11.36	4657.1	--	--	--	--	4667.848	-112.41100	39.05243	USGS
119	--	--	--	3/11/2022	38.82	4627	--	--	--	--	4665.691	-112.41000	39.05897	USGS
120	--	--	--	3/11/2022	72.98	4657.4	--	--	--	--	4728.584	-112.37200	39.10562	USGS
121	385150112302501	(C-22- 6)27ddc-S1	--	2/23/2023	2	4761.058	--	--	--	--	4763.058	-112.50800	38.86426	USGS

APPENDIX B

Clear Lake Spring flow by calendar year (Division of Water Rights, 2023)

Appendix B. *Clear Lake Spring flow by calendar year.*

Date	ac-ft/yr
1959	9170
1960	16,169
1961	14,844
1962	15,441
1963	13,692
1964	14,286
1965	14,973
1966	14,816
1967	14,277
1968	15,350
1969	14,664
1970	15,495
1971	16,753
1972	14,709
1973	16,674
1974	18,941
1975	18,029
1976	17,506
1977	14,310
1978	13,071
1979	13,458
1980	13,649
1981	13,843
1982	13,813
1983	18,502
1984	40,202
1985	56,866
1986	47,172
1987	39,949
1988	34,223
1989	31,073
1990	26,979
1991	22,644
1992	17,669
1993	17,034
1994	16,282
1995	17,949
1996	15,640
1997	13,272
1998	13,890
1999	14,983
2000	15,210
2001	13,966
2002	11,989
2003	9369
2004	9879
2005	11,397
2006	9421
2007	7973
2008	7686
2009	7052
2010	7215
2011	8275
2012	8741
2013	8316
2014	4771
2015	4363
2016	4109
2017	4139
2018	3385
2019	4573
2020	4505
2021	2071
2022	484

APPENDIX C

Map of ET fraction for Pahvant Valley

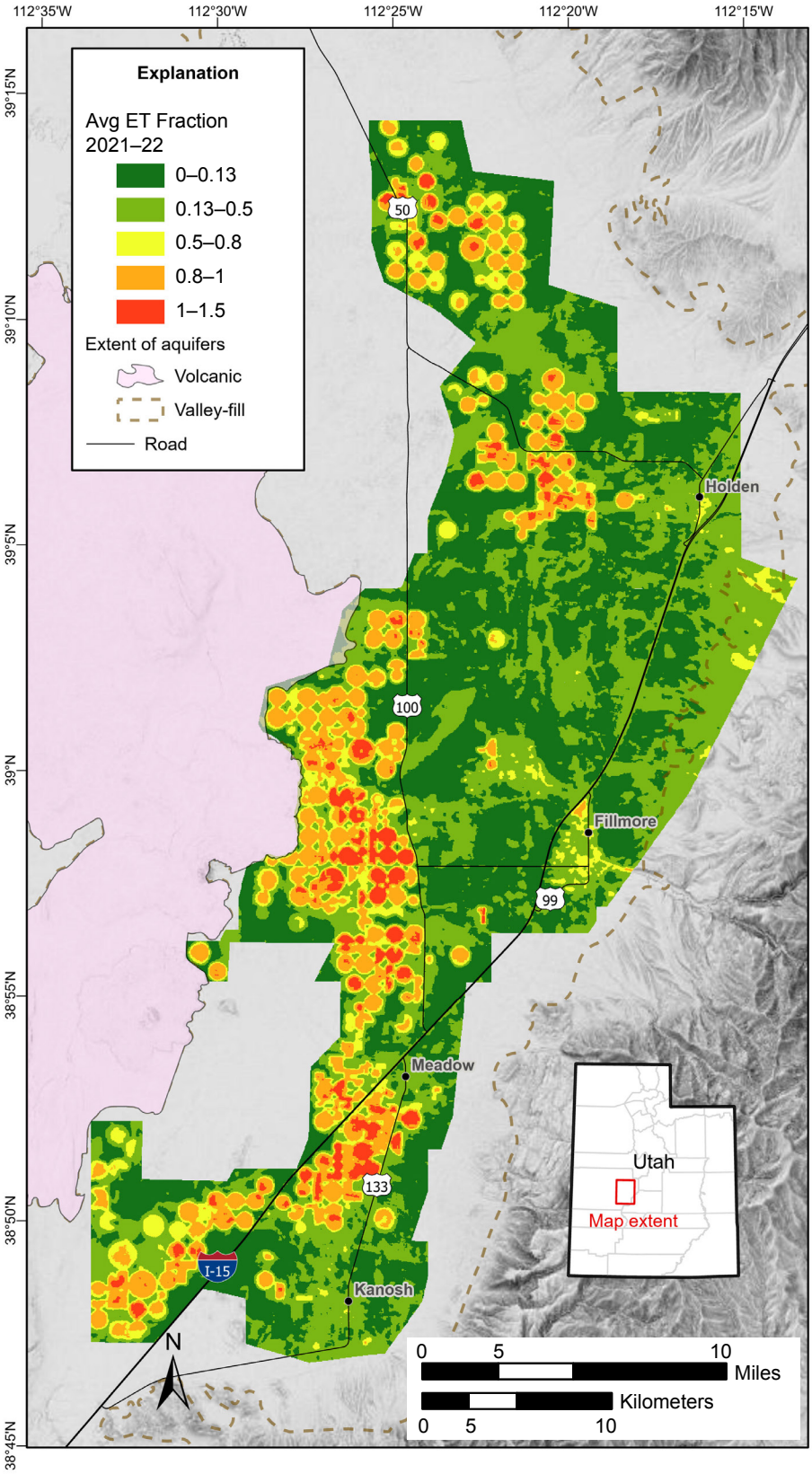

Appendix C. *Map of ET fraction for Pahvant Valley.*

APPENDIX D

Tabulated geochemical data for Pahvant Valley

Appendix D. *Tabulated geochemical data for Pahvant Valley.*

Source	Date	Sample ID	Sampling agency	Latitude	Longitude	Source aquifer or name	Bicarbonate (mg/L)	Calcium (mg/L)	Chloride (mg/L)	Magnesium (mg/L)	Potassium (mg/L)	Sodium (mg/L)	Sulfate (mg/L)	Temperature (°C)	Specific conductance (µS/cm)	Total dissolved solids (mg/L)
Groundwater	10/10/1953	USGS-385806112263201	USGS	38.9683	-112.4429	Valley-fill	320	225	410	100	8	222	601	-	2610	1750
Groundwater	12/21/1953	USGS-385806112263201	USGS	38.9683	-112.4429	Valley-fill	306	202	370	86	10	180	455	19	2310	1480
Groundwater	12/23/1953	USGS-385839112263101	USGS	38.9775	-112.4428	Valley-fill	292	104	121	45	5	91	223	17	1220	755
Groundwater	3/4/1954	USGS-385725112261501	USGS	38.9569	-112.4383	Valley-fill	288	119	174	47	8	99	212	-	1350	822
Groundwater	3/25/1954	USGS-385806112263201	USGS	38.9683	-112.4429	Valley-fill	306	206	380	86	10	181	469	-	2340	1510
Groundwater	1/1/1955	USGS-385746112254003	USGS	38.9627	-112.4286	Valley-fill	298	146	182	60	8	137	377	-	1650	1080
Groundwater	6/1/1955	USGS-385822112264801	USGS	38.9710	-112.4476	Valley-fill	290	214	368	101	7	183	561	-	2420	1600
Groundwater	5/25/1961	USGS-384953112325101	USGS	38.8314	-112.5485	Pahvant Flow	365	357	1130	101	61	526	558	15	4720	2920
Groundwater	5/25/1961	USGS-385026112261001	USGS	38.8403	-112.4368	Valley-fill	316	107	70	21	2	34	64	13	810	480
Groundwater	5/25/1961	USGS-390005112262301	USGS	39.0014	-112.4404	Valley-fill	261	73	52	20	1	32	47	17	640	377
Groundwater	5/26/1964	USGS-384953112325101	USGS	38.8314	-112.5485	Pahvant Flow	362	377	1450	146	60	574	696	14	5460	3875
Groundwater	7/28/1964	USGS-384850112310701	USGS	38.8137	-112.5196	Valley-fill	410	56	1200	253	84	680	690	16	5150	3385
Groundwater	7/29/1964	USGS-385026112261001	USGS	38.8403	-112.4368	Valley-fill	313	88	61	29	2	33	67	12	770	474.5
Groundwater	5/12/1966	USGS-385150112302501	USGS	38.8621	-112.5053	Meadow Hot Spring	314	419	1750	97	16	0	1020	-	*7328	4690
Groundwater	6/22/1971	USGS-384953112325101	USGS	38.8314	-112.5485	Pahvant Flow	288	590	2100	220	10	750	1000	15	7300	4810
Groundwater	6/23/1971	USGS-384748112315801	USGS	38.7961	-112.5339	Pahvant Flow	304	320	1300	180	25	470	560	14	4830	3000
Groundwater	7/12/1972	USGS-384751112312201	USGS	38.7982	-112.5519	Pahvant Flow	229	79	220	58	5	120	180	12	1430	803
Groundwater	7/12/1972	USGS-384829112315901	USGS	38.8078	-112.5333	Pahvant Flow	410	490	1700	150	88	790	990	13	7130	4450
Groundwater	7/12/1972	USGS-384953112325101	USGS	38.8314	-112.5485	Pahvant Flow	345	620	2100	230	77	750	1100	13	8050	5090
Groundwater	7/12/1972	USGS-384910112321401	USGS	38.8191	-112.5380	Valley-fill	326	570	1800	180	78	700	1100	13	7220	4630
Groundwater	7/10/1973	USGS-384748112315801	USGS	38.7961	-112.5339	Pahvant Flow	294	360	1400	190	32	490	640	13	5460	3300
Groundwater	7/10/1973	USGS-384751112312201	USGS	38.7982	-112.5519	Pahvant Flow	227	96	250	72	6	130	250	14	1610	2123
Groundwater	7/10/1973	USGS-384910112321401	USGS	38.8191	-112.5380	Valley-fill	319	620	1900	200	81	740	1100	15	7710	4840
Groundwater	7/10/1973	USGS-385026112261001	USGS	38.8403	-112.4368	Valley-fill	331	93	70	31	3	48	92	13	880	521
Groundwater	7/12/1974	USGS-384751112312201	USGS	38.7982	-112.5519	Pahvant Flow	227	83	220	61	6	150	240	14	1510	934
Groundwater	7/12/1974	USGS-384829112315901	USGS	38.8078	-112.5333	Pahvant Flow	411	400	1500	130	86	740	780	16	6500	3900
Groundwater	7/12/1974	USGS-384953112325101	USGS	38.8314	-112.5485	Pahvant Flow	333	720	2300	250	83	790	1100	15	8820	5460
Groundwater	7/12/1974	USGS-384910112321401	USGS	38.8191	-112.5380	Valley-fill	324	600	2100	210	85	820	1100	15	8080	5130
Groundwater	7/12/1974	USGS-385026112261001	USGS	38.8403	-112.4368	Valley-fill	305	90	81	30	3	62	90	14	950	538
Groundwater	7/8/1975	USGS-385714112264701	USGS	38.9538	-112.4472	Valley-fill	318	260	460	75	23	250	660	20	2950	1910
Groundwater	7/8/1975	USGS-385715112271201	USGS	38.9541	-112.4544	Valley-fill	297	180	320	60	16	170	400	19	2000	1320
Groundwater	7/9/1975	USGS-384748112315801	USGS	38.7961	-112.5339	Pahvant Flow	271	480	1800	230	41	620	670	13	7000	4080
Groundwater	7/9/1975	USGS-384829112315901	USGS	38.8078	-112.5333	Pahvant Flow	379	380	1300	120	82	640	730	16	5800	3500
Groundwater	7/9/1975	USGS-384946112321601	USGS	38.8299	-112.5388	Pahvant Flow	413	620	2400	230	140	1100	1300	17	8760	6050
Groundwater	7/9/1975	USGS-384910112321401	USGS	38.8191	-112.5380	Valley-fill	342	640	2100	210	91	890	1200	15	8000	5350
Groundwater	7/9/1975	USGS-385135112250301	USGS	38.8595	-112.4185	Valley-fill	228	88	92	17	2	29	33	13	730	403
Groundwater	8/6/1975	USGS-385026112261001	USGS	38.8403	-112.4368	Valley-fill	344	93	74	32	3	61	80	13	800	545

Appendix D. *Continued.*

Source	Date	Sample ID	Sampling agency	Latitude	Longitude	Source aquifer or name	Bicarbonate (mg/L)	Calcium (mg/L)	Chloride (mg/L)	Magnesium (mg/L)	Potassium (mg/L)	Sodium (mg/L)	Sulfate (mg/L)	Temperature (°C)	Specific conductance (µS/cm)	Total dissolved solids (mg/L)
Groundwater	8/6/1975	USGS-385303112234801	USGS	38.8841	-112.3975	Valley-fill	299	89	180	30	18	98	75	15	1000	657
Groundwater	8/7/1975	USGS-384953112325101	USGS	38.8314	-112.5485	Pahvant Flow	349	740	2400	290	89	870	1200	15	8880	5810
Groundwater	8/12/1975	USGS-390045112281201	USGS	39.0126	-112.4708	Pahvant Flow	440	200	420	100	7	180	350	12	2600	1530
Groundwater	8/12/1975	USGS-385026112261001	USGS	38.8403	-112.4368	Valley-fill	347	88	65	31	3	61	83	15	860	534
Groundwater	8/12/1975	USGS-385303112234801	USGS	38.8841	-112.3975	Valley-fill	297	82	180	30	18	95	73	15	1190	644
Groundwater	7/19/1976	USGS-385714112264701	USGS	38.9538	-112.4472	Valley-fill	322	270	470	96	22	270	650	20	2860	1960
Groundwater	7/20/1976	USGS-384748112315801	USGS	38.7961	-112.5339	Pahvant Flow	268	540	2300	290	43	640	460	14	8000	4530
Groundwater	7/20/1976	USGS-384953112325101	USGS	38.8314	-112.5485	Pahvant Flow	356	710	2400	270	84	900	1400	14	8950	5990
Groundwater	7/20/1976	USGS-385026112261001	USGS	38.8403	-112.4368	Valley-fill	330	96	68	29	3	51	76	13	850	517
Groundwater	7/20/1976	USGS-385135112250301	USGS	38.8595	-112.4185	Valley-fill	232	89	89	17	2	29	31	13	700	398
Groundwater	7/20/1976	USGS-385303112234801	USGS	38.8841	-112.3975	Valley-fill	294	100	210	31	18	100	84	15	1250	705
Groundwater	7/20/1976	USGS-385715112271201	USGS	38.9541	-112.4544	Valley-fill	299	200	330	69	16	160	390	19	1800	1330
Groundwater	7/22/1976	USGS-384910112321401	USGS	38.8191	-112.5380	Valley-fill	381	640	2200	200	90	980	1300	14	9000	5650
Groundwater	12/10/1976	UTAHDWQ_WQX-5991830	UDWQ	39.1541	-112.4916	Sugar Loaf Well #1	493	116	316	98	11	310	530	-	2840	1850
Groundwater	6/6/1977	USGS-385714112264701	USGS	38.9538	-112.4472	Valley-fill	320	270	460	92	22	260	690	20	2800	1980
Groundwater	6/6/1977	USGS-385715112271201	USGS	38.9541	-112.4544	Valley-fill	300	180	310	68	16	170	410	19	2000	1320
Groundwater	6/7/1977	USGS-384748112315801	USGS	38.7961	-112.5339	Pahvant Flow	260	620	2200	320	44	670	770	14	8210	4910
Groundwater	6/7/1977	USGS-384829112315901	USGS	38.8078	-112.5333	Pahvant Flow	390	330	1100	93	74	600	620	16	5000	3070
Groundwater	6/7/1977	USGS-384953112325101	USGS	38.8314	-112.5485	Pahvant Flow	350	670	2000	240	74	820	1200	15	8300	5230
Groundwater	6/7/1977	USGS-384910112321401	USGS	38.8191	-112.5380	Valley-fill	400	560	1900	180	85	910	1200	15	7810	5080
Groundwater	6/7/1977	USGS-385026112261001	USGS	38.8403	-112.4368	Valley-fill	320	85	61	28	2	49	67	13	850	482
Groundwater	6/7/1977	USGS-385135112250301	USGS	38.8595	-112.4185	Valley-fill	230	80	79	17	2	30	30	13	700	3
Groundwater	6/7/1977	USGS-385303112234801	USGS	38.8841	-112.3975	Valley-fill	300	98	220	32	19	120	89	15	1300	743
Groundwater	6/20/1978	USGS-390045112281201	USGS	39.0126	-112.4708	Pahvant Flow	170	220	450	100	7	190	400	13	2600	1510
Groundwater	6/20/1978	USGS-385715112271201	USGS	38.9541	-112.4544	Valley-fill	200	190	330	67	18	170	420	20	2050	1320
Groundwater	6/21/1978	USGS-384953112325101	USGS	38.8314	-112.5485	Pahvant Flow	210	700	2200	230	83	810	1300	14	8000	5480
Groundwater	6/21/1978	USGS-385135112250301	USGS	38.8595	-112.4185	Valley-fill	140	91	76	17	2	30	23	15	550	334
Groundwater	6/21/1978	USGS-385714112264701	USGS	38.9538	-112.4472	Valley-fill	200	260	470	91	24	250	700	20	2950	1920
Groundwater	6/23/1978	USGS-384748112315801	USGS	38.7961	-112.5339	Pahvant Flow	180	720	2600	330	51	690	960	14	9000	5600
Groundwater	6/23/1978	USGS-384829112315901	USGS	38.8078	-112.5333	Pahvant Flow	340	360	1300	99	87	610	620	17	5750	3300
Groundwater	7/7/1978	USGS-385026112261001	USGS	38.8403	-112.4368	Valley-fill	190	88	73	30	3	53	64	13	810	429
Groundwater	7/7/1978	USGS-390628112201401	USGS	39.1066	-112.3392	Valley-fill	220	230	400	92	4	90	320	14	2150	1300
Groundwater	8/4/1978	USGS-385303112234801	USGS	38.8841	-112.3975	Valley-fill	260	87	190	30	20	100	81	15	1240	654
Groundwater	4/11/1979	UTAHDWQ_WQX-5992340	UDWQ	39.0144	-112.5530	North Pond Well	225	53	129	81	18	67	110	-	*988	632
Groundwater	5/1/1979	USGS-385715112271201	USGS	38.9541	-112.4544	Valley-fill	-	190	320	70	16	160	410	20	2100	1330
Groundwater	5/17/1979	UTAHDWQ_WQX-5992270	UDWQ	38.9347	-112.7663	Black Willow Well	388	43	1702	28	85	1460	1827	-	*9441	6042
Groundwater	5/17/1979	UTAHDWQ_WQX-5992320	UDWQ	38.9966	-112.6994	Kanosh Well	101	247	366	189	140	1700	1255	-	*13,459	8614

Appendix D. *Continued.*

Source	Date	Sample ID	Sampling agency	Latitude	Longitude	Source aquifer or name	Bicarbonate (mg/L)	Calcium (mg/L)	Chloride (mg/L)	Magnesium (mg/L)	Potassium (mg/L)	Sodium (mg/L)	Sulfate (mg/L)	Temperature (°C)	Specific conductance (µS/cm)	Total dissolved solids (mg/L)
Groundwater	5/25/1979	UTAHDWQ_WQX-5991810	UDWQ	39.1136	-112.4613	Sugar Loaf Well #2	620	51	579	38	60	648	351	-	*456	292
Groundwater	5/25/1979	UTAHDWQ_WQX-5991830	UDWQ	39.1541	-112.4916	Sugar Loaf Well #1	430	170	1025	87	107	496	440	-	*4788	3064
Groundwater	5/25/1979	UTAHDWQ_WQX-5992300	UDWQ	38.9764	-112.5866	Peterson Well	307	24	99	15	16	304	351	-	*2084	1334
Groundwater	6/4/1979	UTAHDWQ_WQX-5992330	UDWQ	39.0016	-112.6288	12-A Well	446	61	432	49	51	392	261	-	*2856	1828
Groundwater	6/29/1982	USGS-385715112271201	USGS	38.9541	-112.4544	Valley-fill	-	190	310	71	12	160	420	20	2095	1330
Groundwater	7/20/1984	UTAHDWQ_WQX-5992330	UDWQ	39.0016	-112.6288	12-A Well	338	20	618	2	37	516	156	-	*2881	1844
Groundwater	8/8/1984	UTAHDWQ_WQX-5992280	UDWQ	38.9427	-112.6191	Second Patch Well	280	24	451	1	44	476	871	-	*213	136
Groundwater	8/8/1984	UTAHDWQ_WQX-5992300	UDWQ	38.9764	-112.5866	Peterson Well	241	19	429	1	34	459	457	-	*2156	1380
Groundwater	8/15/1984	USGS-385715112271201	USGS	38.9541	-112.4544	Valley-fill	-	180	300	68	16	170	420	20	2075	1330
Groundwater	8/24/1984	UTAHDWQ_WQX-5992290	UDWQ	38.9430	-112.5405	Squidike Spring	200	529	0	1	63	262	145	-	*4994	3196
Groundwater	6/11/1986	USGS-390052112323801	USGS	39.0143	-112.5530	Pahvant Flow	268	200	1200	140	64	660	690	13	5080	3130
Groundwater	6/12/1986	USGS-385752112224301	USGS	38.9643	-112.3793	Valley-fill	312	74	20	27	1	16	18	15	625	346
Groundwater	6/3/2015	USGS-385150112302501	USGS	38.8621	-112.5053	Meadow Hot Spring	382	437	1805	87	159	0	991	36	7240	*4634
Groundwater	11/7/2022	SP-CLRLK-221107	UGS	39.0946	-112.6125	Clear Lake	190	163	980	133	52	532	649	12	4230	*2707
Groundwater	11/7/2022	SP-MHSP-221107	UGS	38.8621	-112.5053	Meadow Hot Spring	392	455	1870	85	143	1050	1030	25	7740	*4954
Groundwater	11/7/2022	SP-SQSP-221107	UGS	38.9421	-112.5406	Squidike Spring	255	490	2450	226	105	1120	1180	15	8940	*5722
Groundwater	4/11/2023	WL-BFW-041123	UGS	39.0741	-112.4802	Big Flat Well	214	238	480	180	11	152	788	-	-	-
Surface	5/7/1996	UTAHDWQ_WQX-4940200	UDWQ	38.9502	-112.2694	Chalk Creek abv Fillmore	230	49	4	15	1	3	11	9	353.5	196
Surface	8/22/1996	UTAHDWQ_WQX-4940200	UDWQ	38.9502	-112.2694	Chalk Creek abv Fillmore	224	40	6	19	1	5	11	20	357.5	194
Surface	8/11/1999	MEADOW CK @ USFS BNDY	UDWQ	38.8955	-112.3372	Meadow Creek	190	44	9	14	-	7	-	18	307	*197
Surface	11/9/1999	UTAHDWQ_WQX-4940200	UDWQ	38.9502	-112.2694	Chalk Creek abv Fillmore	282	51	6	24	-	6	-	6	390.5	232
Surface	11/13/2001	UTAHDWQ_WQX-4940200	UDWQ	38.9502	-112.2694	Chalk Creek abv Fillmore	242	45	5	21	1	6	-	7	369	222
Surface	11/7/2022	ST-CCUD-221107	UGS	38.9341	-112.2307	Chalk Creek	262	60	6	24	1	6	20	10	439	*281
Surface	11/7/2022	ST-CORNUD-221107	UGS	38.7839	-112.4152	Corn Creek	274	71	26	25	2	19	27	12	557	*356
Surface	11/7/2022	ST-MCUD-221107	UGS	38.8960	-112.3387	Meadow Creek	239	61	5	17	-	5	19	8	390	*250
Surface	11/8/2022	ST-PCMH-221108	UGS	39.0360	-112.2217	Pioneer Creek	250	61	16	22	2	11	20	11	442	*283

Notes:
• Asterisk (*) denotes a calculated value based off either total dissolved solids or specific conductance. The formula TDS=0.64 x EC was used for these conversions.
• Hyphen (-) character indicates no laboratory analysis performed on specific analyte.
• Source aquifer or name is listed as reported by Sampling agency.